THEORETICAL AND EXPERIMENTAL ANALYSIS OF ABSORPTION-CONDENSATION IN A COMBINED POWER AND COOLING CYCLE

By

NITIN GOEL

A DISSERTATION PRESENTED TO THE GRADUATE SCHOOL
OF THE UNIVERSITY OF FLORIDA IN PARTIAL FULFILLMENT
OF THE REQUIREMENTS FOR THE DEGREE OF
DOCTOR OF PHILOSOPHY

UNIVERSITY OF FLORIDA

2005

This work is dedicated to my parents for their constant encouragement, support and love.

ACKNOWLEDGMENTS

This work is accomplished with the contribution of several people. I am highly thankful to my advisor, Prof D. Yogi Goswami, for having an unwavering belief in my capabilities. He has guided, advised and encouraged me throughout this academic program; without him this dissertation would be a daunting task for me. I would like to thank my advisory committee for their invaluable time and comments in the course of this work.

I have learned machine shop skills from Charles Garretson, senior technician at Solar Energy and Energy Conversion Laboratory, which not only helped in this experimental study but will also help me throughout my life. I am also very grateful to my colleagues at Solar Energy and Energy Conversion Laboratory, University of Florida. Christopher Martin, Gunnar Tamm, Saleh Al-Kharabsheh and Sanjay Vijayaraghavan have constantly provided a valuable feedback on my work. I also appreciate the friendship and cooperation of Amit Vohra, Christopher Cheng, Man Su Lee, Patricia Alexander and Shalabh Maroo.

TABLE OF CONTENTS

LIST OF TABLES

LIST OF FIGURES

NOMENCLATURE

A	Area, m^2
b^+	Dimensionless position for developing flows, $b/\left(D_I \, \mathrm{Re}_{D_I} \, \mathrm{Pr}\right)$
b	Axial coordinate, m
B	Length of the coolant tube, m
C_P	Specific heat, kJ/kg-K
D	Diameter of the coolant tube, m
D_{aw}	Volumetric diffusivity, m^2/s
D_h	Hydraulic diameter, m
dm	Mass flux transferred, kg/s
E	Seebeck Voltage, V
F	Volumetric flow rate, l/min
g	Acceleration due to gravity, m/s^2
G	Specific Gibbs energy, kJ/kg
Gz	Graetz number, $\pi/(4b^+)$
H	Specific enthalpy, kJ/kg
h	Heat transfer coefficient, kW/m^2-K
K	Mass transfer coefficient, kmole/m2-s
k	Thermal conductivity, W/m-K
L	Length of the coolant tube assembly, m
M	Molecular weight, kg/kmole

m	Mass flow rate, kg/s
Nu_D	Nusselt number, hD_I/k
P	Total absolute pressure, Pa
Pr	Prandtl number, $\mu C_p/k$
Q	Heat transfer, kW
R	Molar specific gas constant, kJ/kmole-K
Re_{D_I}	Reynolds number for flow in the coolant tube, $\rho u D_I/\mu$
Re_{D_O}	Reynolds number for flow over the coolant tube, $\rho u D_O/\mu$
$\mathrm{Re}_{\mathrm{film}}$	Reynolds number for falling film, $4\Gamma/\mu$
$\mathrm{Re}_{\mathrm{film1}}$	Reynolds number for falling film, $400F/B\eta$
R_{wall}	Conduction resistance, m^2-K/kW
S	Specific entropy, kJ/kg-K
Sc	Schmidt number, $\mu/\rho D_{aw}$
T	Absolute temperature, K
u	Velocity, m/s
U	Overall heat transfer coefficient, $\mathrm{kW/m}^2$-K
UA	Product of the overall heat transfer coefficient and wetted-tube surface area, kW/K
V	Volumetric flow rate, m^3/s
x	Mass fraction of ammonia in the liquid phase
$\tilde{x}$	Mole fraction of ammonia in the liquid phase
y	Mass fraction of ammonia in the vapor phase
$\tilde{y}$	Mole fraction of ammonia in the vapor phase

z	Parameter for estimating ammonia mole flux in the absorbing/desorbing vapor flux, $z = \left(\frac{\frac{dm_{NH_3}}{M_{NH_3}}}{\frac{dm_{H_2O}}{M_{H_2O}} + \frac{dm_{NH_3}}{M_{NH_3}}} \right)$

Greek Symbols

β	Falling film thickness, m
δ	Uncertainty
μ	Dynamic viscosity, kg/m-s
λ	Thermal conductivity, W/m-K
η	Kinematic viscosity, m^2/s
ν	Specific volume, m^3/kg
ρ	Density, kg/m^3
Γ	Mass flow rate of falling film per unit periphery, kg/m-s

Subscripts

abs	Absorber
actual	Actual parameter values
aw	Ammonia-water mixture
b	Bubble
boil	Boiler
B	Reference
c	Critical
cal	Calibration parameter values
C	Coolant
d	Dew
film	Falling film

film1	Falling film
float	Float of the Variable area flow meter
i	Interface
I	Inside
L	Liquid phase
measured	Measured parameter values
mesh	Mesh
O	Outside
r	Reduced
rec	Rectification column
S	Strong solution
tube	Cooling tube
V	Vapor phase
W	Weak solution

Superscripts

*	Modified
E	Excess
mix	Mixing

Abstract of Dissertation Presented to the Graduate School
of the University of Florida in Partial Fulfillment of the
Requirements for the Degree of Doctor of Philosophy

THEORETICAL AND EXPERIMENTAL ANALYSIS OF ABSORPTION-CONDENSATION IN A COMBINED POWER AND COOLING CYCLE

By

Nitin Goel

December 2005

Chair: D. Y. Goswami
Major Department: Mechanical and Aerospace Engineering

Heat-driven absorption thermodynamic cycles offer a possibility of generating both power and cooling with environment friendly refrigerants, such as ammonia. The absorber in such systems is one of the critical components in terms of size, efficiency and cost. In this work, a new concept of enhancing heat and mass transfer processes in a falling film absorber is proposed that could considerably reduce the absorber size without the penalty of high vapor and coolant side pressure drops. The concept utilizes the vertical spacing between the horizontal tubes to form a falling film using a flow guidance medium such as a screen mesh/fabric. In addition to an increase in the liquid-vapor interface area, the design also enhances falling film stability by preventing coalescence of droplets on the horizontal tubes. Furthermore, the design induces thorough mixing of liquid film while it flows progressively over the mesh/cloth and coolant tubes.

This work details a numerical and experimental analysis of the new design with a microchannel falling film absorber design. A finite difference scheme is presented which

models the heat and mass transfer processes in a counter-current flow falling film absorber. The numerical investigation accounts for the liquid and vapor phase mass transfer resistances in the falling film absorption. It also considers the coupled nature of heat and mass transfer processes. Details of the experiments on the proposed concept and the microchannel absorber designs are then presented. The experimental study shows that the absorber heat duty for the proposed design is about 17-26% higher than the conventional microchannel design. The *UA* value is found to increase by about 50% with an introduction of the screen mesh. This is attributable to the fact that the screen mesh enhances both mixing and wetting action in the liquid film. A comparison of numerical and experimental results is also done, which shows a good agreement with some deviation at low temperatures of the coolant and high flow rates of the weak solution.

CHAPTER 1
INTRODUCTION

This chapter describes the motivation behind this research, description of the proposed design and the objectives of this research.

Motivation

In a worldwide fossil fuel based economy, there continues to be an ever-growing demand on fossil fuels, which has created problems in terms of pollution and availability. Sun, being a sustainable, clean and abundant source of energy, is a promising alternative to the fossil fuels. Heat-driven absorption thermodynamic cycles offer a possibility of generating both power and cooling with environmentally friendly refrigerants such as ammonia. A new binary-mixture based thermodynamic cycle capable of producing both power and refrigeration simultaneously was proposed by D. Y. Goswami (1995, 1998). The cycle is an innovative combination of an ammonia-based Rankine cycle and an ammonia-water absorption refrigeration cycle. Figure 1-1 shows the schematic of the cycle.

The basic operation of the cycle is as follows. The ammonia-water solution at high pressure is boiled in the boiler to generate high concentration ammonia vapor and low concentration ammonia liquid. The water-rich solution throttles back to the absorber while the concentrated ammonia vapor is expanded in the turbine to produce work. Expanding the vapor below the ambient temperature can simultaneously provide power and refrigeration. The low-pressure vapor then flows into the absorber where it gets absorbed by the water-rich solution. The cycle is accomplished by pumping back the

liquid mixture of ammonia and water to the boiler. The varying boiling temperature of the binary mixture provides a better thermal match between the working fluid and the sensible heat source leading to an efficient utilization of energy resources. The cycle can use source temperatures as low as 60 ^{o}C, thereby making it a useful power cycle for low-cost solar thermal collectors, geothermal resources and waste heat from existing power plants.

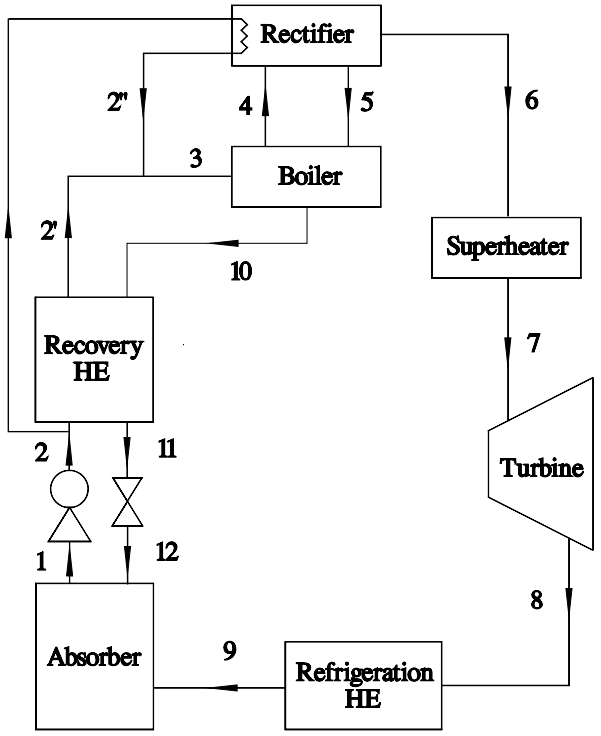

Figure 1-1. Schematic of the ammonia-based combined power and cooling cycle

During experimentations on the cycle at the Solar Energy and Energy Conversion Laboratory of University of Florida, it was realized that the absorber is one of the critical components in terms of size, efficiency and cost. An absorber is a combined heat and mass exchanger that absorbs the vapor phase of the absorbate (NH_3) in a liquid absorbent (H_2O) before pumping the mixture to the high-pressure side of the cycle. The absorption process is exothermic, and thus a substantial amount of heat removal is required from the weak solution to maintain the absorption process. The amount of heat required to be

rejected from the binary mixture in the absorber is nearly equal to the heat requirement of the boiler (Herold et al., 1996).

The key features of an efficient design are low-pressure drop in the liquid, vapor and coolant regimes. Being one of the largest components of the system, it plays a significant role in deciding the overall cost, size and competitiveness of the system. The temperature of the weak solution in absorber is in the range of 40-60 ^{o}C. The low temperature glide between the weak solution and heat rejection source limits the rate of heat loss, and thus requires a larger surface area to accomplish the required heat transfer. In addition, the system is restricted to a penalty of lower pressure drops in the vapor phase. A higher pressure drop in the vapor phase will raise the evaporator temperature, and the cooling temperature of the system will thus be increased.

A detailed literature survey on the existing absorber designs led to the conclusion that the falling film absorption mode possesses lower pressure-drop in the liquid and vapor phases as compared to a much more compact design of the bubble absorption mode. However, the falling film mode poses several practical challenges such as surface wetting, flooding and uniform liquid distribution. It was decided to take the path of falling film absorption mode, and enhance the performance of a falling film absorber by eliminating the significance of the above mentioned constraints on the falling film design.

The absorbers are currently designed on the basis of empirical data. However, numerical analysis is essential for a thorough understanding and development of an efficient design. Absorbers for nonvolatile absorbent-based absorption cycles, such as a LiBr-H_2O cycle, have been studied more extensively as compared to volatile absorbents. In the case of ammonia-water pair, the refrigerant and absorbent are present in both liquid

and vapor phases making the transport phenomena more complex to analyze. The resistance to heat and mass transfer needs to be considered in the liquid and vapor phases, as concentration and temperature gradients are present among liquid, vapor and liquid-vapor interface. In the existing literature, such models for volatile absorbents are mainly limited to co-current systems. The situation becomes more complicated for counter-current flow systems because the inlet liquid and vapor conditions are known at opposite ends. In this work, a finite difference model is developed for a counter-flow system. The model takes into account both liquid and vapor phase mass transfer resistances, and uses empirical correlations to predict the heat and mass transfer coefficients. Empirical correlations for the heat and mass transfer coefficients are useful for simulating wavy-laminar and turbulent flow conditions, the conditions in which numerically calculated coefficients are less reliable.

In the current work, a new design of a falling film absorber is proposed that could considerably reduce the absorber size. The proposed design is based on the fundamental characteristics of an efficient absorber design: large liquid-vapor interfacial area and good wetting characteristics. The design utilizes the unused vertical spacing between the coolant tubes to form a falling film which consequently leads to an increase in the mass transfer area. The proposed design was numerically compared with a microchannel-based conventional horizontal tube type absorber. As horizontal tube-type absorbers with small diameter coolant tubes are very compact, this analysis will help in comparing the proposed design with the current state-of-the-art absorber design.

Proposed Absorber Configuration

It is a well-known fact that the mass transfer process is the dominating factor in the simultaneous heat and mass transfer processes in absorption. An increase in liquid-vapor

contact area and induction of turbulence at the liquid-vapor interface are some of the techniques that can increase mass transfer rates. Bubble absorbers are about 50% more compact in comparison to the traditional falling film absorbers (Kang et al., 2000a). Their compact size results from the generation of an extremely large liquid-vapor interface by bubbling vapor into the bulk liquid. In the case of conventional falling film absorption mode, the interfacial area between the liquid and vapor phases is limited to the surface area of the coolant tubes and liquid droplets falling in between the coolant tubes. However, the surface area of the droplets will be much smaller than that of the coolant tubes. Figure 1-2 provides a schematic representation of the horizontal tube type falling film absorber.

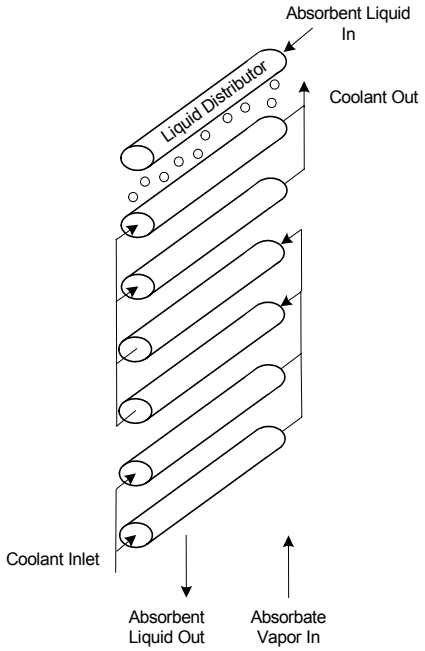

Figure 1-2. Conventional horizontal tube type falling film absorber

Several enhancement techniques have been examined and analyzed to improve the performance of a falling film absorber, but the utilization of vertical space between the adjacent coolant tubes has not yet been reported. A falling film can be formed between the adjacent tubes to increase the liquid-vapor surface area. Operating the falling film in

sheet mode is one way to form a liquid film between the horizontal tubes. However, it requires comparably higher solution flow rates which itself reduces the effective liquid-coolant surface area. Another method, confined to lower solution flow rates would be to have a medium between the horizontal tubes over which a liquid film can be easily formed. Alternatively wrapping a mesh/fabric between the left and right sides of the adjacent tubes, as shown in Figure 1-3, can be utilized to form a liquid film between the horizontal tubes.

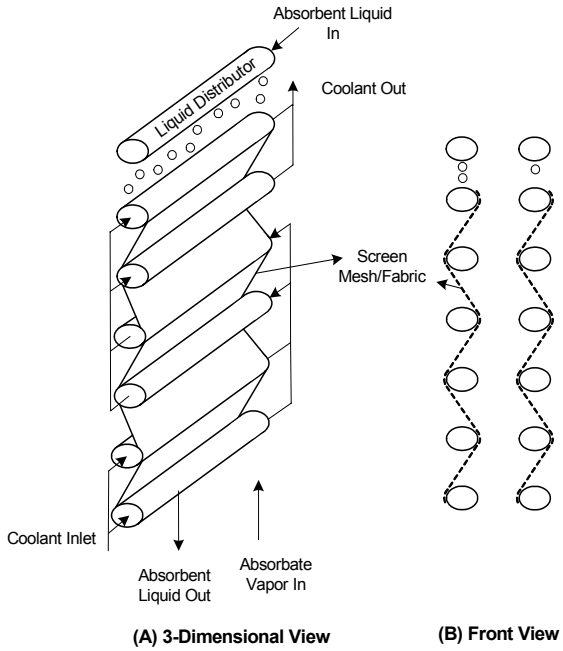

Figure 1-3. Proposed horizontal tube type falling film absorber (with screen mesh/fabric)

The mesh/fabric can be made up of a compatible material such as aluminum, steel, stainless steel, glass fiber, and nylon (Schweitzer, 1998 & 2000). The material should also be flexible, and it should conform to the shape of the coolant tube. In addition, the requirement of forming a uniform falling film on the mesh restricts the use of materials which have good wetting characteristics. It should be noted that a smaller angle between the mesh and vertical plane is desirable. The liquid surface tension will not be able to hold the liquid along the mesh for larger angles, and the liquid will drip in the form of

droplets. However, this effect can be reduced by changing the size of the mesh openings. The openings of the mesh should be sparse enough to just allow the formation of falling film over the mesh. A sparser and thinner mesh will reduce the effect of the mesh on liquid flow over the coolant tubes. The concept is so simple that it can also be incorporated in existing horizontal tube type falling film absorbers.

Availability of a larger liquid-vapor contact area might lead to an extra amount of absorption. The resulting increase in the absorption heat will increase the solution temperature. Hence, a larger temperature gradient between the coolant and liquid solutions will in turn increase the rate of heat transferred to the coolant. In addition to an increase in surface area, the concept also enhances falling film stability by preventing the coalescence of droplets on horizontal tubes. Fabrics have a natural tendency to soak up liquid by capillary action, and this mechanism also helps in redistributing the liquid solution on the coolant tubes. Furthermore, the liquid flow over an irregular surface of the mesh may induce vortices. It may thus promote mixing of the liquid film while it flows alternatively over the mesh/fabric and coolant tubes. Fujita et al. (1980) showed an increase in heat and mass transfer coefficients by 1.5 to 1.8 times on a vertical wetted wall by introducing wire roughness. The falling film mixing replenishes the liquid boundary layer by removing ammonia to the liquid bulk, and thus enhances the absorption rate. The combined effect of increased mass transfer area, liquid film mixing and film stability will improve the absorption flux. Other phenomena associated with the proposed design are the increase in liquid hold-up, prevention of satellite droplets and fin-effect of the metallic mesh. These effects may also enhance the performance of the proposed design.

The use of a large number of smaller diameter cooling tubes can considerably increase the cooling surface area per unit volume as compared to a small number of larger diameter tubes. Very high heat transfer coefficients can also be achieved in small diameter tubes. A parallel-series arrangement of the coolant tubes is usually used to reduce the effect of increase in the pressure drop and restrict the flow rate to the appropriate limits. The coupling of miniaturization of the coolant section and film formation between the horizontal tubes can consequently enhance the absorption flux, and thus lead to an efficient absorber design.

Objectives of the Work

The following are the objectives of this research work:

1. Conduct a literature review of the available absorber designs.
2. Develop a mathematical model to analyze the absorption process in a falling film absorber. The model should consider the coupled nature of heat and mass transfer processes accompanying the falling-film absorption. The model should also take into account the mass transfer resistances in both the liquid and vapor phases, and use the empirical correlations to predict the heat and mass transfer coefficients.
3. Apply the numerical technique to model the horizontal tube type falling film absorber.
4. Conduct a numerical comparison of the effect of screen mesh/fabric on the performance of the horizontal tube type absorber.
5. Design and fabricate both the proposed and conventional designs of horizontal tube type falling film absorber on the basis of the numerical results.
6. Conduct an experimental study to compare the performances of the proposed and conventional designs.
7. Compare the numerical and experimental results to determine the validity of the mathematical model.

CHAPTER 2
LITERATURE REVIEW

Introduction

An absorber in absorption based thermodynamic cycles is a combined heat and mass exchanger that absorbs the vapor phase of the refrigerant or working fluid (such as NH_3) in a liquid absorbent (such as H_2O) for transporting the refrigerant/working fluid to the high-pressure side of the cycle. It is one of the critical components of the power cycle in terms of size, efficiency and cost. It is desirable for an absorber to have low-pressure drops for the liquid, vapor and coolant flows. Size and cost of the absorber also play an important role in designing an absorber. It can be realized by achieving high heat and mass transfer coefficients, and a large surface contact area.

Absorber Designs

Absorbers are usually characterized on the basis of absorption mode. The vapor to be absorbed by the weak solution can be either in bubbles or as bulk phase. Thus, absorbers can be divided into two broad categories, namely, those operating in falling film and bubble absorption modes. Numerous variations of these two types have been extensively analyzed and studied by researchers. Heat and mass transfer enhancement techniques such as extended finned surfaces, sand blasting and use of surfactants have been primarily employed to augment the performance of an absorber. In this work, a literature survey was conducted to explore the existing absorber designs, which is summarized in this chapter. A useful published review on absorber designs is by

Pachhapur and Rane (1998). Killion and Garimella (2001) presented a detailed review of the various numerical modeling techniques.

Falling Film Absorber

Falling film absorption mode has been traditionally utilized in the packed bed columns by chemical industry. In such absorbers, a need for continuous heat removal from the liquid solution led a slight modification of the concept by including a heat rejection mechanism. Packing is replaced by the heat transfer surfaces, namely, vertical/horizontal tubes and plates. The heat transfer surfaces serve the dual purpose of providing a direct contact between the weak solution and the vapor, and an indirect contact between the weak solution and the coolant. The key difference between the falling film and bubble absorption modes is the flow characteristics of the liquid and vapor phases. In the falling film mode, the liquid falls as a film and the vapor flows over it in a continuous phase, whereas in the bubble mode, the liquid flows in a continuous phase and the vapor is dispersed in it as bubbles. In other words, the falling film absorption mode can be visualized as a separated two-phase flow.

Figure 2-1 shows a schematic representation of a typical falling film absorber. It consists of an array of cooling tubes/plates over which the weak solution is uniformly distributed. The weak solution then flows down the cooling surface under the influence of gravity. The vapor to be absorbed enters the absorber and flows through the narrow channels formed by an assemblage of the cooling surfaces. As the vapor flows co-current or counter-current to the weak solution, it is absorbed by the weak solution. The heat of absorption thus released is rejected to the coolant flowing through the cooling tubes/plates.

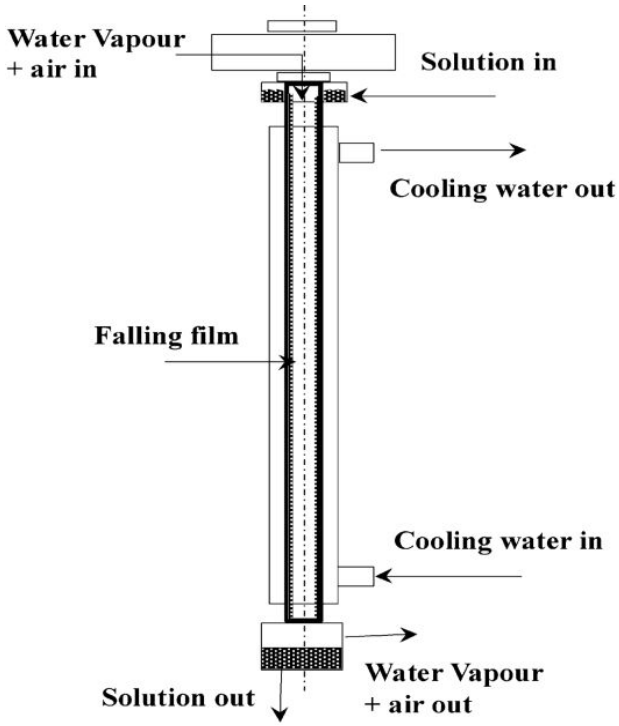

Figure 2-1. Falling film absorber, from Medrano et al. (2003)

Liquid distributors are needed to uniformly distribute the weak solution over the heat transfer surfaces. Good surface wetting and horizontal leveling of the cooling tubes/plates are critical for good design. Another concern is the flooding of adjacent surfaces. Though the falling film mode poses several practical challenges such as surface wetting, flooding and uniform liquid distribution, this absorption mode is widely used due to low pressure-drops in the liquid and vapor phases. Numerous types of cooling surfaces have been employed to augment the performance of the falling film absorbers. The most commonly used types are horizontal/vertical tubes and plates. The falling film of the weak solution can be formed either on the inner or outer surfaces of the tubes/plates. As the field of heat exchangers is comparatively well-researched, the main focus in falling film absorbers has been on heat and mass transfer on the solution-side surface. Numerous investigators have devoted their research to enhance surface wetting,

liquid mixing, and heat/mass transfer coefficients. A brief review of this work is described below.

Surface roughness critically affects the wetting characteristics of a falling film. Several techniques such as sand blasting, surface patterning, scratching, and oxidation have been used to increase the wettability. Micro-scale hatching of the tubular surface has also been utilized to form a uniform falling film (Park et al., 2003). Park et al. did experiments on smooth and micro-scale hatched tubes to analyze the effect of surface roughness in the range of 0.386-6.968 μm. They found the absorption rate for the micro-scale hatched tubes to be about two times greater than that for the smooth tubes.

Yang and Jou (1995) proposed the use of a porous surface to improve the wettability of a surface. The porosity of the surface randomly distributes the falling film, and hence also reduces the flow velocity of the liquid. The effectiveness of a porous medium was numerically analyzed on the basis of Brinkman-Forchhiemer extended Darcy equation. They reported higher absorption rates over smooth film absorption process. They also studied the effect of porosity to maximize the absorption rate and concluded that the optimal porosity of the medium is 0.9.

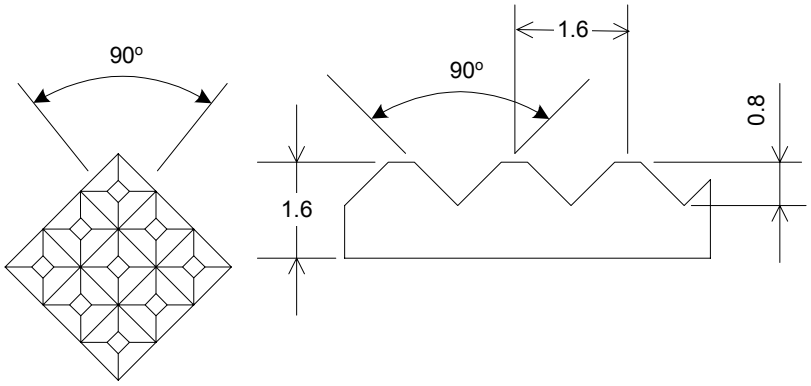

Figure 2-2. Indented tubular surface, from Tongu et al. (1993)

Tongu et al. (1993) designed an air-cooled falling film absorber for a LiBr-LiCl-LiI-$LiNO_3$/H_2O multi-component absorption chiller. The inner surface of the vertical tubes was indented as shown in Figure 2-2. The proposed surface modification not only enhanced the surface wetting but also induced stirring in the liquid solution. In addition, the aluminum louver fins were utilized on the airside to improve the heat transfer coefficient by 20% as compared to the conventional flat fins. However, the paper does not provide any details of the manufacturing procedure used for indenting the inner surface of tubes.

Benzeguir et al. (1991) also profiled the solution-side heat transfer surface to generate large mixing waves. They experimentally compared the performance of a vertical LiBr-H_2O absorber with the smooth, grooved, and wire wound tubes. The tube with grooves was found to be most efficient in terms of heat and mass transfer coefficients. The use of grooved tubes increased the heat transfer coefficient by 1.5 times over smooth tubes.

Miller and Perez-Blanco (1993) studied the effect of solution-side surface configurations on the enhancement of mixing and uniformity of the falling film. They selected the outer surface configurations with pin fins, grooves, and twisted fins and compared them with a conventional smooth surface. These surface configurations are depicted in Figure 2-3. Absorption of water vapor into a solution of aqueous lithium bromide was studied to determine the best solution-side surface configuration. They reported pin fin tubes with 6.44 mm pitch to be the most effective in enhancing the absorption process by 225% over the conventional design. It was followed by the grooved tubes, which reported a 175% increase in mass absorption. The experiments

were not done in the presence of surfactants. The authors further concluded that the enhancement in mass transfer was comparable to systems with surfactants, which frequently faces the problem of breakdown at high temperature.

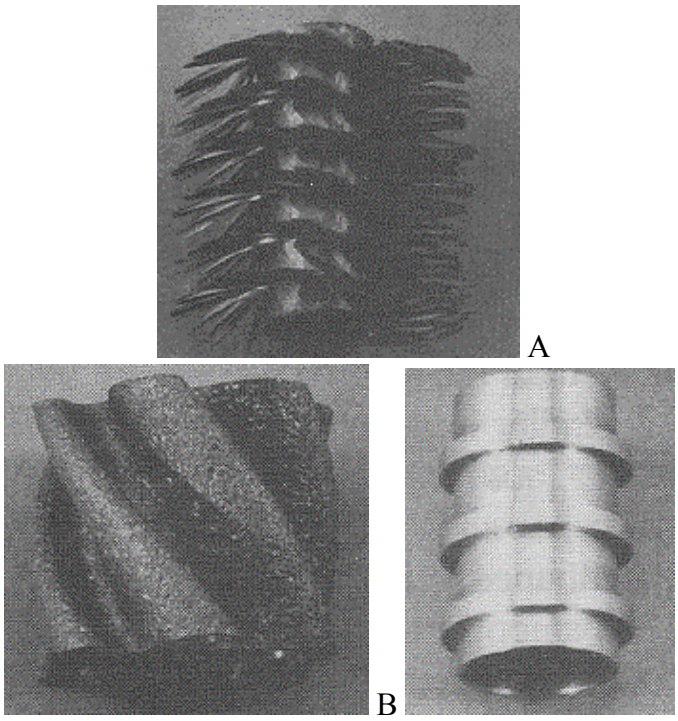

Figure 2-3. Different surface configurations employed by Miller and Perez-Blanco (1993): (A) Pin fin tube, (B) Twisted tube, and (C) Grooved tube

Similar to the above concept, Schwarzer et al. (1993) used spiral steps on the inner periphery of the tubes. In addition to the increase in fluid mixing, the fins act as obstructions in the vapor path that consequently induce turbulence in the flow. Their design was built by assembling individual discs with spiral steps. They observed an increase in heat transfer coefficient with the increase in the slope of the spiral steps.

Constant curvature surfaces (CCS) were studied by Isshiki et al. (1988) for the purpose of forming uniformly thick falling film. A self-elaborative sketch of CCS can be seen in Figure 2-4. They reported formation of uniformly thick liquid film over these surfaces. Experiments on the CCS tubes were done with 50% LiBr-H_2O solution. The

heat transfer coefficient of the CCS was found to be the highest as compared to the triangular and rectangular finned tubes.

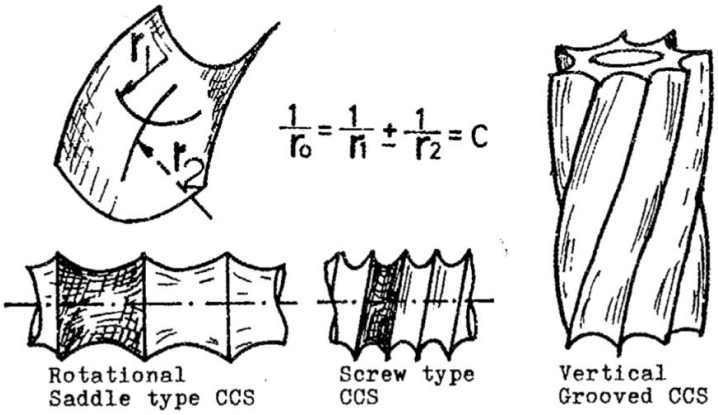

Figure 2-4. Constant curvature surface (CCS) tubes, from Isshiki et al. (1988)

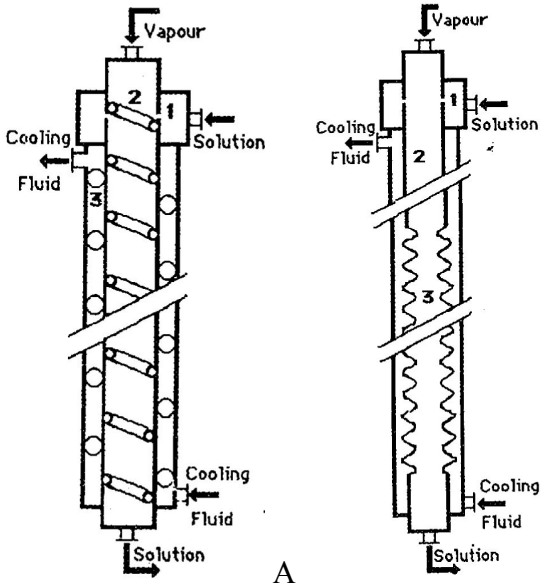

Figure 2-5. Vertical tubular absorbers provided with tangential solution feed (Rignac et al., 1988): (A) Falling film absorber with helical coils, and (B) Falling film absorber with a corrugated tube

The expansion energy of the weak solution has also been utilized to promote turbulence near the feeding zone of a vertical tube absorber (Rignac et al., 1988). The weak solution was tangentially injected on the inner surface of tubes. The spiral movement of the falling film was further guided by the use of helical coils. A similar coil in the annular passage of cooling fluid was also introduced to improve the coolant side

heat transfer coefficient. In another version of the design, corrugated tubes replaced the tube-helical coil assembly. Figure 2-5 shows representative schematics of both systems. Rignac et al. (1988) conducted experiments for the working pairs methanol-LiBr, methanol-glycerol, water-glycerol, and water-ethylene glycol, whereas water and water-ethylene glycol were utilized as the cooling fluids. The second version of the absorber was found to be more favorable; 20-50% greater overall heat transfer coefficient was attained than over the tube-helical coil assembly.

Strenger and Setterwall (1993) used lamella plates as the heat exchange surfaces. Lamellas are commonly utilized as cooling plates in the falling film chillers. Their advantage over the cooling tubes is their ability to achieve higher coolant-side heat transfer coefficients while subjected to lower pressure drops. The front and cross-sectional views of the lamella are shown in Figure 2-6. For the aqueous LiBr flow rate of 0.44 kg/s-m, an overall heat transfer coefficient as high as 1.8 kW/m^{2}K was reported.

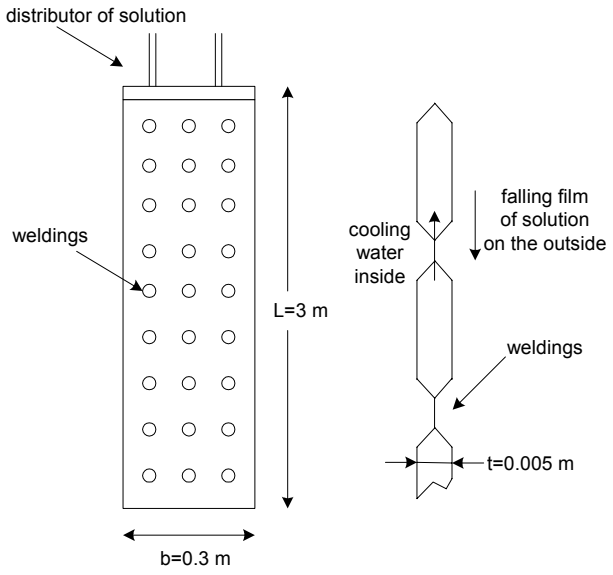

Figure 2-6. Front and cross-sectional view of the Lamella, from Strenger and Setterwall (1993)

Another enhancement technique is the miniaturization of the coolant flow path. It has already shown promising improvements in heat exchanger technology. Very high heat transfer coefficients can be achieved for microchannels, even in the laminar flow regime. In addition, the surface-to-volume ratio increases with the miniaturization of coolant sections. Garimella (2000) proposed the application of small-diameter coolant tubes in the falling film absorber. The experiments conducted by his group also confirmed that a very high absorption heat duty (16 kW) could be accomplished in a compact absorber of a size 0.178 m × 0.178 m × 0.508 m (Meacham and Garimella, 2002).

Recently, Islam et al. (2003b) proposed a unique concept of periodically inverting the falling film while the liquid solution flows over the cooling surface. The liquid surface that was previously in contact with the cooled surface is directly exposed to the vapor by inverting the film. This design not only increases the mass flux, but also induces mixing due to shear forces. However, the effective liquid-coolant surface area was drastically reduced.

Flow behavior has a significant impact on the surface wetting, and heat and mass transfer characteristics of the falling film absorber. Hu and Jacobi (1996a) have thoroughly investigated different falling-film modes on a horizontal tube bundle. As shown in Figure 2-7, the flow modes were characterized as droplet, droplet-jet, in-line jet, staggered jet, jet-sheet, and sheet modes. They also proposed a flow mode transition map on the basis of Reynolds and modified Galileo number. In their companion paper, Hu and Jacobi (1996b) presented the average heat transfer correlation for the sensible heating of the sheet, jet and droplet falling film modes. However, the experiments were carried out

in a quiescent environment, and the effect of tube bundle depth was also neglected. Later, Wei and Jacobi (2002) studied the effect of tube spacing, tube diameter and tube bundle depth in the presence of airflow. The imposed gas flow destabilized the sheet and jet flow modes, and consequently, the hysteretic effect from the flow mode transitions was eliminated. In addition, the deeper tube bundle also tends to destabilize the flow patterns. It should be noted that experiments conducted by Jacobi and coworkers did not consider the absorption process. Other studies on the transition of a falling film mode, droplet spacing, and heat transfer from a horizontal tube are reported by Mitrovic (1986), Roques et al. (2002), Tang et al. (1991), and Hu and Jacobi (1998).

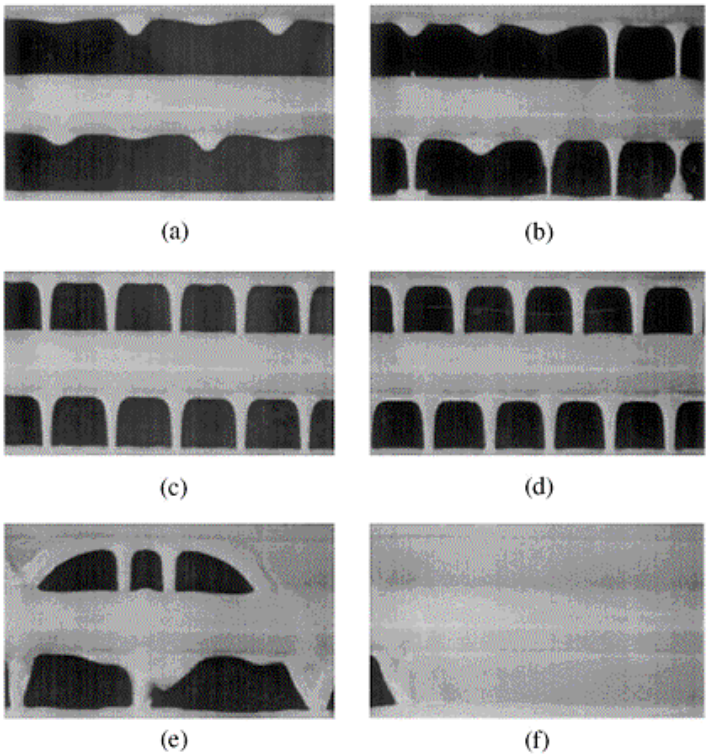

Figure 2-7. Different falling-film modes on horizontal tube bundles, from Hu and Jacobi (1996a). The modes are classified as: (a) Droplet mode, (b) Droplet-jet mode, (c) In-line jet mode, (d) Staggered jet mode, (e) Jet-sheet mode, and (f) Sheet mode

Gas flow also induces shear stresses at the liquid-vapor interface. It is well established that the interfacial shear across the gas/liquid interface enhances the fluid

mixing and improves the mass transfer rates. However, excessive increase in the vapor flow rates can cause liquid bridging between the adjacent falling film paths. The occurrence of flooding relies heavily on the flow velocities of the vapor and liquid phases. The flooding phenomenon critically affects the performance of falling film absorbers. A large amount of pressure drop for the vapor regime can be experienced. Also, the inherent advantage of falling film to achieve a large heat transfer rate with less amount of liquid is also diminished. Numerous studies on flooding phenomenon in the vertical tube channels have been conducted. The Wallis and Kutateladze correlations are widely used to predict the onset of flooding in the vertical tubes (Wallis, 1970a & 1970b; Kutateladze, 1972).

Bubble Absorber

In a bubble absorber, the refrigerant bubbles through the weak solution while flowing co/counter current to the liquid flow direction. The bubble mode provides a very large liquid-vapor interfacial area. It also achieves very good liquid-vapor mixing. Its simple design leads to a decrease in the capital and operating costs of the absorber. A typical schematic of a bubble absorber is depicted in Figure 2-8. The common wettability problem faced by falling film absorption mode is not present in the bubble mode. Therefore, the bubble absorber does not require a liquid distributor but does require a vapor distributor. The vapor distributor is typically a set of orifices that produce very small bubbles. The downside of this type of absorbers is the large pressure drop in both the vapor and liquid phases. Unfavorable pressure gradient in the vapor phase due to the orifice and hydrostatic pressure of the solution column can adversely affect the vapor absorption. Accordingly, it puts restriction on the height of the bubble absorber. Also the bulk-flow of liquid leads to a smaller coolant-solution heat transfer area as compared to

the falling film absorption. A very small amount of fluid can wet a very large surface area by the falling film mechanism.

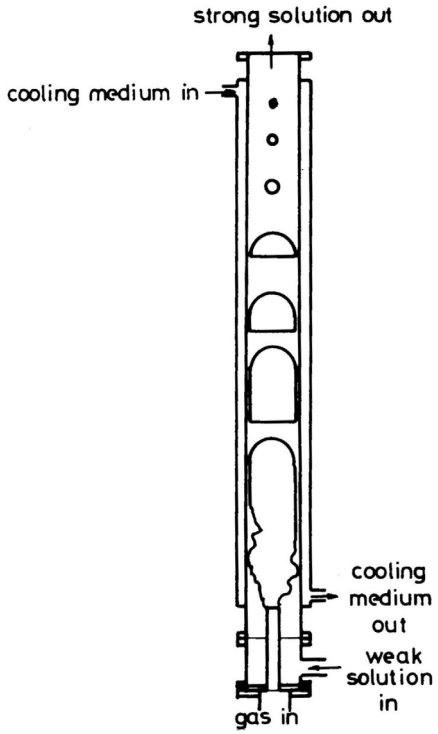

Figure 2-8. Typical schematic of a bubble absorber, from Infante Ferreira et al. (1984)

The early attempts to investigate compact bubble absorbers were made by Keizer (Sujatha et al., 1999), and Infante Ferreira et al. (1984). Infante Ferreira and coworkers developed a differential model while considering simultaneous heat and mass transfer processes in vertical tubular columns for the ammonia-water absorption system. In addition, experiments were conducted with adiabatic and non-adiabatic wall conditions. A major fraction of vapor absorption was found in the slug flow regime. Finally, they concluded that the performance of a bubble absorber critically depends on its geometry, and consequently, proposed a design correlation for the absorber height. Keizer (Sujatha et al., 1999) experimentally showed that the bubble absorbers could be two times smaller than the falling film absorbers. In addition, they found that the bubble absorber operates

closer to the saturation conditions, and the heat transfer coefficient can be twice that encountered in a falling film absorber. Herbine and Perez-Blanco (1995) presented a model to analyze the absorption process in a co-current bubble absorber for NH_3-H_2O working pair. They estimated the water mass flux transferred across the liquid-vapor interface by relating it to the ammonia mass flux and the degree of saturation of the vapor phase. They did not provide an explanation of this uncommon method of estimating the water mass flux. A common practice is to find the water mass flux by using equilibrium relations for the liquid-vapor interface.

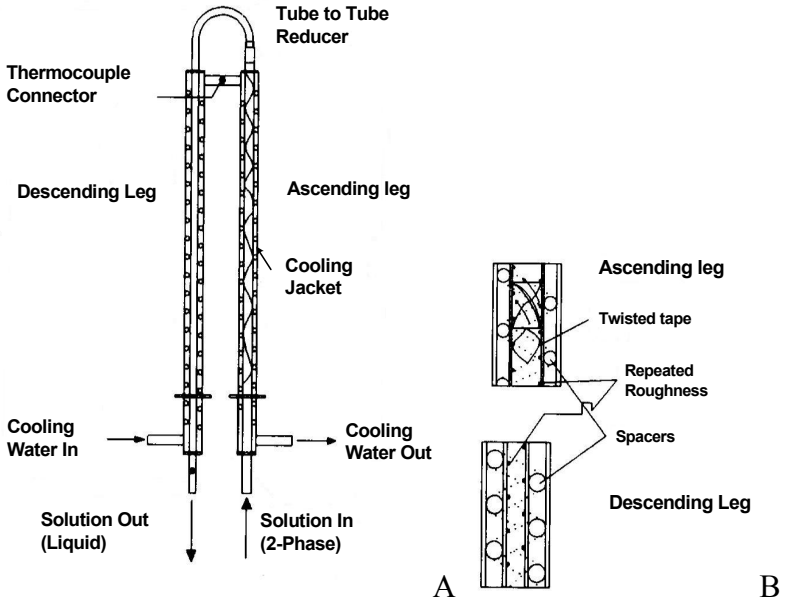

Figure 2-9. Schematic of bubble absorber design studied by Merrill et al. (1995): (A) Bubble absorber schematic, and (B) Bubble absorber enhancements

Merrill et al. (1995) analyzed the performance of a compact bubble absorber for a NH_3-H_2O generator-absorber heat exchange (GAX) cycle. Various heat and mass transfer enhancement techniques (repeated roughness, spiral flutes, and flow spacer) were employed to improve the absorber performance over a baseline case. They fabricated and tested three different bubble absorbers with the above-mentioned augmentation

techniques. As shown in Figure 2-9, their design consists of an inverted U-tube with a coolant jacket. It traps the bubble, and thus increases the residence time for the liquid-vapor interaction. The performance of the absorbers was reported in terms of GAX load. The absorber with internal repeated roughness and external flow spacers was found to be superior, and GAX load was increased by 38%. Helbing et al. (2000) experimentally investigated non-adiabatic falling film and bubble absorption modes for the ammonia-water system. They compared the two absorption modes with constructively different configurations: falling film in a vertical tube and bubble flow in a rectangular plate channel. For the design considered, they found significantly higher liquid heat transfer coefficients for the bubble mode over the falling film mode. The liquid heat transfer coefficient for the falling film mode was in the range of 3000-4000 W/m^2K, whereas its value was from 6000 to 7000 W/m^2K for the bubble mode. However, a large exergy loss was reported for the bubble absorber.

The bubble dynamics play an important role in the bubble absorption mode. The key parameters affecting the bubble behavior are surface tension, orifice diameter, orifice spacing, liquid concentration, vapor flow rate, and co/counter current flow. Numerous studies have been conducted to investigate their effect on the absorption process. Most of the experimental studies have focused on the transient visualization of the bubble behavior from formation to collapse.

The initial diameter of bubbles has attracted several people to investigate and propose a correlation for it. The most commonly used bubble diameter correlation is by Akita and Yoshida (1974). They visualized bubble diameters for different gas-liquid pairs, and proposed a correlation as a function of the orifice diameter, and gas velocity.

They also reported the bubble size to be independent of the surface tension, liquid viscosity, and densities of liquid and vapor. Later, Kumar (1976) and Bhavaraju (1978) also reported a correlation for bubble size. The general trend from the various correlations showed that the bubble diameter increases with increase in the orifice diameter. Another effort was made to numerically analyze the bubble behavior while it flows through the subcooled liquid (Merrill and Perez-Blanco, 1997). They employed a finite difference scheme, and the resulting bubble heat and mass transfer parameters were compared to the existing semi-empirical correlations. Recently, Kang et al. (2002b) visualized the bubble formation for the ammonia-water pair. They found that the residence time of a bubble increases with the increase in initial bubble diameter and liquid concentration. The correlation for bubble diameter as proposed by them was a function of inertial force, viscous force, surface tension, buoyancy, absorption potential, orifice diameter, and inlet vapor flow rate. The shape of the departing bubble was found to be solely dependent on the surface tension and inertial forces: spherical shape for surface tension dominant flow conditions, whereas hemispherical for the inertial force dominant conditions. Terasaka et al. (2002) studied the mass transfer mechanism while bubbling ammonia-nitrogen mixture into a stagnant pool of water. A non-spherical bubble model was also developed, and the results from simulation were compared with the experimental results. They found liquid phase resistance to be dominant for the entire bubble formation process. The major portion of ammonia (about 80-90%) was absorbed during the bubble formation. They also reported a decrease in bubble diameter with the increase in ammonia composition and decrease in gas flow rate. Kang et al. (2002c) analyzed the effect of parameters such as orifice diameter, vapor velocity, and liquid

concentration on the performance of ammonia-water bubble absorber, and later, formulated a mass transfer correlation on the basis of their experimental study.

Packed Bed Absorber

The packed bed columns are extensively used in petrochemical processes. In refrigeration systems, they have found applications in rectification and dehumidification applications. A typical schematic of a packed bed column is shown in Figure 2-10. The column is filled with packings of inert/catalytic material. The liquid, distributed over the packing, flows down the column with continuous subdivision and mixing of the fluid streams. The design allows uniform distribution of the solution, and thus provides a very large contact area between the liquid and vapor phases. However, the packed bed column does not have an arrangement to remove the heat of absorption, and the absorption process is due solely to the subcooled nature of the weak solution. The combined contribution of absorption heat and mass transfer eventually makes the solution saturated.

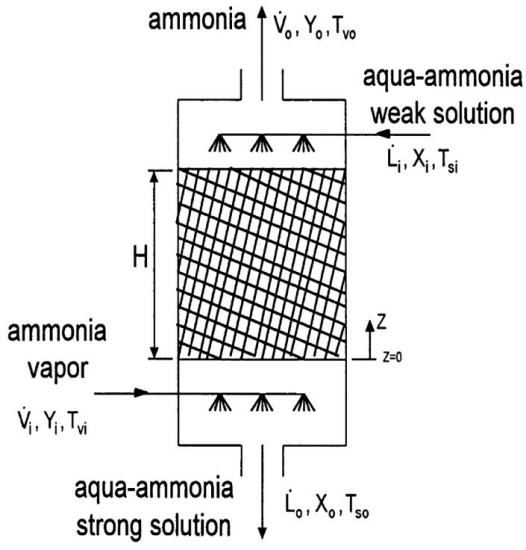

Figure 2-10. Packed bed absorber, from Selim and Elsayed (1999a)

Selim and Elsayed (1999a & 1999b) did numerical investigation of a packed bed absorber for an ammonia-water absorption system. They reported that high absorption

rate is achievable by multistage absorption while cooling the solution between the absorption stages. Their proposed two-stage packed bed absorber system is shown in Figure 2-11. Although multistage packed bed column will work, it will further increase the cost, size and complexity of the system. A better way is to simultaneously accomplish the mass transfer and heat rejection processes.

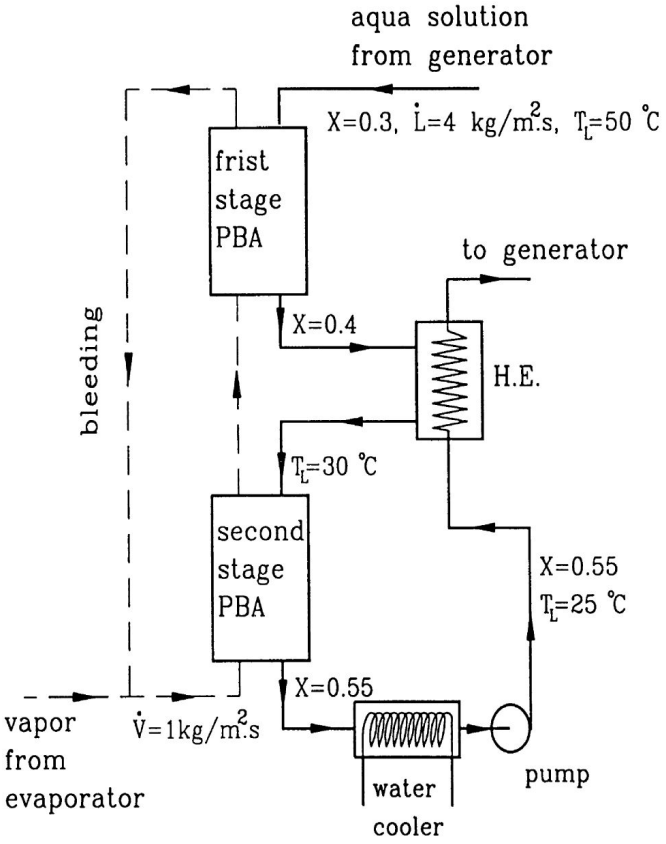

Figure 2-11. Schematic of a two-stage packed bed absorber proposed by Selim and Elsayed (1999b)

Rotating Disc Absorber

The concept relies on the application of centrifugal force to make very thin liquid film. As shown in Figure 2-12, a typical system consists of two concentric cylinders. The weak solution is injected in the inner cylinder while the cylinder rotates about its own axis. The centrifugal force forms a uniform thin film of solution on the periphery of the inner cylinder. It increases the surface contact area and also promotes turbulence and

uniform mixing of the liquid film. Refrigerant entering the rotary cylinder is eventually absorbed in the liquid film. The heat of absorption is rejected to the coolant flowing in the annulus of concentric cylinders. Pathanjali and Rahman (1996) developed a numerical model for the absorption in a rotary absorber. They found that the rotational speed and absorbent flow rate strongly effect the absorption process. Kang et al. (1995) have also analyzed a rotary absorber for LiBr-H_2O absorption system. Though high heat and mass transfer coefficients can be achieved by this concept, the arrangement needs energy to rotate the cylinders, limiting the design to small capacity systems.

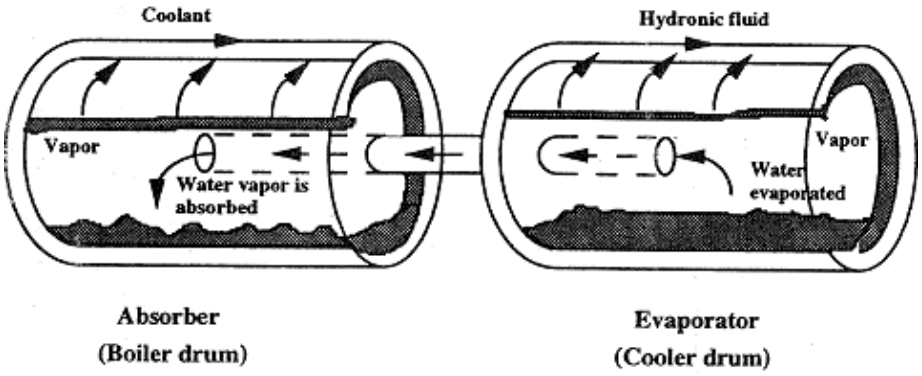

Figure 2-12. Rotary drum absorber, from Kang et al. (1995)

Jet Ejector Absorber

Stirring has been traditionally used to achieve homogeneity of the reactant mixture. One way to create turbulence in the mixture is by means of nozzles. High pressure of the weak solution can be utilized to impart momentum and, hence, promote uniform mixing of the liquid-vapor mixture. For this purpose, a jet ejector as shown in Figure 2-13 can be incorporated at the inlet port of the absorber. The jet ejector consists of a nozzle and diffuser, and consequently, does not contain moving parts. The weak solution at high pressure passes through the nozzle, and its potential energy is converted into kinetic energy. The vapor phase to be absorbed mixes with the weak solution at the inlet of the

diffuser. With the increased kinetic energy of the weak solution, a uniform dispersion of liquid and vapor phases can be achieved. The diffuser is used to partially recover the pressure by reconverting kinetic energy into potential energy. Daltrophe et al. (1993) developed a numerical model to analyze the use of jet ejectors in an absorption system. They reported that almost 40% of the absorption process could be achieved in the jet-ejector arrangement. The feasibility of the concept has not been duly analyzed. The author feels that the diffuser with appropriate cooling arrangements can itself be utilized as an absorber.

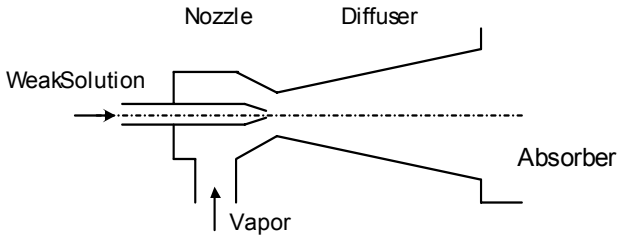

Figure 2-13. Jet ejector, from Daltrophe et al. (1993)

Solution Heat Recovery Absorber

It is beneficial to utilize the heat content of the weak solution leaving the generator. As shown in Figure 2-14, the heat recovery is accomplished by the use of a solution heat exchanger (SHX) between the weak and strong solutions. Thus, the weak solution entering the absorber will be cooled to a lower temperature. It leads to a reduction in the cooling load of the absorber and, consequently, reduces the absorber size. The decrease in temperature of the weak solution also increases its driving potential to absorb the refrigerant. Furthermore, the strong solution is preheated before it enters the boiler. In this way, the addition of a solution heat exchanger not only reduces the cooling requirement of the absorber but also reduces the heat load of the boiler.

Another means to further utilize the low heat content of the strong solution leaving the absorber is to use a solution-cooled absorber. As the name suggests, strong solution is used as a cooling medium to extract the absorption heat produced in the absorber. The strong solution is first pumped to the high pressure which subcools the solution and eliminates any chance of evaporation. As shown in Figure 2-15, the absorber can be divided into two parts; the first is cooled by the strong solution, whereas the second is externally cooled.

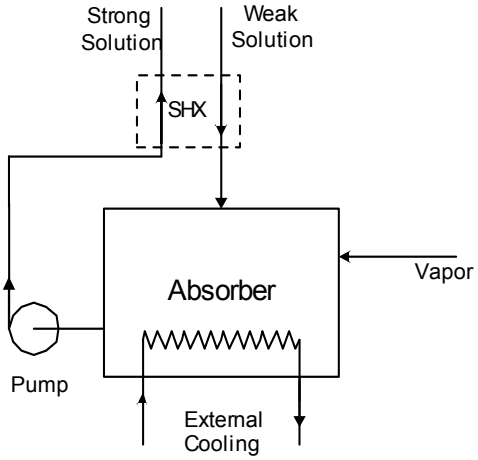

Figure 2-14. Absorber with a solution heat exchanger (SHX)

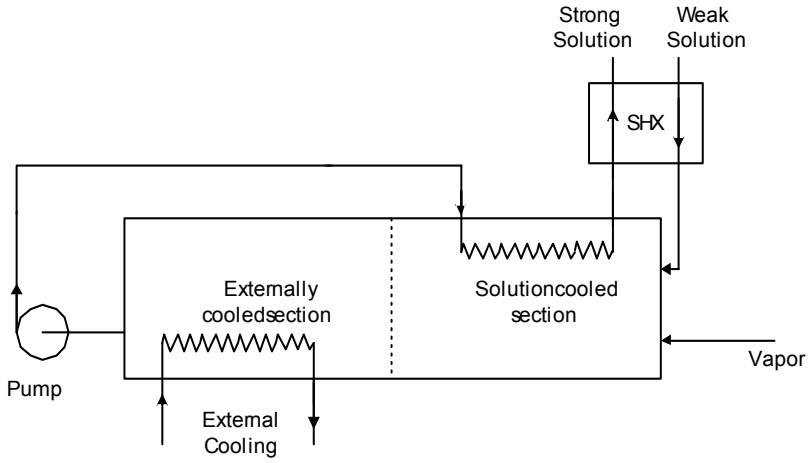

Figure 2-15. Solution cooled absorber

If the increased capital and pumping cost due to the implementation of a solution heat exchanger/solution cooled absorber are taken into account, this approach is only

viable in situations where a large temperature difference between the weak and strong solutions is possible. Also, specific heat of the strong solution plays an important role in deciding its feasibility. For instance, the solution heat exchanger is typically less effective in LiBr-water absorption systems (Herold et al., 1996).

Absorbers can also be characterized on the basis of the cooling medium used:

1. Air-cooled Absorber
2. Water-cooled Absorber
3. Solution-cooled Absorber
4. Evaporative Absorber

Air-cooled Absorber

Air is used to remove heat from the air-cooled absorber by natural or forced draft. Fins are provided to improve the air-side heat transfer rate. Due to their large size, they are normally used in small capacity applications. Generally, low temperature gradient between the air and solution, and low heat transfer coefficient lead to an increase in the absorber size. Furthermore, high head pressure, excessive power consumption and noise are the other sources of concern.

Water-cooled Absorber

Water is the most popular option among the numerous cooling mediums considered. Very high heat transfer rates are possible because of the high specific heat and thermal conductivity of water, and, consequently, the absorber size can be drastically reduced. However, a drawback is the need of a continuous low temperature water source. Many investigators have proposed the use of underground/river water. The cooled underground/river water is fed to the absorber where it removes the heat from the absorber and then the heated water is dumped back into the water body. But many environmentally conscious nations have enacted laws against the usage of such water in

heat exchangers. Furthermore, their usage nullifies the environment friendly advantage of the absorption systems. Therefore, the common practice is to use cooling towers in conjunction with water-cooled absorbers. The heated water from the absorber is cooled in the cooling tower and then re-circulated through the absorber. Various water-cooled absorbers have already been described in detail in the previous sections.

Solution-cooled Absorber

The strong solution exiting the absorber is itself used to extract the heat of absorption. The configuration eliminates the need of an external cooling medium. In addition, it preheats the solution before it enters the boiler. The solution-cooled absorber has already been described in the section on solution heat recovery.

Evaporative Absorber

An evaporative absorber utilizes the latent heat of cooling water to reject the absorption heat. Figure 2-16 shows a representative schematic of such an absorber. As evident, it combines the objectives of having a water-cooled absorber and a cooling tower. The cooling water flows down in the form of falling film, whereas air flows in the counter-current direction of the water. The absorption heat is first rejected to the water, and then water rejects the heat to air in the form of latent heat. The evaporation process increases the humidity of air and the humidified air exits from the top of the absorber. The remaining water re-circulates in the evaporative absorber, and the addition of more water makes up the loss. In some instances, the system might need a large amount of refrigerant. This is due to the fact that the refrigerant-absorbent mixture itself is connected to the spray chamber and, thus requires longer piping connections. Pachhapur and Rane (1998) demonstrated the idea to work with ammonia-water absorption systems. They reported that an overall heat transfer coefficient in the range of 2-4 kW/m^2K was

achieved for a co-current flow of liquid and vapor phases. Though evaporative absorbers have not found much use, they are promising candidates in dry climate regions.

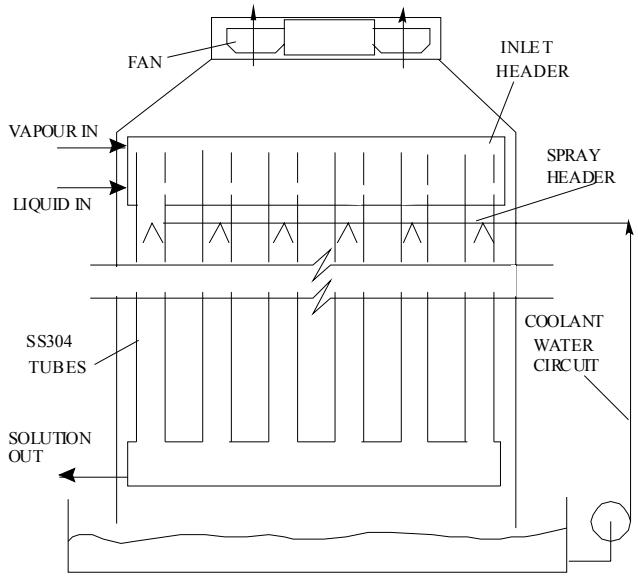

Figure 2-16. Evaporative absorber, from Pachhapur and Rane (1998)

Effect of Non-condensable Gases

Non-absorbable gases are often produced by corrosion and passivation processes inside the absorption system. Leakage of air can add to the problem. The presence of such gases has an adverse effect on the absorption process. The diffusion of absorbate towards the liquid regime sweeps non-absorbable gases near the liquid-vapor interface. Due to the impermeability of the liquid phase towards the non-absorbable gases, such unwanted gases tend to accumulate near the liquid-vapor interface. This creates an additional resistance to mass transfer resulting in a reduction of absorption flux. The influence of non-absorbable gases on the performance of the absorber has been extensively investigated both theoretically and experimentally (Ameel et al., 1997; Medrano et al., 2003; Yank and Wood, 1993; Cosenza and Vliet, 1990). These researchers have shown that the effect of non-absorbable gases is significant and

detrimental to mass absorption. Yang and Wood (1993) did experiments to investigate their influence on a LiBr-H2O system. They found that the absorption rate was reduced by 75% when the air concentration was increased from 5 to 30%. The experimental work of Cosenza and Vliet (1990) showed that the air concentration of 0.1% reduced the heat and mass transfer rates by about 2%. Recently, Medrano et al. (2003) analytically predicted the effect of non-absorbable gases on a LiBr-H2O absorber. They reported that for cooling water at 35 ^{o}C, an increase in air concentration from 0 to 20% results in an absorption reduction of 61%. A remedy is to remove the deleterious gases by periodic purging and prevent their further generation/entrance.

Effect of Surfactants

Surface tension has a significant effect on the fluid dynamics. It not only increases the surface wetting area but also induces interfacial turbulence. In the case of a bubble absorber, a decrease in a surface tension favors the formation of smaller diameter bubbles. Investigations have shown that the presence of surfactants enhances the absorber performance. A small amount of a surfactant can considerably reduce the surface tension of fluids. Much research has been devoted to quantifying and understanding the effect of surfactants. It has been accepted that the heat and mass transfer enhancement due to the reduction of surface tension is largely attributed to interfacial turbulence. The effect of interfacial turbulence is often termed as the Marangoni convection. The presence of surfactants causes local variation in the surface tension, which in turn induces turbulence at the liquid-vapor interface. Though several models, namely, “salting-out” and Kashiwagi models, have been developed to explain the mechanism of Marangoni convection, they contradict each other and a satisfactory description of the concept is still needed (Kashiwagi, 1988; Hozawa et al., 1991; Kim et al., 1996; Kang et al., 1999;

Kulankara et al., 1999). Various additives are known to promote interfacial turbulence in LiBr-H_2O absorbers, the most recognized among them being n-Octanol. Kashiwagi (1988) found that heat transfer was enhanced by four times by the introduction of n-Octanol in a LiBr- H_2O mixture. Similarly, Beutler et al. (1996) investigated the effect of different surfactants on LiBr-H_2O absorbers. They reported a significant increase in the value of heat transfer coefficients by adding n-Octanol and 2-Ethyl-1-Hexanol, an isomer of n-Octanol. Ammonia-water systems are less focused in this direction, partly due to the unpopularity of the system, and partly due to the unavailability of chemically stable additives at higher operating temperatures. Kim et al. (1996) also experimentally investigated the effect of 2-Ethyl-1-Hexanol on vapor absorption in an aqueous LiBr-H_2O solution flowing over a vertical tube. They varied the concentration of the surfactant, and found 20-30 ppm to be the optimal concentration to induce maximum enhancement in mass transfer rates. No further improvement was observed for higher concentration of the surfactant. Möller and Knoche (1996) experimentally analyzed the effect of five surfactants on an ammonia-water absorber: two anionic, two non-ionic surfactants and n-Octanol. They reported that the enhancement in mass transfer is possible with n-Octanol, and the ionic and non-ionic surfactants have a negligible effect on mass absorption.

CHAPTER 3
THEORETICAL ANALYSIS

Absorbers are currently designed on the basis of empirical data. However, numerical analysis is essential for a thorough understanding and development of an efficient design. Absorbers for cycles with nonvolatile absorbents such as LiBr-H_2O cycle have been studied more extensively as compared to volatile absorbents. In the case of ammonia-water pair, the refrigerant and absorbent are present in both liquid and vapor phases making the transport phenomena more complex to analyze.

Background

Falling film absorbers have been extensively studied over the last few decades. Several investigators have developed computational models to predict the performance of these absorbers. There is a disagreement among researchers regarding the existence of dominant resistance to mass transfer in either liquid or vapor phase (Killion and Garimella, 2001). The mass transfer resistance is quite often neglected in either phase to simplify the numerical models (Ruhemann, 1947; Briggs, 1971; Kang et al., 1996a & 1996b; Colburn and Drew, 1937; Garimella, 2000; Kang et al., 1993; Price and Bell, 1974). Mass transfer resistances in both liquid and vapor phases were considered by Gommed et al. (1999, 2001), Kim (1998), Perez-Blanco (1988), Potnis et al. (1997) and Kang et al. 1998). The analysis by Gommed et al. (1999, 2001) and Potnis et al. (1997) predicted that the vapor phase mass transfer resistance is dominant, whereas, Kim (1998) and Perez-Blanco (1988) concluded that the liquid phase mass transfer resistance controls the overall absorption process. Models developed by Gommed et al. (1999, 2001) and

Kim (1998) were self-reliant and did not require empirical correlations for heat and mass transfer coefficients. Gommed et al. (1999, 2001) studied falling film absorption on vertical tubes for a co-current vapor flow system. They used a finite volume technique to formulate their model. Kim (1998) developed a model based on an integral formulation of momentum, heat and mass transfer equations to compare co-current and counter-current absorbers. Velocity, temperature and concentration profiles were assumed to be parabolic. The flow was assumed to be laminar and fully developed. Further, the coolant wall was assumed to be either adiabatic or isothermal. Perez-Blanco (1988), on the other hand, simulated their design model using empirical correlations for the heat and mass transfer coefficients. The model considered was for falling film absorption around coiled tubes. They used a finite difference scheme to solve the model. The issue of similar lack of consensus in neglecting the liquid/vapor phase mass transfer resistance is also addressed by Killion and Garimella (2001), in their comprehensive review on the existing numerical models for the falling film absorption mode.

In addition, most of these models were developed and analyzed for co-current vapor flow systems (Gommed et al., 1999 & 2001; Perez-Blanco, 1988). However, the situation is more complicated for counter-current vapor flow systems. Due to the opposite flow direction of the fluids, inlet conditions need to be defined at opposite ends of the absorber. There are very few models of counter-current absorbers. Kang et al. (1993) adapted a model originally developed by Price and Bell (1974) for a vertical-fluted tube absorber. They considered a counter-current system under the assumption that weak solution is well mixed, and consequently, both liquid bulk and liquid-vapor interface are always at thermodynamic equilibrium. Their model neglects the liquid-phase mass

transfer resistance. Garimella (2000) used similar assumptions in his design model for counter-current vapor flow absorption over very small diameter horizontal tubes. In the literature, models for volatile absorbents which consider the mass transfer resistance in both the liquid and vapor phases are mainly limited to co-current systems. The numerical analysis by Kang et al. (1998, 2000a) predicted the required length of the counter-current absorber. Their models considered resistance to mass transfer in both the phases. However, the computational details of the scheme were not provided.

In this work, an attempt is made to avoid the above mentioned controversy by considering the heat and mass resistances in both the liquid and vapor phases. A finite difference model is developed to analyze falling film absorption mode in a counter-flow absorber. It takes into account the liquid and vapor phase mass transfer resistances, and uses empirical correlations to predict the heat and mass transfer coefficients. Empirical correlations for the heat and mass transfer coefficients are useful for simulating wavy-laminar and turbulent flow conditions, the conditions in which numerically calculated coefficients are less reliable.

Mathematical Model

A numerical model is developed to compare the performance of the proposed absorber with the microchannel-based horizontal tube type absorber design. The falling film absorber considered here consists of an array of horizontal coolant tubes over which a weak solution is distributed. The weak solution then flows over the coolant tubes and mesh/fabric under the influence of gravity. The absorbate vapor enters from the bottom of the absorber and flows through the narrow channels formed by an assemblage of coolant tubes. The vapor is absorbed by the weak solution flowing counter-current to it. The heat of absorption thus released is rejected to the coolant that flows through the coolant tubes.

The model considered here is a two-dimensional model that neglects the temperature and concentration variation along the axis of the horizontal tubes. However, the coolant flow is in a cross-counter direction to the solution while the coolant enters at the bottom and leaves at the top of the absorber. The flow of coolant in the individual tubes being cross-flow to the weak solution leads to a variation in coolant temperature along the tubes. In order to improve the model, the coolant temperature in an individual tube is assumed to be equal to the mean of the inlet and outlet temperatures of the tube. The parallel-series arrangement of the coolant tubes is used to decrease the coolant-side pressure loss to acceptable limits. The presence of mesh/fabric in the proposed design is the only difference between the proposed and horizontal tube type falling film absorber designs which are considered for the numerical analysis. Continuity and energy balance equations are applied at each differential control volume of the proposed design, as shown in Figure 3-1. Due to the presence of falling film in between the horizontal tubes, associated heat and mass transfer processes in that region also need to be considered. Hence, the model for the proposed design consists of two types of differential control volumes: the control volume in the cooling region and the control volume in mesh/fabric region. Similarly, the model for the horizontal tube type absorber design only consists of control volumes present in the cooling region.

The following assumptions were made in building the model:

1. The absorption process is assumed to be in steady state.
2. System pressure is constant.
3. Thermodynamic equilibrium exists at the liquid-vapor interface.
4. The heat transfer surface under the conditions is completely wet (i.e., there is no direct heat transfer between the vapor and the coolant surface).

5. Heat losses to the environment are negligible.

6. Adiabatic absorption in droplets is neglected.

7. No flooding occurs between the two adjacent horizontal tubes.

8. Mass transfer due to thermal and pressure difference is negligible (mass transfer occurs only because of the concentration gradient).

9. Effect of non-absorbable gases is ignored.

10. The coolant temperature along the radial coordinates of the tubes is assumed to be constant.

11. Conduction heat transfer between the mesh/fabric and coolant tubes is negligible.

12. The flow of absorbent along the periphery of coolant tubes is unaffected by the presence of mesh/fabric.

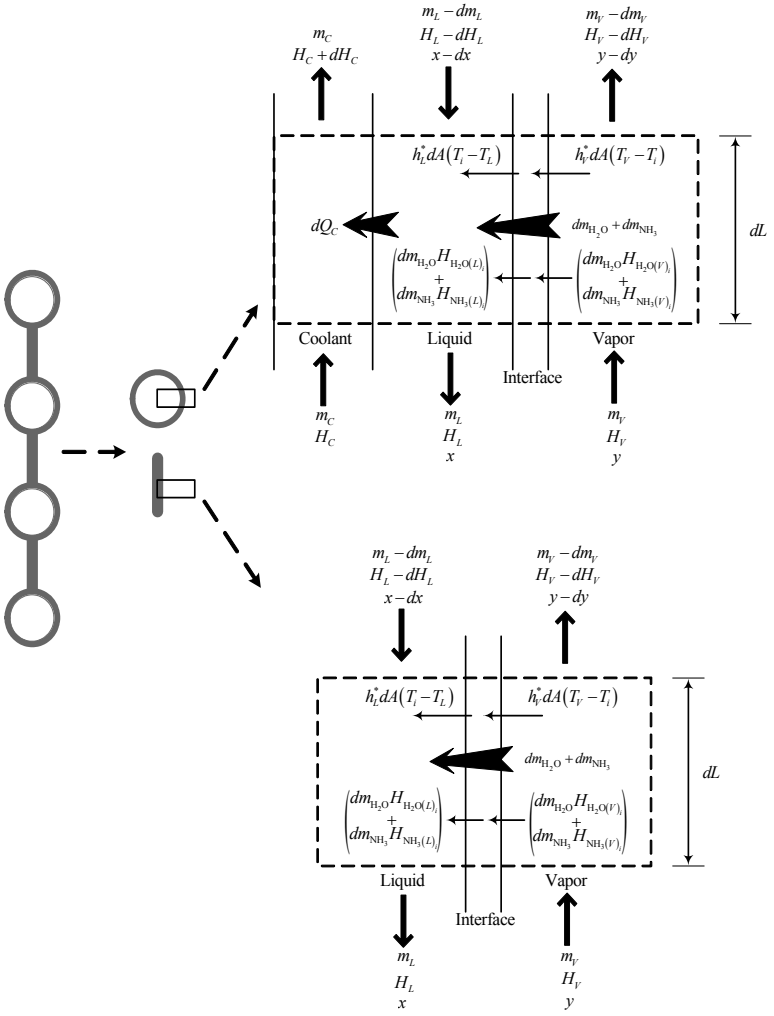

Figure 3-1. Schematic of the differential control volume of the proposed design

The mass transfer between the liquid and vapor phases is due to the combined effect of bulk transport and molecular diffusion of NH_3 and H_2O across the liquid-vapor interface. For steady state, the mass flux of the vapor absorbed by the weak solution is given by (Treybal, 1980)

$$\frac{dm_{NH_3}}{M_{NH_3}} + \frac{dm_{H_2O}}{M_{H_2O}} = dA_i K_V \ln\left(\frac{z - \tilde{y}_i}{z - \tilde{y}}\right) \tag{3-1}$$

$$\frac{dm_{NH_3}}{M_{NH_3}} + \frac{dm_{H_2O}}{M_{H_2O}} = dA_i K_L \ln\left(\frac{z - \tilde{x}}{z - \tilde{x}_i}\right) \tag{3-2}$$

Subscripts *L*, *V*, and *i* denote the liquid, vapor, and liquid-vapor interface, respectively. The positive value of mass flux, namely, dm_{NH3} and dm_{H2O}, signify the mass transfer from vapor to liquid phase. As both ammonia and water are being absorbed/desorbed, the absorption mass flux consists of both constituents. The mole fraction of ammonia in the absorbing/desorbing vapor is defined as *z* and can be expressed by Eq. (3-3). For the working pair, the value of *z* is normally expected to be between zero and one. However, its value can also be just greater but close to one for some design conditions.

$$z = \left(\frac{\dfrac{dm_{NH_3}}{M_{NH_3}}}{\dfrac{dm_{H_2O}}{M_{H_2O}} + \dfrac{dm_{NH_3}}{M_{NH_3}}}\right) \tag{3-3}$$

The similarity between heat and mass transfer processes can be utilized to deduce the analogous heat and mass transfer coefficients (Chilton and Colburn, 1934). The heat and mass transfer analogy is particularly useful when either one of the heat and mass transfer coefficients is difficult to obtain. So, in this case, liquid heat transfer coefficient

h_L and vapor mass transfer coefficient K_V are obtained by the use of the following equation for the liquid and vapor phases separately:

$$\frac{h}{M} = C_P K \left(\frac{\mathrm{Sc}}{\mathrm{Pr}} \right)^{2/3} \tag{3-4}$$

Yih and Chen (1982) developed liquid-side mass transfer correlations for laminar, wavy, and turbulent falling films in a wetted-wall column. The correlations were based on the motion of eddies near the liquid-vapor interface, and the value of the constants were obtained by fitting to their own experimental results and the work of ten other researchers. Their correlations are applicable to fully developed conditions only. Even though the wetted-wall columns formed by wrapping mesh between the coolant tubes is not similar to the wetted-wall columns on which the mass transfer relations were established, the application of correlations in the current geometry is a reasonable approximation. However, it must be noted that the extent of potential error due to this assumption has not been established. The correlation for the laminar flow regime was established in the range of $49 < \mathrm{Re}_{\mathrm{film1}} < 300$ and 8.5 °C < T < 50 °C, and can be expressed as

$$K_L = \left(0.01099\, \mathrm{Re}_{\mathrm{film1}}^{0.3955}\, \mathrm{Sc}_L^{0.5} \right) \left[\frac{D_{aw(L)} \rho_L}{M_L} \left(\frac{g}{\eta_L^2} \right)^{1/3} \right] \tag{3-5}$$

The liquid solution flows alternatively on the mesh and coolant tubes. The convective heat transfer between the vapor and falling film on horizontal tubes $h_{V,\mathrm{tube}}$ is modeled as gas flow over a circular cylinder. The equation is valid for $40 < \mathrm{Re}D < 4000$, and the evaluation of fluid properties is required at a mean boundary layer temperature (Incropera and DeWitt, 2002)

$$h_{V,\text{tube}} = \left(\frac{k_V}{D_O}\right) \times 0.683\,\text{Re}_{D_O}^{0.466}\,\text{Pr}_V^{1/3} \tag{3-6}$$

The convective heat transfer coefficient for the vapor and falling film on the mesh $h_{V,\text{mesh}}$ is based on the flow inside a parallel-plate channel under laminar conditions. The correlation assumes uniform surface temperature, and neglects the edge effect due to the finite width of parallel-plate channels. Though the correlation is not exactly applicable to finite rectangular ducts formed by a screen mesh across the tubes, it can be considered as a reasonable approximation for large aspect ratios. The relation is also restricted to fully developed profiles of velocity and temperature, and is given by (Shah and London, 1978)

$$h_{V,\text{mesh}} = 7.541\left(\frac{k_V}{D_h}\right) \tag{3-7}$$

where the hydraulic diameter D_h is defined as

$$D_h = \frac{4\left(\text{Cross-sectional Area of the Duct}\right)}{\left(\text{Wetted Perimeter}\right)} \tag{3-8}$$

The heat transfer between the liquid and vapor phases occurs due to the combined contribution of convective heat transfer and sensible heat load of the mass transferred across the interface. The ordinary convective heat transfer is due to the temperature gradient between the fluid in motion and the bounding surface. If the convective heat transfer is also accompanied by mass transfer across the bounding surface, an extra amount of heat will transfer due to the heat capacity of the mass being transferred. This sensible heat transfer is primarily due to the temperature gradient between the liquid and vapor phases, and consequently between the liquid, liquid-vapor interface, and vapor regimes. The convective heat transfer coefficient can be modified to account for the

effect of mass transfer. The modified heat transfer coefficient h^* for simultaneous heat and mass transfer is given by (Treybal, 1980)

$$h^* = h\frac{c}{1-e^{-c}} \tag{3-9}$$

where $$c = \frac{\frac{dm_{\mathrm{NH_3}}}{M_{\mathrm{NH_3}}}C_{p,\mathrm{NH_3}} + \frac{dm_{\mathrm{H_2O}}}{M_{\mathrm{H_2O}}}C_{p,\mathrm{H_2O}}}{h} \tag{3-10}$$

The mass and concentration balance between the liquid and vapor phases are given by

$$dm_L = dm_V \tag{3-11}$$

$$m_V y + (m_L - dm_L)(x - dx) = (m_V - dm_V)(y - dy) + m_L x \tag{3-12}$$

The energy balance equation for the control volume of liquid phase will depend on the location of the falling film on the coolant tubes or the screen mesh as indicated below.

Control volume of liquid phase in the coolant region

$$\begin{aligned} m_L H_L + dQ_C = {} & (m_L - dm_L)(H_L - dH_L) + h_L^* dA(T_i - T_L) + dm_{\mathrm{H_2O}} H_{\mathrm{H_2O}(L)_i} \\ & + dm_{\mathrm{NH_3}} H_{\mathrm{NH_3}(L)_i} \end{aligned} \tag{3-13}$$

Control volume of liquid phase in the mesh region

$$\begin{aligned} m_L H_L = {} & (m_L - dm_L)(H_L - dH_L) + h_L^* dA(T_i - T_L) + dm_{\mathrm{H_2O}} H_{\mathrm{H_2O}(L)_i} \\ & + dm_{\mathrm{NH_3}} H_{\mathrm{NH_3}(L)_i} \end{aligned} \tag{3-14}$$

The energy balance equation for the control volume of vapor phase is given by

$$\begin{aligned} m_V H_V = {} & (m_V - dm_V)(H_V - dH_V) + h_V^* dA(T_V - T_i) + dm_{\mathrm{H_2O}} H_{\mathrm{H_2O}(V)_i} \\ & + dm_{\mathrm{NH_3}} H_{\mathrm{NH_3}(V)_i} \end{aligned} \tag{3-15}$$

The liquid-vapor interface is assumed to be at thermodynamic equilibrium. Concentration, temperature and pressure of the binary mixture are coupled to each other

at the saturation state. In particular, only two of these properties are sufficient to determine the thermodynamic state of a binary mixture. The concentration of ammonia in the vapor and liquid at the interface can then be expressed as

$$y_i = f\left(T_i, P\right) \tag{3-16}$$

$$x_i = f\left(T_i, P\right) \tag{3-17}$$

Energy balance at the liquid-vapor interface gives

$$\begin{aligned} h_L^* dA\left(T_i - T_L\right) + dm_{\mathrm{H_2O}} H_{\mathrm{H_2O}(L)_i} + dm_{\mathrm{NH_3}} H_{\mathrm{NH_3}(L)_i} &= h_V^* dA\left(T_V - T_i\right) \\ &\quad + dm_{\mathrm{H_2O}} H_{\mathrm{H_2O}(V)_i} + dm_{\mathrm{NH_3}} H_{\mathrm{NH_3}(V)_i} \end{aligned} \tag{3-18}$$

The heat absorbed by the coolant can be found by an energy balance over the coolant, coolant-liquid interface, and global control volumes

$$dQ_C = U dA_C \left(T_L - T_C\right) \tag{3-19}$$

$$dQ_C = m_C dH_C \tag{3-20}$$

$$dQ_C = \left(m_L - dm_L\right)\left(H_L - dH_L\right) + m_V H_V - m_L H_L - \left(m_V - dm_V\right)\left(H_V - dH_V\right) \tag{3-21}$$

where the overall heat transfer coefficient U combines the various thermal resistances in the path of the heat flow between the weak solution and coolant, and can be expressed as

$$\frac{1}{U} = \frac{1}{h_C} + R_{\mathrm{wall}} + \frac{1}{h_{\mathrm{film}}} \tag{3-22}$$

The coolant-side heat transfer coefficient h_C is based on the developing laminar flow conditions in the coolant tube. The correlation for the local Nusselt number for the uniform surface heat flux is of the form (Churchill and Ozoe, 1973)

$$\frac{\mathrm{Nu}_D + 1}{5.364\left[1+\left(\mathrm{Gz}/55\right)^{10/9}\right]^{3/10}} = \left[1+\left(\frac{\mathrm{Gz}/28.8}{\left[1+\left(\mathrm{Pr}/0.0207\right)^{2/3}\right]^{1/2}\left[1+\left(\mathrm{Gz}/55\right)^{10/9}\right]^{3/5}}\right)^{5/3}\right]^{3/10} \tag{3-23}$$

The mean value of Nusselt number for the coolant tube will be an average of local Nusselt number over the entire length of the tube.

The correlation developed by Wilke (Yih, 1986) is used to calculate the falling film heat transfer coefficient for the laminar flow regime. The Wilke correlation was established for $Re_{\mathrm{film}} < 2460\ \mathrm{Pr}^{-0.646}$

$$h_{\mathrm{film}} = 1.88\left(\frac{k_L}{\beta}\right) \tag{3-24}$$

where the average film thickness β for the laminar flow is given by Nusselt's theory (Yih, 1986)

$$\beta = 0.91\mathrm{Re}_{\mathrm{film}}^{1/3}\left(\frac{\eta_L^2}{g}\right)^{1/3} \tag{3-25}$$

The model requires the thermodynamic and transport properties of ammonia-water mixture. Thermodynamic properties of ammonia-water mixture are based on the empirical correlations given by Ziegler and Trepp (1984). The correlations use Gibbs excess energy method for the mixtures and bubble and dew point temperature correlations for the phase equilibrium. They provided separate equations of state for the liquid and vapor phases of the pure components; while in the case of mixtures the deviation from ideal solution behavior was accounted by the Gibbs excess energy method. Developed correlations are valid in the 0.2-110 bar pressure range and 230-600

K temperature range. The transport properties, namely viscosity, thermal conductivity and molecular diffusivity, are required to calculate the heat and mass transfer coefficients. A literature survey was conducted for the transport property correlations valid for our design conditions. The correlations of thermodynamic and transport properties of the mixtures are given in Appendices A and B, respectively.

Numerical Technique

Finite difference method is used to solve the system of nonlinear ordinary differential equations. The model is subjected to the given inlet conditions of the liquid, vapor and coolant flow regimes. The absorber is divided into differential segments of an incremental length *dL*. The system considered here has already been explained in detail. In brief, coolant and vapor are introduced at the bottom and flow upward while the liquid flows down from the top, and hence the inlet liquid and vapor conditions are known at opposite ends. The conventional and straightforward way to simulate such finite difference model is to first guess either vapor and coolant conditions at the top section or liquid conditions at the bottom section of the absorber. Then iteratively perform the simulation from the location of assumption to the other end until known inlet conditions are achieved. However, there are three unknowns for each vapor/liquid conditions: temperature, mass flow rate and concentration, and, thus the iteration has to be done by assuming at least three unknowns.

A simpler way is to calculate the coolant, liquid and vapor conditions for successive states in their respective flow directions, which is described in the subsequent paragraphs. Each incremental segment was further divided into liquid, vapor, and coolant differential segments. The entire liquid region has to be solved first by marching top to bottom while the vapor and coolant segments are computed later from bottom to top.

Figure 3-2 give a general idea of the numerical technique for a horizontal tube type absorber. In Figure 3-2 Elements 1-4 represent a coolant tube, whereas Elements 5-7 represent a mesh in between the horizontal tubes.

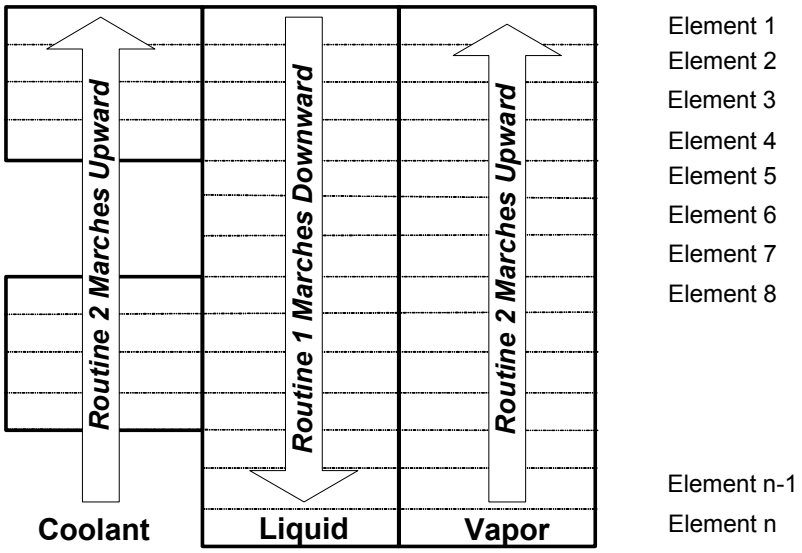

Figure 3-2. Schematic of the numerical technique for the horizontal tube type absorber

Before the complete explanation of the algorithm, the calculation procedure for a single liquid, vapor or coolant differential segment needs to be understood. The liquid differential segment at the top of the absorber is chosen to understand this approach. The conditions at this liquid segment are known, as they are the inlet conditions of the weak solution. However, the vapor and coolant conditions are not known at this segment, and, thus the vapor and coolant conditions are assumed to be equal to the known inlet conditions. The liquid differential segment can now be solved to determine the conditions of the next downstream differential segment. Similarly, by assuming the vapor and coolant conditions, all the liquid differential segments can be solved while marching downward. Once the liquid conditions are known for the entire absorber, the vapor and coolant control volumes can be solved by marching in their flow direction. The obtained liquid, vapor and coolant conditions are not the actual conditions. The actual coolant,

liquid and vapor conditions are obtained by iteratively solving the liquid, vapor and coolant control volumes until their values converge to a stable solution.

The model is primarily based on two routines. Routine 1 solves the liquid differential segments by marching in the downward direction, whereas Routine 2 marches upward to solve the vapor and coolant differential segments. The model starts by first simulating Routine 1 and later Routine 2. Due to the interlinking of the liquid, vapor and coolant control volumes, the vapor and coolant conditions are needed to solve Routine 1. An initial guess for the conditions of all the vapor and coolant differential segments is taken to be equal to the inlet vapor and coolant conditions. With the above assumption, the liquid regime can be simulated with the given inlet liquid conditions at the top section, and assumed vapor and coolant conditions across the entire absorber. The calculations for the liquid region are made in incremental steps while marching downward. At each incremental step in the routine 1, the values at each liquid differential segment are computed with respect to the conditions at the respective vapor and coolant differential segments. These vapor and coolant conditions are kept constant throughout the routine 1, before the second routine changes them. In other words, the mass and energy balance equations are solved only for the liquid control volume.

Routine 2 uses the values for liquid differential segments obtained from the first routine to calculate the new refined vapor and coolant conditions. The second routine marches upward in incremental steps to calculate the state of vapor and coolant at each segment. The second routine calculates the vapor and coolant conditions prevailing in the absorber for a given set of fixed liquid conditions across the absorber.

The model iteratively loops over these two routines to achieve better approximations of an unknown solution. This is repeated until all unknown variables converge to stable values. The final coolant, liquid and vapor conditions at each differential segment satisfy the given system of simultaneous nonlinear equations. This is repeated until all unknown variables converge to stable values. The algorithm developed to model the proposed design is also utilized to model the conventional horizontal tube type absorber (i.e. an absorber without mesh) by assuming the length of mesh to be equal to zero. The solution method can be summarized as follows:

1. Assume a length of the absorber and divide the absorber, i.e., coolant tubes and screen mesh, into differential segments of incremental length dL.
2. Equate the vapor and coolant conditions of all incremental steps to the inlet vapor and coolant conditions.
3. Solve the liquid control volume for each segment by marching downward. The values of vapor and coolant conditions at each node are obtained by step 2 in case of first iteration or by Routine 2 in case of later subsequent iterations. The following steps describe Routine 1:
    a. Guess the liquid-vapor interface temperature T_i.
    b. Calculate the liquid- and vapor-side mass fractions of the ammonia, x_i and y_i, at the interface using Eqs. (3-16) and (3-17).
    c. Guess z.
    d. Calculate a new value of z by using Eqs. (3-1) and (3-2).
    e. If the difference between the old and new values of z is less than the assumed convergence criterion, go to step f, otherwise go to step c.
    f. Calculate the mass flux of ammonia and water using Eqs. (3-1) - (3-3).
    g. Calculate a new value of T_i from an energy balance of interface control volume using Eq. (3-18).
    h. If the difference between the old and new values of T_i is less than the assumed convergence criterion, go to step i, otherwise go to step a.

i. Calculate the mass flow rate and concentration of the liquid phase for the next segment using Eqs. (3-11) and (3-12).

j. Calculate the enthalpy of the liquid phase for the next segment from an energy balance of liquid control volume using Eq. (3-13) or (3-14). The use of Eq. (3-13) or (3-14) depends on the location of the falling film in the coolant or mesh region.

4. Solve the vapor and coolant differential segments by marching upward. The values of the liquid conditions at each node are obtained by Routine 1. The following steps describe Routine 2:

a. If the differential segment contains the coolant tube, follow the following steps:

i. Guess the average coolant temperature T_C of the coolant tube.

ii. Guess the liquid-vapor interface temperature T_i.

iii. Calculate the liquid- and vapor-side mass fractions of the ammonia, x_i and y_i, at the interface using Eqs. (3-16) and (3-17).

iv. Guess z.

v. Calculate a new value of z by using Eqs. (3-1) and (3-2).

vi. If the difference between the old and new values of z is less than the assumed convergence criterion, go to step vii, otherwise go to step iv.

vii. Calculate the mass flux of ammonia and water using Eqs. (3-1) - (3-3).

viii. Calculate a new value of T_i from the energy balance of the interface control volume using Eq. (3-18).

ix. If the difference between the old and new values of T_i is less than the assumed convergence criterion, go to step x, otherwise go to step ii.

x. Calculate the mass flow rate and concentration of the vapor phase for the next segment using Eqs. (3-11) and (3-12).

xi. Calculate the heat absorbed by the coolant in the differential coolant segment dQ_C using Eq. (3-19).

xii. Calculate the enthalpy of the vapor phase for the next segment from an energy balance for the vapor control volume using Eq. (3-15).

xiii. If the next differential element contains mesh, go to step xiv, otherwise go to step ii to calculate the conditions of the next differential element.

xiv. Calculate the total amount of heat absorbed by the coolant tube by adding all dQ_C of the differential segments pertaining to that coolant tube.

xv. Calculate the outlet coolant temperature of the tube using Eq. (3-20).

xvi. Calculate a new value of T_C by taking the average of the inlet and outlet coolant temperatures of the tube.

xvii. If the difference between the old and new values of T_C is less than the assumed convergence criterion, go to step xviii, otherwise go to step i.

xviii. If the next coolant tube is not in parallel connection with the current tube, equate the inlet coolant temperature of the next parallel tube assembly to the mean of the outlet coolant temperatures of the current parallel tube assembly.

b. If the differential segment contain the mesh, follow the following steps:

i. Guess the liquid-vapor interface temperature T_i.

ii. Calculate the liquid- and vapor-side mass fractions of the ammonia, x_i and y_i, at the interface using Eqs. (3-16) and (3-17).

iii. Guess z.

iv. Calculate a new value of z by using Eqs. (3-1) and (3-2).

v. If the difference between the old and new values of z is less than the assumed convergence criterion, go to step vi, otherwise go to step iii.

vi. Calculate the mass flux of the ammonia and water using Eqs. (3-1) - (3-3).

vii. Calculate a new value of T_i from an energy balance of the interface control volume using Eq. (3-18).

viii. If the difference between the old and new values of T_i is less than the assumed convergence criterion, go to step ix, otherwise go to step i.

ix. Calculate the mass flow rate and concentration of the vapor phase for the next segment using Eqs. (3-11) and (3-12).

x. Calculate the enthalpy of the vapor phase for the next segment of the incremental steps from an energy balance of the vapor control volume using Eq. (3-15).

5. Repeat steps 3 and 4 until the rate of change of any variable between two successive iterations is $< 10^{-10}$.

6. Check the mass flow rate of the vapor at the outlet of the absorber. If it is a negative value, decrease the length of the absorber and go to step 2; if it is a positive value and is greater than 1% of the inlet vapor flow rate, increase the length of the absorber and go to step 2; if the value lies between zero and 1% of inlet vapor flow rate, assume the convergence.

Numerical Results and Discussion

A computer code was developed to numerically predict the performance of both designs. The code yields the mass flow rate, temperature, and concentration distribution for liquid and vapor phases along the absorber length. In addition, temperature and concentration conditions at the liquid-vapor interface, and heat and mass fluxes across the interface are also obtained. A wide range of operating conditions were used to test the code. The code also incorporates a check on the occurrence of flooding between the adjacent cooling plates. The flooding criterion used for this purpose is based on Wallis equation (Wallis, 1969). Overall mass and energy balance were done for each test condition, and accuracies better than 99.9% and 99.7%, respectively were achieved. The numerical technique thus showed a good agreement with the mass and energy conservation laws.

The mathematical model was then used to analyze the performance of the proposed falling film absorber with the microchannel absorber design. The analysis of both the

designs is based on the geometric dimensions and operating conditions listed in Tables 3-1 and 3-2. The operating conditions considered here are typical conditions encountered in the absorption based combined power/cooling thermodynamic cycle. These conditions are also typical to the single-stage ammonia-water absorption systems. The design conditions were selected such that a uniform distribution of the weak solution on the horizontal tubes is practically feasible, and thus the numerical results are based on a realistic situation. The finite difference scheme is modeled to calculate the minimum number of tubular rows required to accomplish the given amount of vapor absorption in both designs.

Table 3-1. Operating conditions of the proposed and microchannel falling film absorber designs used in numerical analysis

System Pressure, bar	2.81
Coolant medium	Water
	Inlet Conditions
Coolant mass flow rate, kg/s	0.0887
Reynolds number for coolant inlet flow, Re_{D_I}	946
Coolant bulk temperature, K	300.15
Solution mass flow rate, kg/s	0.0145
Reynolds number for inlet falling film, $\mathrm{Re}_{\mathrm{film}}$	75
Solution bulk temperature, K	316.15
Solution mass fraction	0.3
Vapor mass flow rate, kg/s	0.002
Reynolds number for vapor inlet flow, Re_{D_O}	100
Vapor bulk temperature, K	300.15
Vapor mass fraction	0.995

The computational results are summarized in Table 3-3. As depicted in the table, an absorber with the falling film guidance mechanism in between the coolant tubes will require a lesser number of tubes as compared to a similar horizontal tube type falling film absorber design. This accounts for a size reduction of about 29%. In order to thoroughly

analyze the proposed design with respect to the horizontal microchannel tube type absorber design, the temperature, concentration, and mass flow profiles of the different fluid regions were obtained as a function of the coolant tube rows.

Table 3-2. Geometric dimensions of the proposed and microchannel falling film absorber designs used in numerical analysis

Tube outer diameter, mm	3.2
Tube inner diameter, mm	2.3
Tube material	316 Stainless Steel
Tube length, cm	10
Number of tubes per row	4
Number of tube rows per pass	15
Tube vertical pitch, mm	7.6
Tube traverse pitch, mm	16

Table 3-3. Computational comparison of the proposed and microchannel type falling film absorber designs

	Proposed Design	Microchannel Absorber Design
Required length of the coolant tube assembly (L), m	0.45	0.63
Required minimum number of tube rows	59	83
Absorber heat duty, kW	3.71	3.84
Liquid-vapor interface area, m^2	0.33	0.32
Coolant surface area, m^2	0.23	0.32
	Outlet Conditions	
Solution mass flow rate, kg/s	0.0165	0.0165
Solution bulk temperature, K	308.6	306.1
Solution mass fraction	0.384	0.384
Vapor mass flow rate, kg/s	1.18×10^{-5}	1.4×10^{-5}
Vapor bulk temperature, K	318.1	316.9

Figures 3-3 and 3-4 show the variation in bulk mean temperature of the coolant, solution, and vapor along the absorber length for the proposed and microchannel falling film absorber designs, respectively. For both designs, the solution temperature increases for a while as the liquid flows down the cooling surface. At the top section of the absorber, heat transfer from the liquid to coolant region is less than the heat transferred to

the liquid phase by the heat of absorption. This is due to the fact that subcooling has a combined contribution on the heat transfer from liquid to coolant region, and the mass transfer from vapor to liquid region. The solution temperature reaches a maximum value, and thereafter it decreases as the solution flows down in both designs. Due to the rejection of heat to the coolant, the coolant temperature increases while flowing through the coolant tubes. Also note that the interfacial temperature is always greater than the solution temperature. This is due to the generation of absorption/condensation heat at the liquid-vapor interface. For both designs considered, the vapor temperature initially increases quite rapidly as it flows in the upward direction, and then it gradually approaches the interface temperature. The coolant mean temperature sharply increases after every 15 rows of the coolant tubes. It represents the entry of the coolant in the next parallel assembly of the coolant tubes. Thus, the periodic surge in the coolant temperature is in agreement with the parallel-series arrangement of the coolant tubes.

The difference between the vapor, liquid, liquid-vapor interface, and coolant temperatures can lead to the conclusion that the liquid-side heat transfer resistance is negligible in comparison to the other constituents of heat transfer resistance. However, the vapor phase heat transfer resistance also becomes comparable to the liquid phase heat transfer resistance at the upper section of both absorbers. It is the coolant-side heat transfer resistance that dominates the overall heat transfer resistance at the absorbers' upper section. A noticeable trend for the proposed design is the liquid temperature profile, which decreases and increases alternatively as the solution flows over the coolant tube and mesh, respectively. The flow of solution on the coolant tubes decreases the solution temperature and makes the solution more subcooled. As the solution flows on

the screen mesh, it absorbs vapor and the unavailability of a heat rejection mechanism on the screen mesh causes the solution to reach closer to saturation conditions. However, the effect of the coolant tubes to decrease the solution temperature is more significant than the effect of the screen mesh to increase the solution temperature, and the net result is a decrease in the solution temperature from the top to the bottom of the absorbers.

Figures 3-5 and 3-6 illustrate the mass flow rate of the liquid and vapor phases at various axial positions of both absorbers. The flow rate of the vapor decreases as it flows upward in the absorber, eventually becoming zero at the top section of both cases. This is consistent with the design criterion of complete absorption of the vapor phase. The absorption of vapor results in an increase of the solution flow rate.

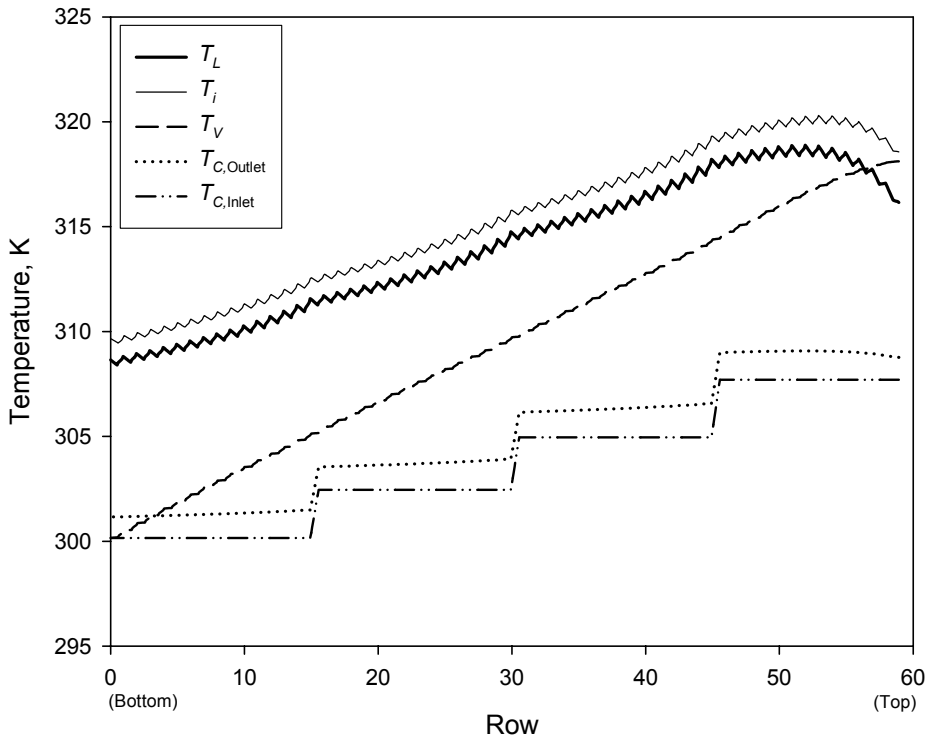

Figure 3-3. Variation of temperature for the proposed falling film absorber

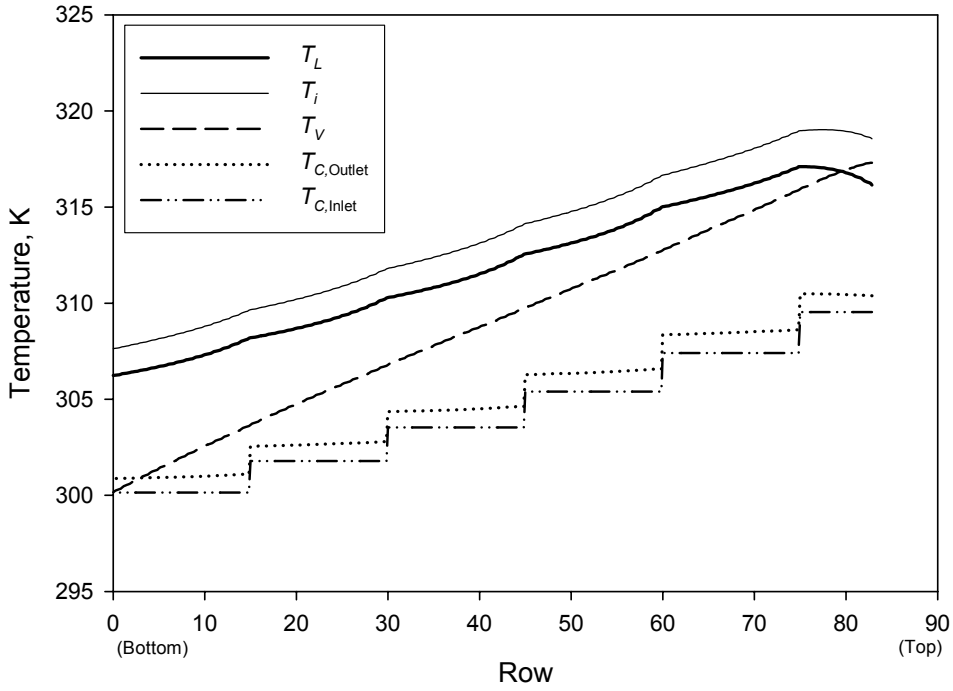

Figure 3-4. Variation of temperature for the microchannel falling film absorber

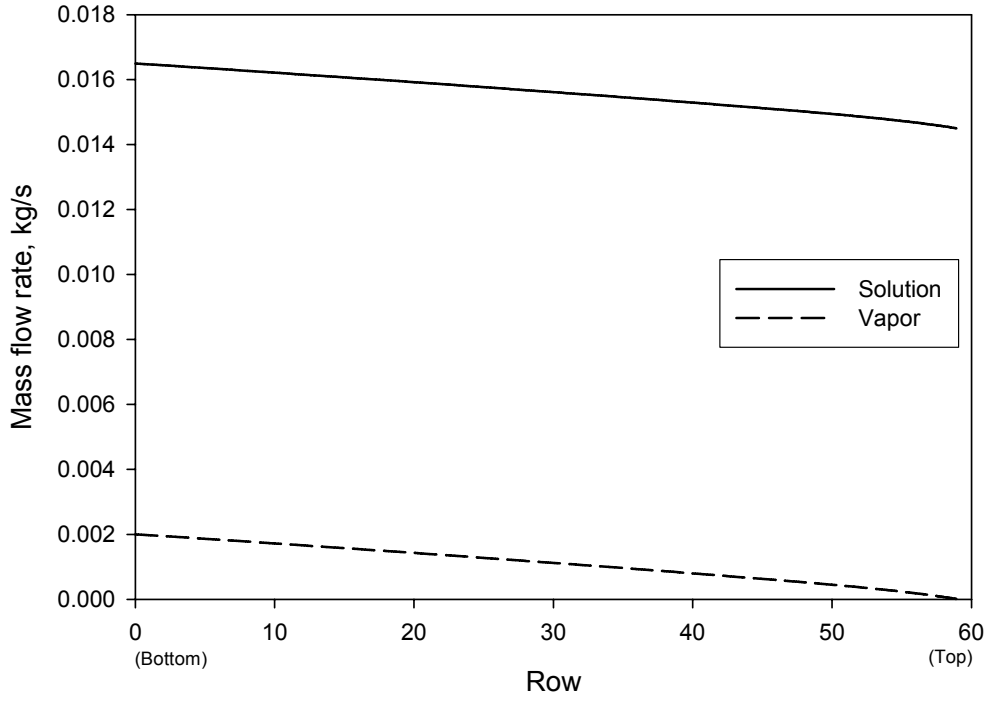

Figure 3-5. Variation of mass flow rate for the proposed falling film absorber

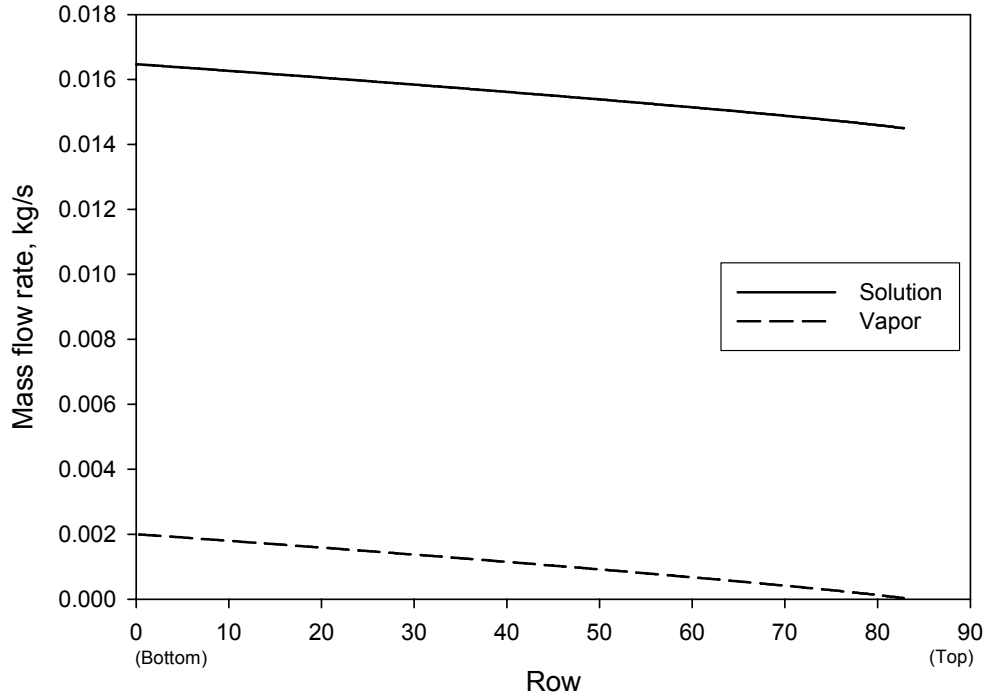

Figure 3-6. Variation of mass flow rate for the microchannel falling film absorber

The profiles of the composition of absorbing flux, and the concentration of the liquid and vapor phases are shown in Figures 3-7 and 3-8. It was found that the parameter z is more than 1 near the inlet vapor region, and thereafter its value decreases to less than 1 for both designs. It implies that a small amount of water vapor is being evaporated in the bottom section of the absorbers. The inlet concentration of vapor considered in the current operating conditions is 0.997. A very low concentration of water in the vapor phase leads to the transfer of water from the liquid to vapor phase by a diffusion mechanism. The results by Kang et al. (2000a) and Herbine and Perez-Blanco (1995) also confirm that desorption of water can occur near the entrance location of the vapor phase. However, in their case, they considered the absorption process in a cocurrent ammonia-water bubble absorber. The alternative decrease and increase in the value of *z* for the proposed design is due to the flow of liquid alternatively over the coolant tubes and mesh.

The value of *z* also remains higher than the vapor concentration for both designs. However, the difference between the value of *z* and the vapor mass fraction is quite small. The higher concentration of ammonia in the absorbing flux as compared to that in the vapor phase leads to the decrease in vapor mass fraction from the bottom to the top of the absorbers. Similar reasoning stands behind the increase in concentration of the solution as it flows in the downward direction. It was also found that the concentration difference between the vapor and liquid-vapor interface is lower than the difference between the liquid and liquid-vapor interface. It implies that for the operating conditions considered, a major fraction of the overall mass transfer resistance lies in the falling film. Perez-Blanco (1988) and Kim (1998) also considered both the liquid- and vapor-side mass transfer resistances in their numerical model, and found the liquid-side mass transfer resistance to be dominant.

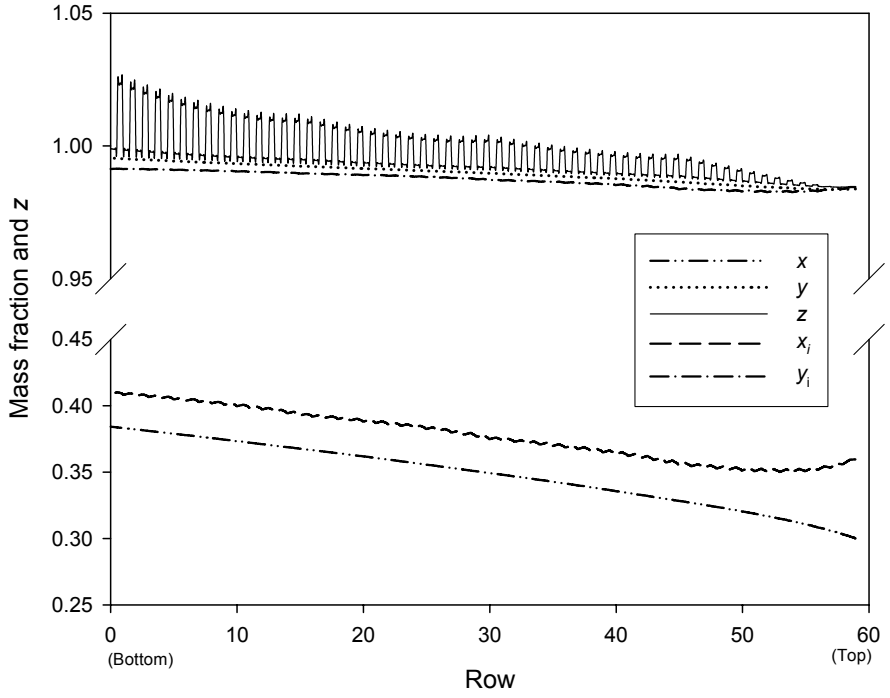

Figure 3-7. Variation of concentration for the proposed falling film absorber

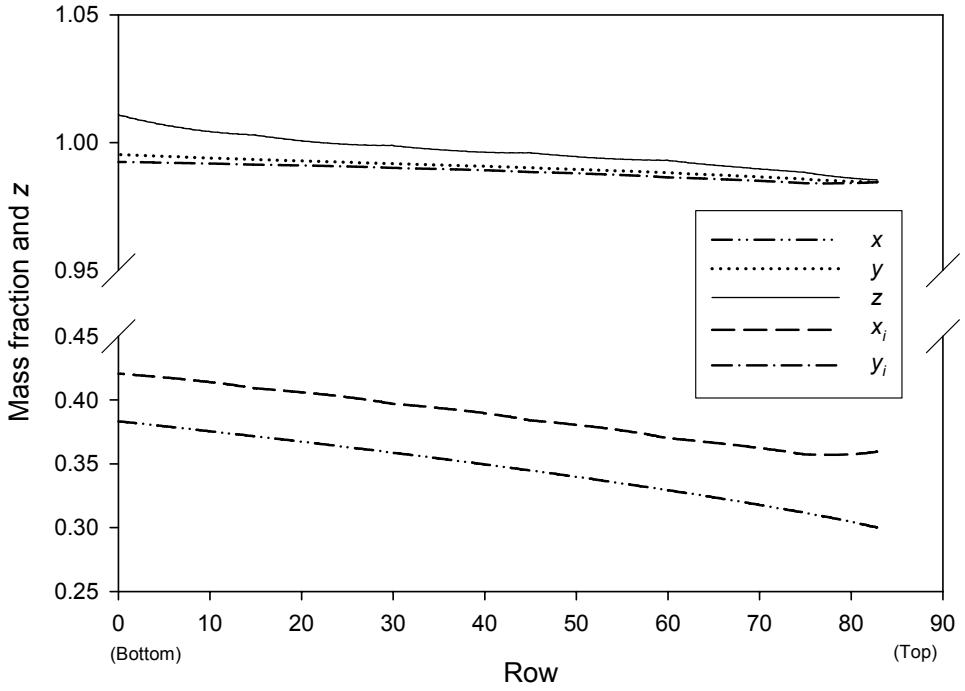

Figure 3-8. Variation of concentration for the microchannel type falling film absorber

Conclusion

The numerical analysis shows the promising prospects of a new concept of forming a falling film in between the horizontal coolant tubes by a flow guidance medium like a screen mesh/fabric. The proposed design is more compact and efficient than the falling film absorber based on small diameter coolant tubes. A size reduction of about 29% is possible for the operating conditions considered. The new design will induce thorough mixing of the liquid film while it flows alternatively over the mesh and coolant tubes.

The current theoretical modeling is a preliminary attempt to analyze the proposed design with the currently available numerical models. Several flow mechanisms associated with the flow over the horizontal tubes and fabric/mesh are not considered in order to realize a numerical model. For example, the effect of the fabric/mesh on the larger residence time of the falling film, lack of adiabatic adsorption in droplets, fin effect

of the metallic mesh, wettability enhancement, prevention of the satellite droplets, etc, are neglected in the current analysis. A complete analysis of the complex heat and mass transfer processes coupled with a flow analysis of falling film is not available in the literature. In addition, the current literature also lacks numerical and experimental flow analysis of a falling film over an irregular mesh. It necessitates an experimental study which will help in considering the complex phenomena that were unaccounted for in this numerical scheme.

CHAPTER 4
EXPERIMENTAL METHODOLOGY

An experimental investigation was carried out to compare the effect of a screen mesh stretched between coolant tubes of a microchannel falling film absorber. As horizontal tube type absorbers with small diameter coolant tubes are very compact, this analysis will help in comparing the proposed design with the current state-of-the-art absorber design. Descriptions of the test facility, absorber configuration and experimental procedure are outlined in this chapter.

Experimental Setup Description

Experiments were done on the prototype of combined power-cooling cycle installed at Solar Energy and Energy Conversion Laboratory, University of Florida. The test facility was initially built by Tamm, and he experimentally studied the performance of the combined power and cooling cycle (Tamm, 2003). Later, Martin incorporated a rectification column and an expander to the facility to conduct his experiments on the expander (Martin, 2004). However, the setup required modifications to improve the system operation, and therefore was modified according to the needs of this experimental investigation. The modified system features a better rectification system, larger suction head at the pump inlet and a smaller separator tank. The modified design reduces the pressure drop across the suction line by a larger diameter of piping and lesser number of constraints in the flow path.

In the experimental setup used by Martin, the rectification column was configured in a manner that the condensate produced in the reflux cooler was directly brought into

the absorber through the vapor line. The flow rate of condensate was also not measured. Thus, the entry of unaccounted liquid into the absorber hindered the mass and energy balance across it. In addition, the rectification column suffered from frequent flooding problems due to its small diameter (2 inch schedule 40 pipe). In this work, a new rectification column was fabricated and installed into the test facility. The rectification column is a 3 inch schedule 40 pipe of 6 ft length, which is filled with 1/2 inch ceramic Berl Saddle packings to a length of about 2 ft. The reflux cooler is installed in the remaining space of 4 ft in the rectification column. It is a water cooled helical coil with 56 turns of inner diameter 7.5 inch, which was fabricated in the laboratory by using 3/8 inch aluminum tubing. It was also found that the piping installed between the absorber and suction pump was causing a large pressure drop, and thus creating cavitation problems. The suction head was increased by changing the piping from 1/2 inch tube to 3/4 inch tube, and reducing the unwanted bends in the flow path. In addition, the vessel utilized as the separator in the setup was found to be quite large, providing an excessive containment of ammonia vapor in the separator. The separator was thus replaced with another vessel of smaller size. Apart from the modifications to the test facility, the proposed and conventional absorber designs were also fabricated and incorporated into the experimental setup. The new absorber vessel is connected in parallel with the old absorber. The old absorber is essentially a bubble absorber, which was not properly designed. The proposed and conventional assemblies of horizontal coolant tubes were alternatively installed in the new absorber vessel. The experiments were first done on the conventional design, and later on the proposed design. The details of the new absorber unit are presented in the next section.

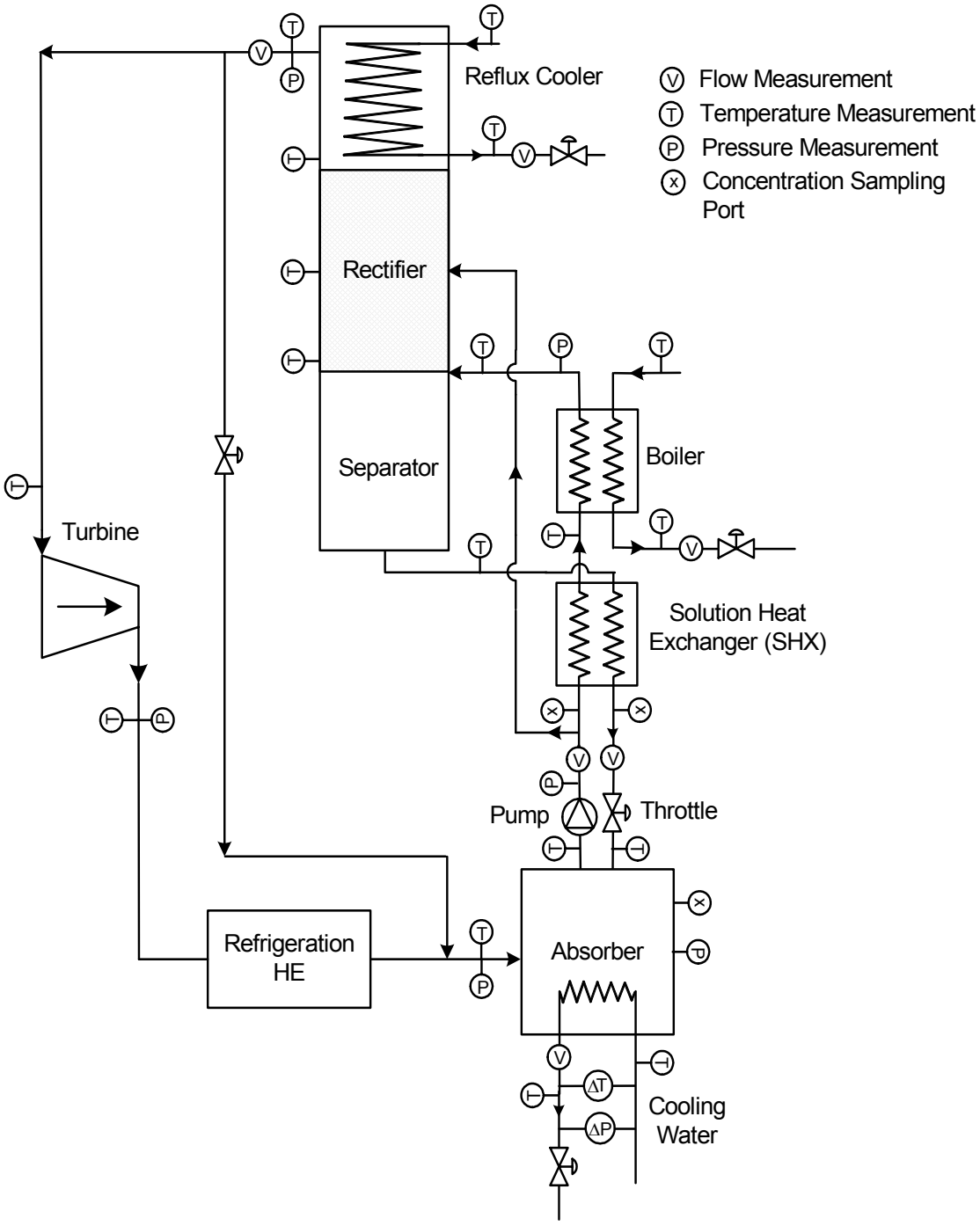

Figure 4-1. Schematic of the prototype of combined power and cooling cycle

A schematic and a photograph of the modified test facility are shown in Figures 4-1 and 4-2, respectively. The strong solution is directly fed to a hot water heated plate-type heat exchanger to produce the liquid-vapor mixture. A counter-flow arrangement between the strong solution and hot water provides the exit temperature of the ammonia-

water mixture to be closer to the inlet temperature of the heat source fluid. The liquid-vapor mixture leaving the boiler is brought into the separator. The low concentration ammonia liquid separates from the high concentration ammonia vapor by gravity, and settles at the bottom of the separator, whereas, the vapor stream enters the rectification column.

Figure 4-2. Photograph of the prototype of combined power and cooling cycle

The rectification column consists of a packed bed and a reflux cooler. The exchange of heat and mass between the liquid and vapor phases enhances the purity of the vapor stream. The vapor leaving the packed bed column is finally enriched by partial condensation of the vapor in the reflux cooler. Condensation is achieved by keeping the heat-exchanging surface below the dew point of the vapor. The condensate returns back to the separator by gravity. In addition, the experimental system has a provision to

directly feed a fraction of the strong solution into the packed bed column by bypassing the vapor generation step. It enables heat and mass exchange between the strong solution and vapor streams in the packed bed column.

The vapor stream exits the rectification column, and expands through a turbine to produce work. After expansion through the turbine, the low temperature vapor provides cooling to the refrigeration unit. The ammonia vapor is finally absorbed by the weak solution in the absorber. An extra vapor flow path is also installed to bypass the turbine and refrigeration heat exchanger, and to adiabatically throttle the vapor by using a needle valve.

The low-pressure vapor then flows into the absorber where it gets absorbed by the weak solution. The current setup does not have a condenser and an evaporator. The weak solution which settles down in the separator is throttled back to the absorber where it is uniformly distributed on the outer-surface of the horizontal coolant tubes. The vapor entering the absorber flows upward though the tubular assembly. The vapor and weak solution flow counter-currently leading to the absorption of vapor in the weak solution to form the strong solution. The cooling water flows counter and cross-currently to the falling film through coolant plates. The absorption heat thus produced is rejected to the coolant to continue the absorption process. The cycle is completed by pumping back the strong solution through a rotary vane pump to the high pressure side. Before entering the boiler, the strong solution recovers heat from the weak solution by a counter-current plate-type heat exchanger.

The heat of absorption is rejected to chilled water flowing through a shell-and-tube heat exchanger installed in the coolant loop. The coolant flow is controlled by a

centrifugal pump and a ball valve, whereas its temperature is controlled by varying the flow rate of a 50/50 mixture of ethylene glycol/water circulating across the chiller. The chiller is thermostatically controlled to maintain the temperature of ethylene glycol/water mixture in the range of 8-14 °C.

The heat source for the test facility is a 5 kW electric water heater whose capacity is augmented by using phase change thermal energy storage. The thermal storage tank was pressurized to about 80 psig with city water, which facilitated the temperature of hot water to exceed 100 °C. A centrifugal pump was used to circulate a controlled amount of hot water between thermal storage and plate type heat exchanger of the test facility. A ball valve was also installed between suction and discharge ports of the pump to control the amount of liquid flowing back into the pump, and thereby regulating the flow of hot water into the test facility.

Absorber Configuration

The vessel used in this experimental study was a flanged container made from a 6 inch steel pipe. The conventional assembly of horizontal tubes and proposed design were alternatively experimented in the same absorber unit. The schematic and photograph of the absorber system are shown in Figures 4-3, 4-4 and 4-5. An 8 inch long section of the pressure vessel made from a transparent borosilicate glass was also installed in the middle of the absorber vessel to view the wetting conditions of the falling film. However, the idea of using transparent vessel did not work up to the expectations due to the optical distortion by the cylindrical curvature of glass and condensation over the inner surface.

The coolant tubes used in this experimental study are stainless steel tubing of 1/8 inch outer diameter and 0.016 inch wall thickness. The length of each horizontal tube is about 10 cm. The entire tube assembly consists of 4 columns each having 60 horizontal

tubes with their ends brazed to a stainless steel header of 1/2 inch outer diameter and 0.12 inch wall thickness. In a column, the tubes are connected in a parallel-series arrangement with 15 rows of tubes in parallel. The geometric dimensions of the coolant tube assembly are listed in Table 4-1. The entire tube assembly was fabricated in the laboratory by oxy-acetylene based nickel brazing. The top and bottom ends of all the four columns of tubular assembly are connected with manifolds to allow equal distribution of coolant between them. The coolant flows in cross-counter direction to the solution entering at the bottom and leaving at the top of the absorber. A thermopile with an accuracy of ±0.085 °C was installed between the inlet and outlet ports of coolant to measure the temperature rise across the coolant loop.

Table 4-1. Geometric dimensions of the coolant tube assembly used in experimental analysis

Tube outer diameter, mm	3.2
Tube inner diameter, mm	2.3
Tube material	316 Stainless Steel
Tube length, cm	10
Number of tubes per row	4
Number of tube rows per pass	15
Tube vertical pitch, mm	8
Tube traverse pitch, mm	16

The weak solution is distributed over the horizontal tubes by means of a drip tray arrangement. The drip tray has several perforations which are equidistant and located above the center axis of each column of horizontal tubes. It was made by punching a stainless steel sheet, and the indentations/downward edges on the perforation caused by punching were not completely removed. However, the shape of the indentation was made uniform to prevent the coalescence of droplets dripping through the tray. After conducting some preliminary tests with flowing water through the tray, the vertical

distance between the perforations and horizontal tubes was decided to be about 1/8 inch. The drip tray and coolant tube assembly were screwed together to prevent any misalignment. In order to flow the entire amount of vapor through the horizontal tubes, the tubular assembly was enclosed in an aluminum case. The photographs of coolant assembly are shown in Figure 4-6. The assembly was then housed in a pressure vessel of 6-inches inner diameter. A level gauge was installed in the vessel to check the strong solution level in the absorber vessel. The level of strong solution was kept high enough to prevent the vapor from leaking through the bottom opening of the aluminum enclosure, whereas the top opening of the enclosure was open to the absorber vessel. The overall dimensions of the coolant assembly are approximately 6.35 cm × 12 cm × 63.5 cm, and the total surface area of the horizontal tubes is about 0.24 m^2.

The main difference between the two designs is an aluminum screen mesh in the case of the proposed absorber design. The experiments were first conducted done on the microchannel absorber design, and then the same tubular assembly was modified with an aluminum woven wire mesh as described before. The wire mesh has a diameter of 0.2 mm and 16 × 16 meshes per square inch. A close view of the screen mesh wrapped in between the horizontal tubes is shown in Figure 4-6. The wetting characteristics of the coolant tubes also play a major role in the formation of the falling film. The outer surface of the coolant tubes was sand blasted to increase the roughness, and thereby wettability. The wetting characteristics of the aluminum mesh used in this study were enhanced by keeping it in hot water at about 80 °C for a period of 30 min (Min and Webb, 2002).

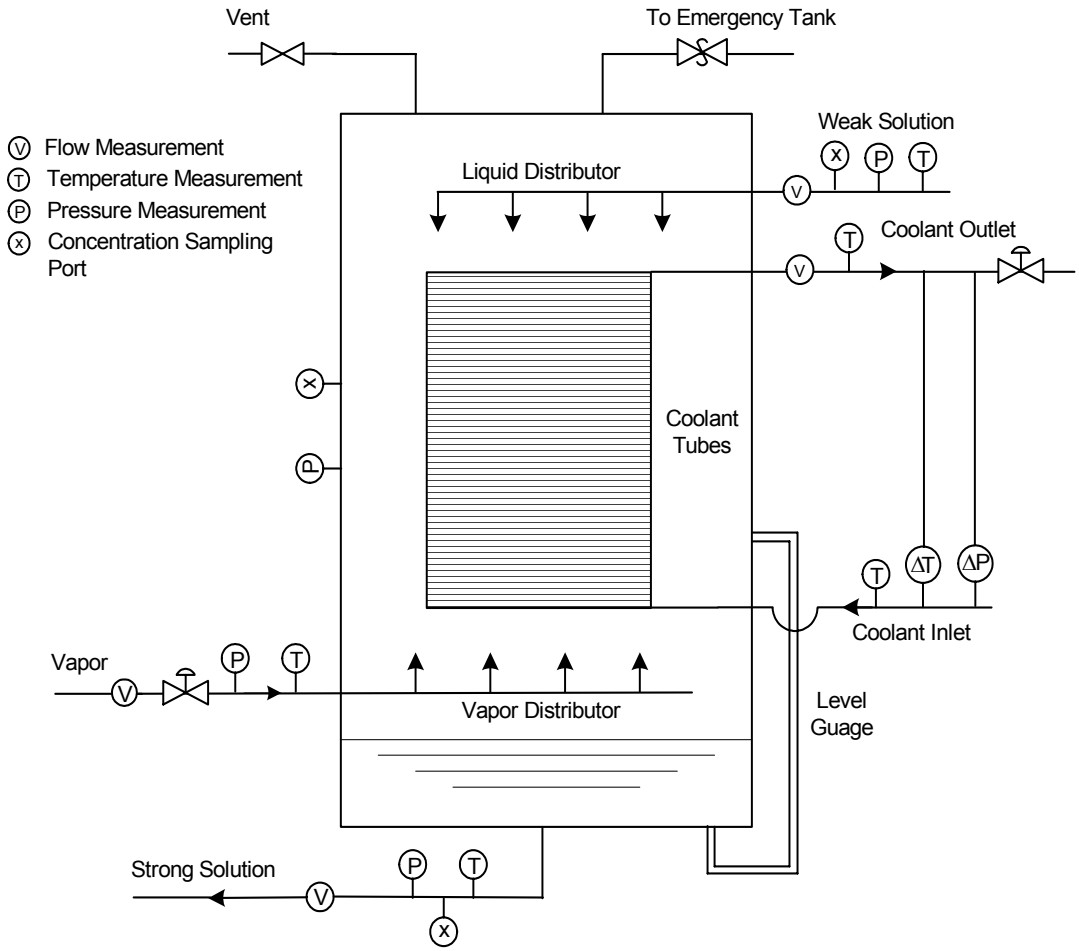

Figure 4-3. Schematic of the absorber in the combined power and cooling cycle

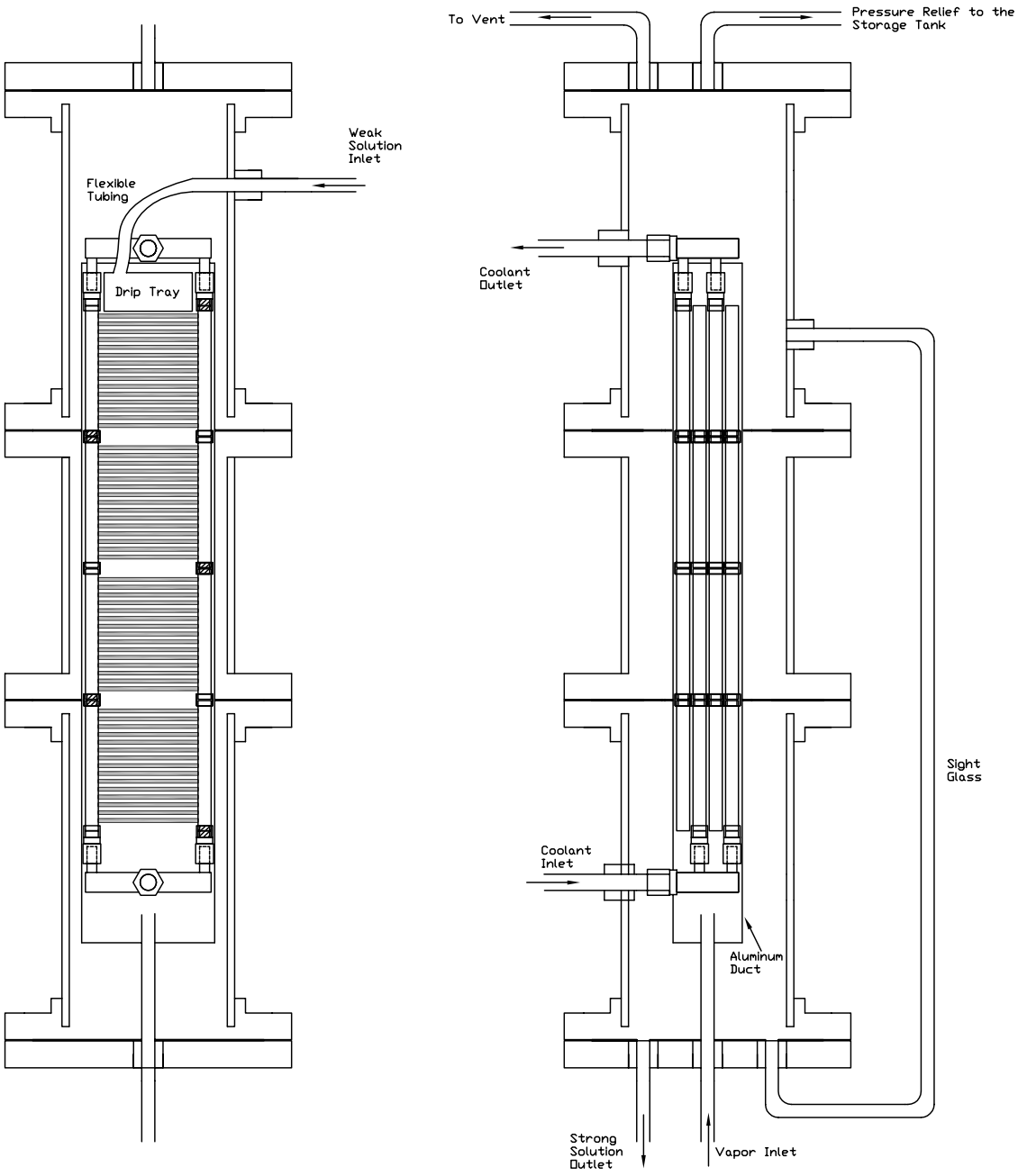

Figure 4-4. Detailed sketch of the absorber in combined power and cooling cycle

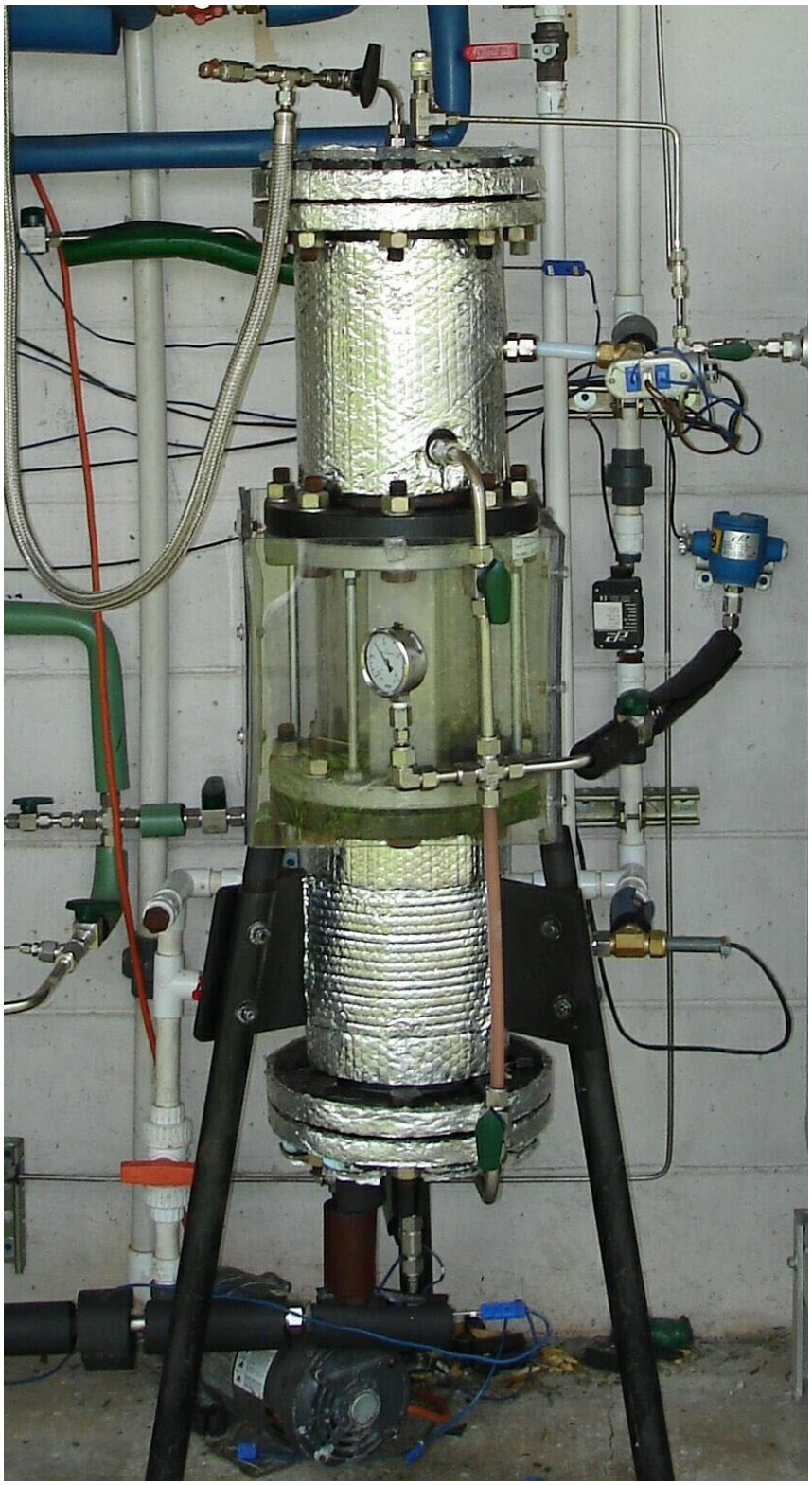

Figure 4-5. Photograph of the absorber in combined power and cooling cycle

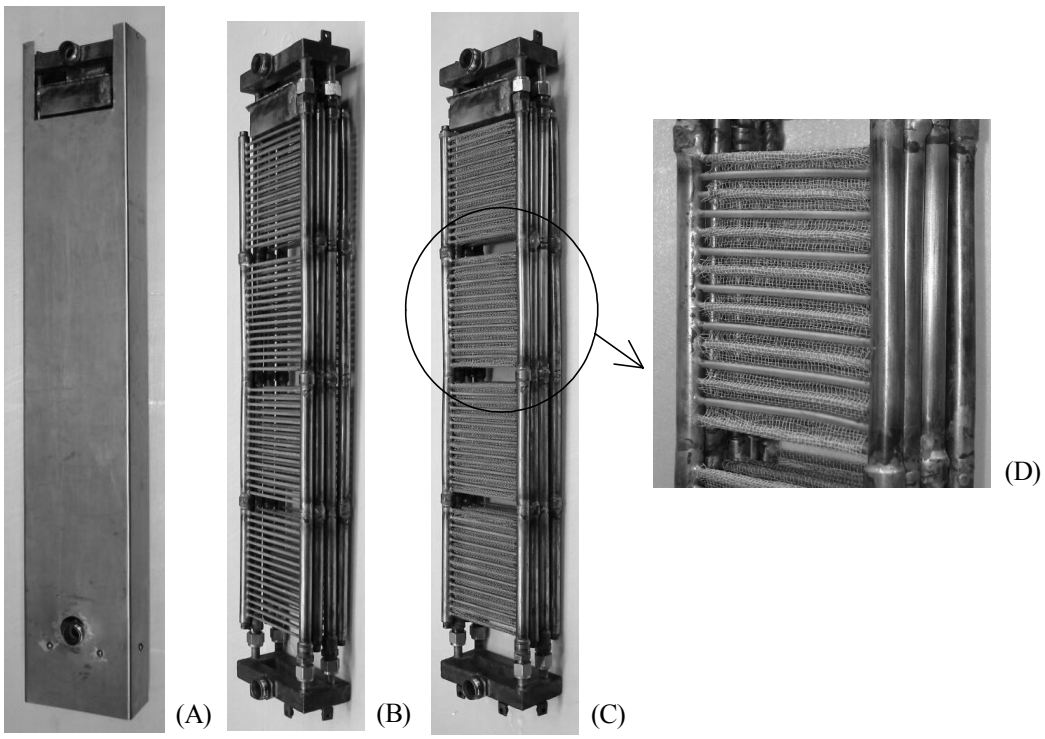

Figure 4-6. Photographs of the coolant assembly: (A) External view of the tubular array housed in an aluminum casing, (B) Internal view of the microchannel array, (C) Internal view of the tubular array with screen mesh, and (D) Closer view of the screen mesh wrapped in between the tubes

Instrumentation

Temperature, pressure, flow rate and concentration were measured at the locations shown in Figure 4-3. T-type thermocouples and pressure transducers measure the temperature and pressure respectively of various flow streams in the test facility. The flow rates of the strong and weak solutions are measured with variable area flow meters, whereas the coolant flow rate is measured with a paddle wheel flow meter. The volumetric flow rate of vapor is determined by a turbine flow meter. A thermopile was fabricated and characterized in laboratory to accurately measure the rise in temperature across the coolant loop.

In order to determine the concentration of the ammonia-water solution, the samples of binary mixture are collected in a syringe and then analyzed by a Gas Chromatograph.

Septum ports are installed on the flow streams of strong and weak solutions to take samples in a syringe from the pressurized system. While collecting vapor samples, it was found that a small amount of the vapor was getting condensed on the surface of the syringe. This implied that the syringe should be pre-heated to a temperature higher than the vapor sample. However, the temperature of vapor to be sampled was more than 65°C in all the operating conditions, which made this option difficult. Therefore, the concentration of vapor was determined by the application of thermodynamic property correlations on the measured value of temperature and pressure at the exit of the rectification column. A number of pressure relief valves were also installed in the test facility for protection against any excessive pressure in the system. The pressure relief valves discharge into a large emergency tank.

The readings of thermocouples, pressure transducer, differential pressure, differential temperature and vapor flow rate were recorded by a data acquisition PC interface, whereas the flow rate values of variable area and paddle wheel flow meters were manually documented. The concentration of weak and strong solutions was also manually recorded after analyzing the solution by a Gas Chromatograph. The details of the instruments are given in Appendix C.

Experiments Conducted

The experiments were carried out to compare the performance of both designs for typical conditions encountered in the combined power and cooling cycle. It should be noted that these conditions are also typical to single-stage ammonia/water absorption systems (Herold et al., 1996). A parametric analysis was also performed to analyze the influence of various parameters affecting the system performance. It was initially desired to consider the influences of the following parameters on the absorber: weak solution

flow rate, coolant inlet temperature and vapor fraction. These parameters are usually considered in an experimental analysis on an absorber (Meacham and Garimella, 2004; Deng and Ma, 1999; Islam et al. 2003a). The flow rate of a weak solution has a significant impact on the wetting characteristics of the falling film, which thereby influences the overall performance of the absorber. The temperature of the coolant varies with location, and thus it will be useful to know its effect on the absorption performance. The ratio of vapor to weak solution is typically in the range of 8-10% for combined power and cooling cycle and single-stage absorption systems. It was found that the operating range of turbine flow meter, which is used to measure the vapor flow rate, limits the system operation at lower vapor fraction. In addition, the absorber size limits a drastic increase in vapor fraction unless the absorption rate is increased by unrealistic means such as, very low inlet coolant temperature. Thus, the experiments were conducted on a fairly narrow range of vapor fraction, and the influence of vapor fraction was not considered in this experimental study.

CHAPTER 5
EXPERIMENTAL ANALYSIS

This chapter presents the experimental comparison of the proposed absorber design with the microchannel absorber. The experimental results are also compared with the theoretical model. An explanation of the deviation of the theoretical model from the experimental results is finally presented.

Operating Conditions

The experimental analysis is primarily based on the conditions encountered in the combined power and cooling cycle. The experiments were first conducted on the microchannel absorber design, and then the same tubular assembly was modified with an aluminum screen mesh as described before. The temperature, vapor flow rate and pressure measurements were recorded in a real time manner through a PC-based data acquisition system. The initial warm-up of the test facility and steady state operation required about 2 hours. The occurrence of steady state was determined through the readings from the data acquisition system, flow meters, and the level of strong solution in the absorber. The experiments were conducted by first maintaining the desired inlet temperature and flow rates of the weak solution and coolant, and then the vapor flow rate was increased to an extent that the absorber pressure reaches the desired value. Measurements for each experiment were averaged values of the data recorded at a rate of 100 Hz for a period of 5 min. The experiments were repeated by re-establishing the operating conditions after a period of at least 6 hours.

The analysis of both designs is based on the baseline conditions listed in Table 5-1. The resultant absorber heat duty was obtained by varying the flow rate of the vapor such that the conditions described in the table were achieved. The weak solution flow rate and inlet coolant temperature were also individually varied to study their influence on the performance of both designs. The weak solution flow rate was varied from 11.1 to 17.8 g/s, whereas the inlet temperature of the coolant was in the range of 20 to 30 °C.

Table 5-1. Baseline experimental conditions of the proposed and microchannel falling film absorber designs

Absorber Pressure, bar	2.81±0.02
Coolant medium	Water
	Absorber Inlet Conditions
Coolant mass flow rate, g/s	88.7±1.7
Inlet coolant bulk temperature, °C	27.0±0.5
Weak solution mass flow rate, g/s	14.46±0.424
Weak solution bulk temperature, °C	43.0±0.5
Weak solution concentration, kg/kg	0.30±0.015
Vapor bulk temperature, °C	58.0±0.5
Vapor concentration, kg/kg	0.956±0.004

Data Analysis

The parameters selected to assess the performance of both designs are absorber heat duty, and product of the overall heat transfer coefficient and wetted-tube surface area. The absorber heat duty is the amount of heat rejected to the coolant in order to continue the vapor absorption into the weak solution at a steady state. Its value can be determined by conducting an energy balance across either the solution side or the coolant side of the absorber. At steady state loss of energy by the solution side is equal to the gain in energy by the coolant side. The mass flow rate and enthalpy of each fluid stream exiting/entering the absorber are thus required to conduct an energy balance over the absorber.

The volumetric flow rates of the weak solution and vapor were measured by a variable flow meter and a turbine flow meter, respectively. The weak solution

concentration was measured through a gas chromatograph, whereas the vapor concentration was determined by the application of liquid-vapor equilibrium correlations on the measured temperature and pressure of vapor stream. Thermodynamic property correlations were finally used to compute the density of liquid and vapor phases at the given temperature, pressure and concentration. The enthalpies of the liquid and vapor streams were then estimated by thermodynamic property correlations. The heat duty of the absorber was calculated for both coolant and solution loops to confirm an energy balance between them.

The overall heat transfer coefficient U can be estimated from the given absorber heat duty, coolant tube wetted-surface area, and log mean temperature difference LMTD between the coolant and solution sides. The LMTD is based on the assumption of constant specific heat of both heat transferring fluids. However, in the case of absorbers, the specific heat of solution changes as it absorbs the vapor phase. The approach of estimating the overall heat transfer coefficient on the basis of LMTD is thus an approximation to a complex analysis. However, this approach has been widely used to present the performance of an absorber (Lee et al. 2002; Sujatha et al., 1999; Jeong et al. 1998). The wetted surface area of the coolant tube is unknown, and thereby the value of U can not be reasonably estimated. Therefore, it was decided to estimate the value of UA, which represents the effective thermal performance of a falling film. The uncertainties in indirect measurements were also estimated to determine the confidence in the experimental results. It was estimated by ascertaining the sensitivity of various directly measured parameters through perturbation method.

Results and Discussion

A comparison of both designs for a representative experiment conducted at the baseline operating conditions is presented in Table 5-2. The heat duties of both coolant and solution sides are within the estimated limits of error, which validates energy balance over both absorbers. The coolant side heat load for the proposed design is 4.085±0.084 kW, whereas the microchannel absorber design has a heat load of 3.378±0.072 kW. The difference between the two designs is due to the inclusion of an aluminum mesh in the new proposed design. The experiments on both absorber designs were conducted on same coolant assembly with equal coolant flow rates, and thus all coolant-side conditions for the two designs are same. The presence of screen mesh increases the heat duty of the absorber by about 20.5% for the representative experiment considered. The higher heat load for the proposed design is primarily due to an increase in the mass transfer area, and an enhancement in the turbulence and wettability of the falling film. However, increase in the residence time of the liquid-vapor contact, and heat conduction through the metallic screen mesh are some of the other reasons that cannot be neglected. The higher heat load of the proposed design can also be confirmed by the requirement of higher vapor flow rate. The mass flow rate and concentration measurements of the strong solution were also higher for the proposed design than the conventional microchannel absorber design. The value of *UA* is found to increase by more than 44.6% with the proposed design. It is not possible to conclude as to the exact reason for the observed results without more detailed experimental data as well as flow visualization. However, increased mixing and tube wetting due to the introduction of wire roughness over the coolant tubes are the possible reasons for this increase. Repetition of experiments at the same baseline operating

conditions also provided similar results. The results for both designs are represented in Figures 5-1 to 5-4.

Table 5-2. Experimental comparison of the proposed and microchannel absorber designs for the representative test at baseline operating conditions

	Proposed Design	Microchannel Absorber Design
Absorber heat duty (Coolant-side), kW	4.085±0.084	3.378±0.072
Absorber heat duty (Solution-side), kW	3.878±0.127	3.218±0.127
Overall heat transfer coefficient × Wetted-tube surface area *UA*, W/K	483±42	334±26
Absorber pressure, bar	2.797±0.02	2.795±0.02
Weak solution mass flow rate, g/s	14.461±0.424	14.450±0.424
Weak solution bulk temperature, °C	43.3±0.5	43.7±0.5
Weak solution concentration, kg/kg	0.298±0.015	0.302±0.015
Strong solution mass flow rate, g/s	16.513±0.535	15.995±0.535
Strong solution bulk temperature, °C	39.6±0.5	40.0±0.5
Strong solution concentration, kg/kg	0.381±0.015	0.370±0.015
Vapor mass flow rate, g/s	2.061±0.023	1.774±0.021
Vapor bulk temperature, °C	59.4±0.5	57.1±0.5
Vapor concentration, kg/kg	0.956±0.0018	0.959±0.0015

The influence of the weak solution flow rate and the coolant inlet temperature on both designs was also studied experimentally. These two parameters were alternatively varied for the baseline operating conditions listed in Table 5-1. The volumetric flow rate of weak solution was varied in the range of 0.2±0.00076 gpm to 0.32±0.00076 gpm with incremental steps of 0.02 gpm. As shown in Figure 5-1, the absorber heat duty of both designs increases as the weak solution flow rate is increased. Since, the coolant side conditions were kept constant, it can be concluded that the absorption process in falling film absorber is controlled by the mass transfer process. The rate of vapor absorption is dependent on the concentration gradient between the liquid-vapor phases, and the mass transfer coefficients. The increased flow rate of weak solution not only enhances the turbulence and wetting characteristics but also reduces the effective concentration

difference between the two phases. Thus, the amount of vapor absorption increases with the increase in weak solution flow rate, which translates into higher absorber heat duty for both designs. There is a consistent enhancement in absorber heat duty with the proposed design. The heat load of the proposed design is found to be about 17-26% higher than the microchannel absorber design.

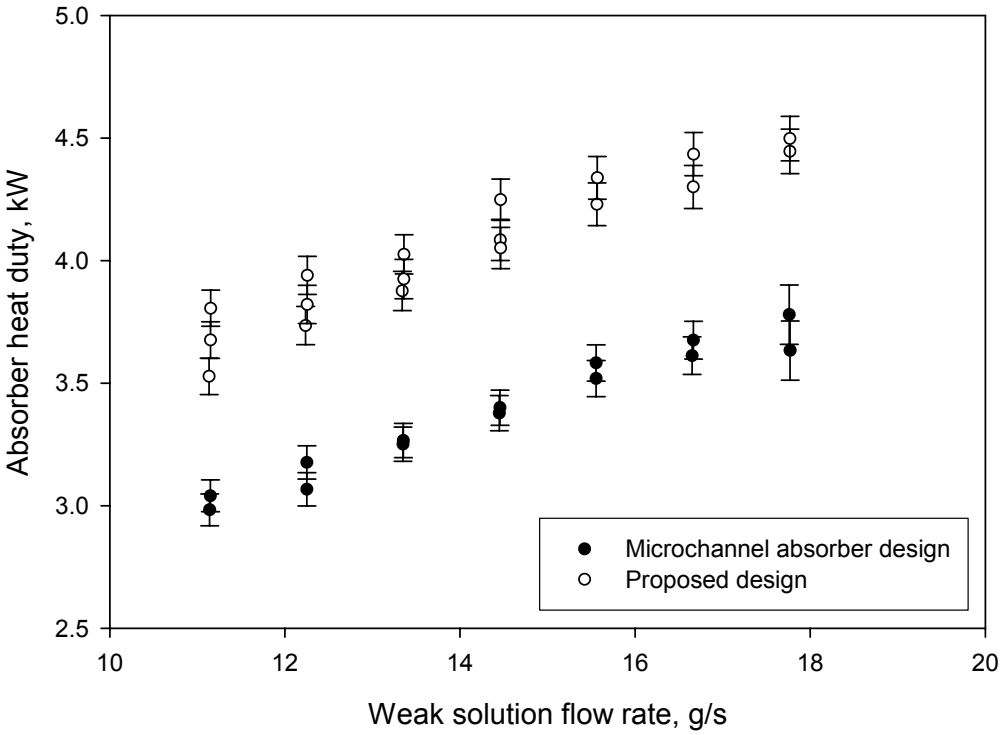

Figure 5-1. Absorber heat duty with the variation in weak solution flow rate (The baseline conditions listed in Table 5-1 and other experimental conditions were used as input to the numerical model)

The effect of weak solution flow rate on *UA* (product of the overall heat transfer coefficient and wetted-tube surface area) is illustrated in Figure 5-2. The value of *UA* is relatively constant over the operating range of weak solution flow rate. Its average values are 0.34 and 0.5 kW/K respectively for the microchannel and proposed absorber designs. In the case of proposed design, some experiments at low weak solution flow rates (11.15-

12.25 g/s) show a relatively high value of $UA \approx 0.62$ kW/K. While other experiments at the same flow rates show lower value of $UA \approx 0.48$ kW/K. We do not have an explanation for these differences. However, our speculation is that the instability in wetting conditions at the low flow rates might have resulted in the unexpected different values of *UA* for these experiments. The average increase in the *UA* value for the proposed design is about 49% in comparison to the microchannel design for all the experiments conducted at various weak solution flow rates.

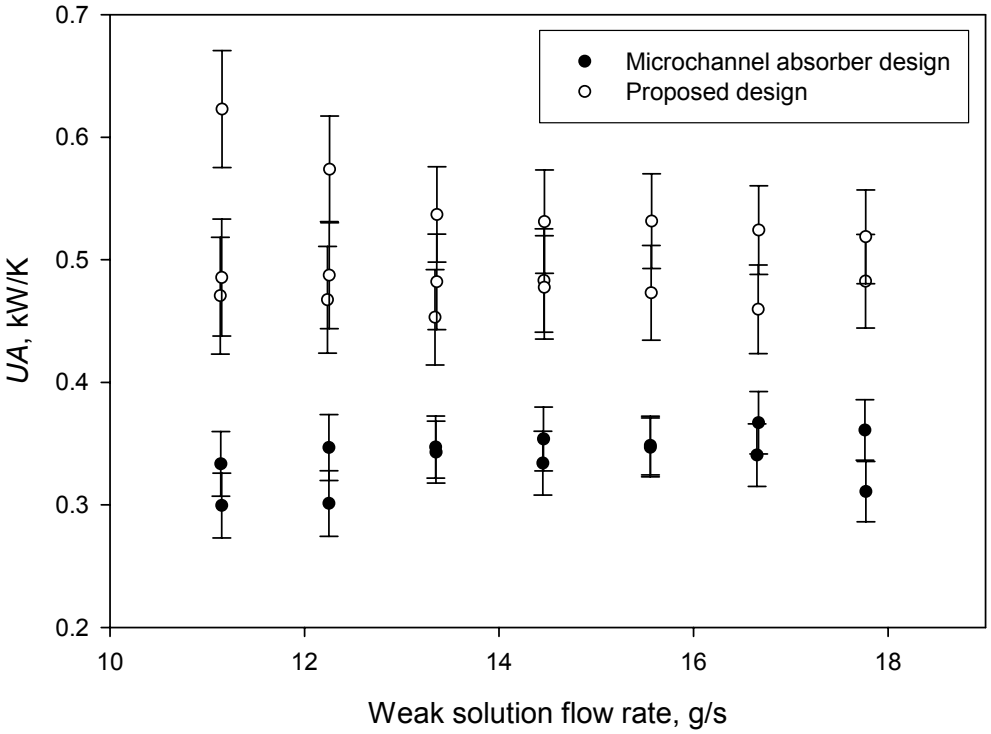

Figure 5-2. Variation of *UA* value with the weak solution flow rate (The baseline conditions listed in Table 5-1 and other experimental conditions were used as input to the numerical model)

Figure 5-3 shows the effect of the inlet coolant temperature on the absorption capacity of both designs. The temperature range was selected as 20-30 ^{o}C (68-86 ^{o}F), which covers typical thermal conditions for the cooling towers. As expected, a decrease

in the inlet coolant temperature results in an increase in the absorber heat duty for both designs. The effect is very prominent and can be utilized in places where the option of lower inlet coolant temperature is viable. The absorber heat duty of the proposed design is consistently higher (17 to 25%) than the microchannel absorber design. The variation of *UA* with the coolant inlet temperature is shown in Figure 5-4. The value of *UA* is essentially not affected by the coolant temperature. Its average values are 0.32 and 0.5 kW/K respectively for the microchannel and proposed absorber designs. A consistent enhancement in *UA* was noticed with the introduction of the metallic screen mesh. The average increase in the *UA* value for the proposed design is found to be about 55% in comparison to the microchannel design.

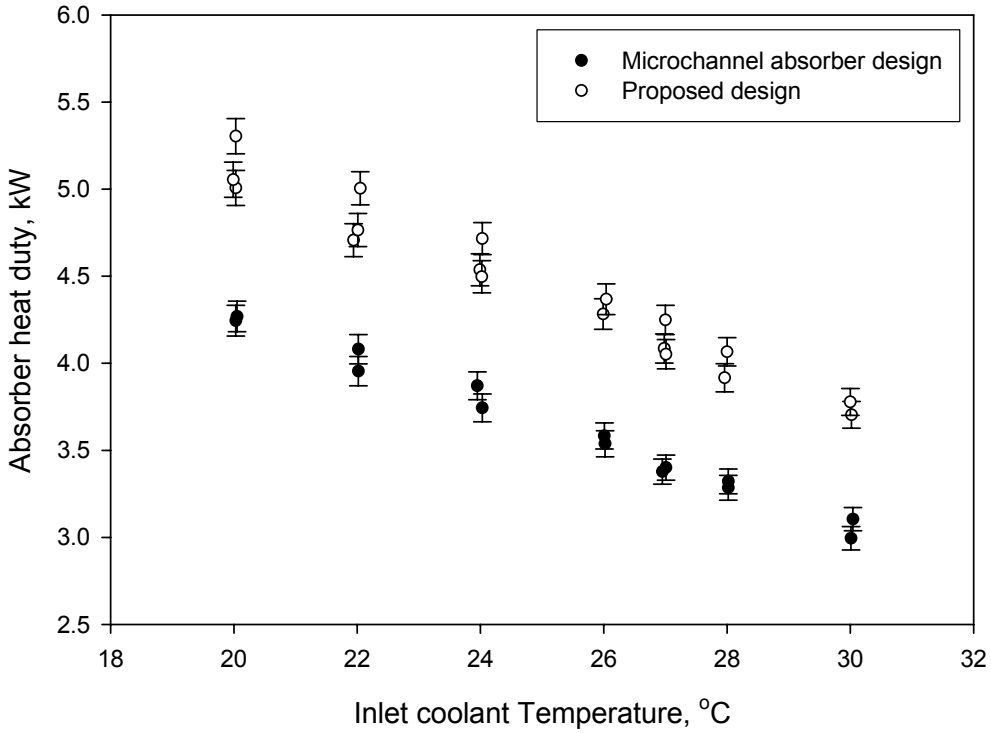

Figure 5-3. Absorber heat duty with the variation in inlet coolant temperature (The baseline conditions listed in Table 5-1 and other experimental conditions were used as input to the numerical model)

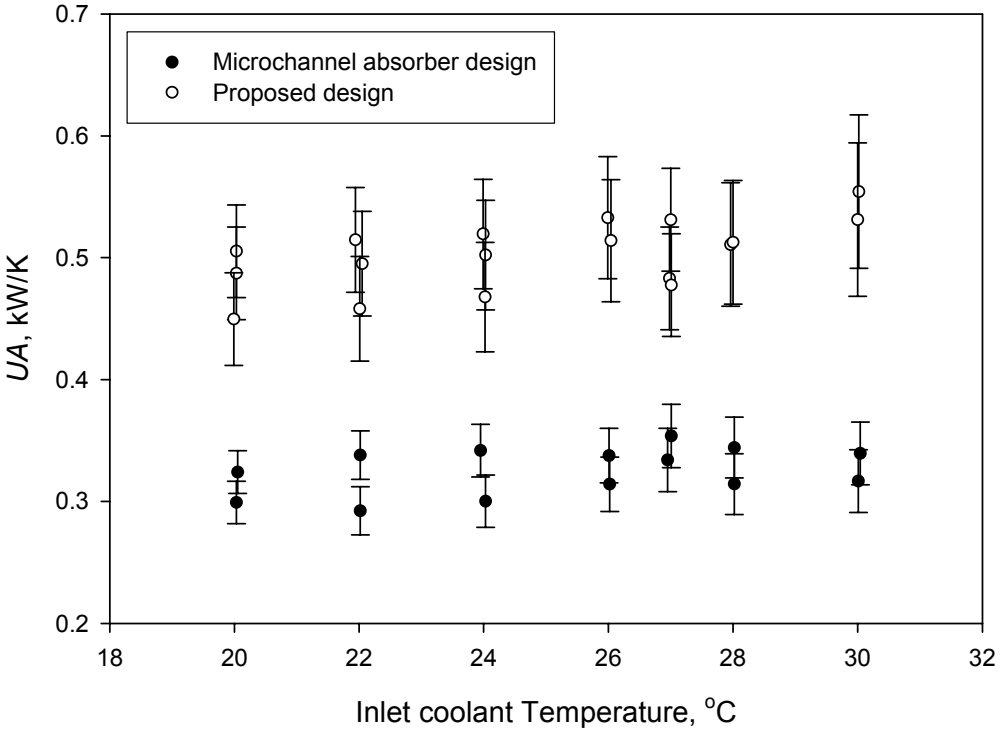

Figure 5-4. Variation of *UA* with the inlet coolant temperature (The baseline conditions listed in Table 5-1 and other experimental conditions were used as input to the numerical model)

Comparison of Theoretical and Experimental Analysis

As described earlier, the experimental analysis was performed on the proposed and conventional microchannel absorber designs. The coolant assembly consists of a fixed number of 240 horizontal small-diameter tubes, which was created by stacking 4 columns of 60 tubes each. The experiments were conducted at various inlet coolant temperatures, and weak solution flow rates. For each experiment, the vapor flow rate was varied until a pressure of about 2.8 bar was achieved in the absorber vessel. The given absorber size was thus sufficient to accomplish complete vapor absorption at the corresponding experimental conditions.

A finite difference numerical model was developed to predict the minimum absorber size needed to accomplish complete absorption in both designs. A comparison

between numerical and experimental results was then performed to determine the validity of the numerical model. Numerical simulations were run for each experiment to find the theoretical minimum number of rows of tubes needed to accomplish complete absorption. The input parameters of the numerical simulation were obtained from the corresponding experiment which includes temperature, pressure, concentration, and flow rates of the weak solution, vapor, and coolant. The predicted number of rows was then compared with the actual number of rows used in the experimental analysis.

An assessment of the uncertainty associated with the numerical analysis is also required when a comparison between experimental and numerical results is done. The major reasons for deviation include the errors in the theoretical representation of a physical phenomenon, the errors in their numerical implementation, and the uncertainty of the input parameters of the numerical analysis. The errors in numerical implementation are primarily due to the mathematical approximation of a 3-dimensional system with a 1-dimensional analysis at a set of discrete locations in space, and the round-off error from the computer. An uncertainty analysis was performed on the numerical model to account the effect of the uncertainty of the input parameters. The measured experimental values of temperature, pressure, concentration and flow rates of weak solution, vapor and coolant are input into the numerical model. Thus, uncertainties in these measurement results in uncertainty in the numerical results. The dimensional parameters are also the input in the numerical model. However, the uncertainties in dimensional parameters are quite small, and their effect on the overall uncertainty in predicting the absorber size is negligible. Perturbation method was used to estimate the sensitivity of predicted number of rows to uncertainties in various input parameters. The uncertainty in the prediction of

absorber size for a representative test at the baseline conditions was estimated to be ±12.3 rows of tubes for both designs.

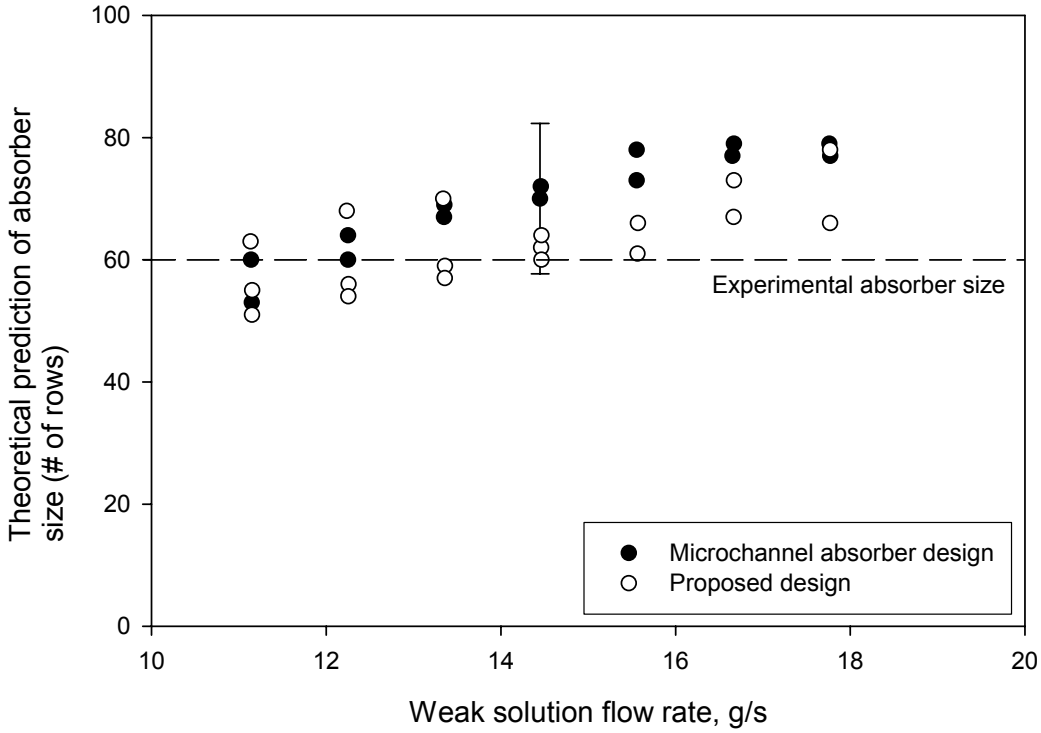

Figure 5-5. Comparison of numerical and experimental results for the variation in weak solution flow rate (The baseline conditions listed in Table 5-1 and other experimental conditions were used as input to the numerical model)

Figures 5-5 and 5-6 show the deviation of the size predicted by the numerical model from the actual absorber size in the experimental investigation. The numerical and experimental results compare reasonably well with some deviation at low temperature of coolant and high flow rate of weak solution. If an uncertainty of ±12.3 rows of tubes is assumed to hold for all the experiments conducted for various weak solution flow rates and coolant inlet temperatures, 58% and 79% of the total experiments on microchannel absorber and proposed design, respectively, show a good agreement with the experimental results.

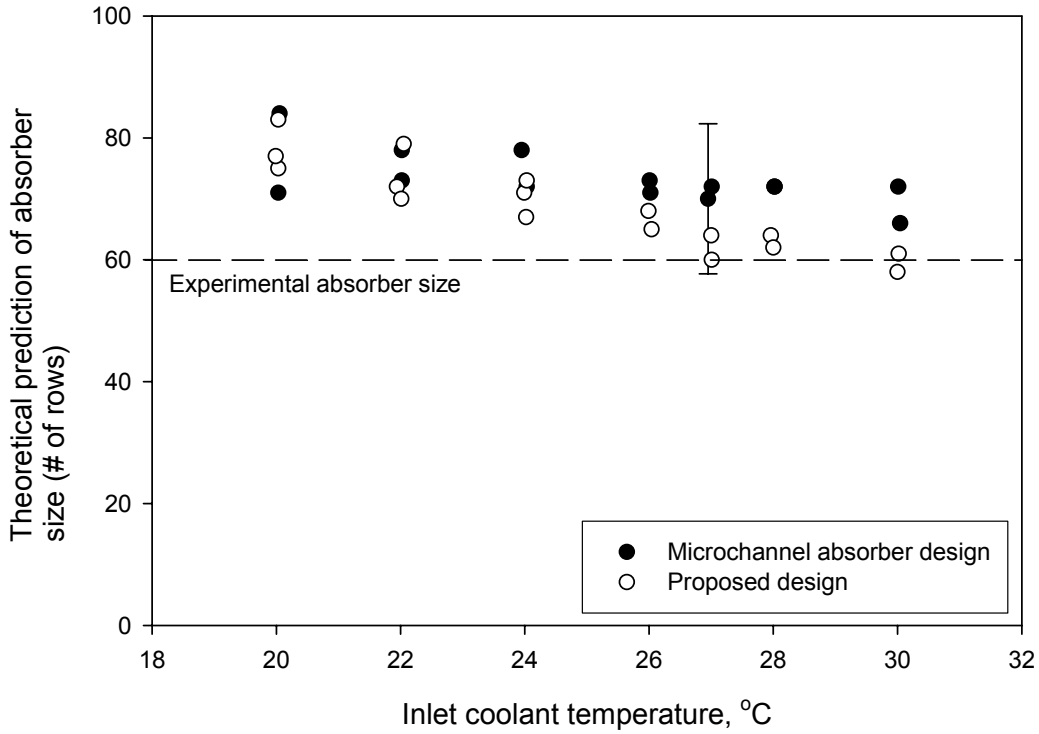

Figure 5-6. Comparison of numerical and experimental results for the variation in coolant inlet temperature (The baseline conditions listed in Table 5-1 and other experimental conditions were used as input to the numerical model)

As shown in Figures 5-5 and 5-6, the numerical model mostly over-predicts the size for both designs. This trend is more pronounced in the case of the microchannel absorber than the proposed design. This trend is expected as the current numerical analysis completely neglects the adiabatic absorption of vapor that takes place between the horizontal tubes of the microchannel absorber. The transfer of weak solution between the horizontal tubes of the microchannel absorber occurs in the form of droplets, and the surfaces of these newly formed droplets provide extra areas for vapor absorption.

The over prediction of absorber size in the case of proposed design may be largely due to the non consideration of heat conduction from the coolant tubes to the metallic mesh in the numerical model. The screen mesh used in this experimental investigation is

made of aluminum, which is a highly thermally conductive material with conductivity of about 200 W/m-K. As the screen mesh is mechanically wrapped around the horizontal tubes, the thermal resistance between the coolant tubes and screen mesh to be assumed very large, and thus heat conduction was neglected in the numerical analysis. However, the metallic screen mesh can dissipate heat through conduction by acting as a fin.

There is also a visible trend in the deviation between the predicted and the actual sizes with the variation of the weak solution flow rate. As the flow rate of weak solution is increased, the deviation of the numerical model increases in the positive direction for both designs. The correlation used to estimate the heat transfer coefficient of a falling film, and the assumption of complete wetting conditions can lead us to the possible explanation behind this trend. The correlation developed by Wilke (Yih, 1986) is based on simple convective heating of a laminar falling film over the vertical flat plates. The unavailability of the correlation for the falling film over horizontal tubes led to the use of the heat transfer correlation for wetted wall columns. The correlation predicts a decrease in the falling film heat transfer coefficient with the increase in the flow rate of the falling film. The assumption of complete wetting of the coolant tubes will therefore cause a decrease in the *UA* product with an increase in the flow rate of the falling film. However, the experimental results for *UA* show that its value is unaffected by the weak solution flow rate. This discrepancy is due to the estimation of falling film heat transfer coefficient and assumption of complete wetting conditions of the falling film, which thereby can lead to an over-prediction of the absorber size with the increase in the weak solution flow rate.

As evident from Figure 5-6, a similar increase in the extent of over prediction of the absorber size is observed with a decrease in the inlet temperature of the coolant stream. A reason behind this deviation is unknown. The coolant tubes are brazed to stainless steel headers of 1/2 inch outer diameter and 0.12 inch wall thickness. The headers in the current experimental study were not insulated. The heat transfer due to forced convection between the metallic header and vapor was neglected in the numerical model, which could be a possible reason behind the increase in over prediction of absorber size with the decrease in inlet coolant temperature.

CHAPTER 6
SUMMARY, CONCLUSIONS AND RECOMMENDATIONS

A new concept of forming a falling film in between the horizontal coolant tubes by a flow guidance medium like a mesh is proposed. The design utilizes the unused vertical spacing between the coolant tubes to form a double-sided falling film which consequently leads to an increase in the mass transfer area. The new design is numerically and experimentally compared to the horizontal microchannel type falling film absorber.

The numerical technique is developed to model the counter-current flow absorbers while accounting for the liquid and vapor phase mass transfer resistances in the falling film absorption. It also considers the coupled nature of heat and mass transfer processes. The advantage of increasing the mass transfer area by forming the falling film between the non-utilized vertical spacing is evident from the numerical results. The numerical analysis showed that

1. For the operating conditions considered, the liquid mass transfer resistance was found to control the overall absorption process.
2. The liquid-vapor interface temperature is always greater than the bulk liquid temperature.
3. The liquid-side heat transfer resistance is negligible in comparison to the other constituents of heat transfer resistance.
4. The proposed design is more compact and efficient than the falling film absorber based on small diameter coolant tubes. Size reduction of about 29% is possible for the operating conditions considered.

The experiments conducted on the proposed design and the conventional microchannel absorber shows that the absorber heat load of the proposed design is about

17-26% higher than the microchannel design. The *UA* value is found to increase by about 50% with an introduction of the screen mesh. This is attributable to the fact that the screen mesh enhances both mixing and wetting action in the liquid film. Some other phenomena associated with the proposed design are the increase in liquid hold-up, prevention of satellite droplets and fin-effect of the metallic mesh. These effects may also contribute in enhancing the performance of the proposed design.

The following recommendations should be considered for future work in this area:

1. The numerical model should be improved to consider adiabatic absorption of vapor taking place in between the horizontal tubes of the microchannel design.

2. If the screen mesh wrapped in between the horizontal tubes is made up of a highly thermally conductive material like aluminum, the screen mesh can act as fins. Thus, heat conduction from the coolant tubes to the metallic mesh should be considered in numerical modeling of the proposed design. This improvement in the current numerical scheme can be done by determining the thermal resistance between the coolant tubes and the screen mesh.

3. A better correlation for estimating the heat transfer coefficient of the falling film is required. The liquid-side heat transfer coefficient used in the current numerical analysis is based on simple convective heating of a falling film over the vertical flat plates.

4. The coolant tubes used in this experimental study are stainless steel tubing of 1/8 inch outer diameter and 0.016 inch wall thickness. The selection of coolant tubes in the current analysis was based on the practical constraints in fabricating the assembly. However, it is recommended that the diameter and the material of the coolant tubes be optimized in the future. The use of smaller diameter coolant tubes can further enhance the coolant side heat transfer coefficient for laminar flow. However, the pressure drop across the coolant tubes should also be considered while deciding on the parallel-series arrangement of the tubes.

5. The properties of mesh strongly affect the wettability, turbulence and liquid-interface area of the falling film. Heat conduction from a thermally conductive mesh can also play a major role in the selection of mesh. Therefore, it is recommended that the screen mesh properties such as material, mesh style, open area and mesh size be optimized in the future.

6. A visual observation of the wetting characteristics of the falling film is highly desired. In the current experimental setup, the transparent vessel had optical

distortion due to the cylindrical curvature of glass and presence of condensate over the inner surface.

7. The experiments were conducted for the operating conditions encountered in the combined power and cooling cycle. These operating conditions are also common to single-stage ammonia-water absorption systems. It is recommended to also experimentally verify the compactness of the proposed design for the NH_3-H_2O generator-absorber heat exchange (GAX) cycle. The GAX cycle is widely used in water chiller applications, and has slightly higher absorber pressure.

APPENDIX A
THERMODYNAMIC PROPERTIES OF AMMONIA-WATER MIXTURE

Thermodynamic properties of ammonia-water mixture are based on the empirical correlations given by Ziegler and Trepp (1984). The correlations use Gibbs excess energy method for the mixtures, and bubble and dew point temperature correlations for the phase equilibrium. They provided equations of state for the liquid and vapor phases of the pure components, while in case of mixtures the deviation from ideal solution behavior was accounted by the Gibbs excess energy method. Developed correlations are valid in the 0.2-110 bar pressure range and 230-600 K temperature range. The correlation reproduces the experimental data available in the literature with good accuracy (Xu and Goswami, 1999).

The Gibbs energy in integral form is defined as

$$G = H_0 - TS_0 + \int_{T_0}^{T} C_P dT + \int_{P_0}^{P} \nu dP - T\int_{T_0}^{T} \frac{C_P}{T} dT \qquad \text{(A-1)}$$

where subscript 0 signifies the reference state of the pure component. Ziegler and Trepp assumed the liquid heat capacity to be second order in temperature, and the liquid phase volume to be first order in pressure and second order in temperature. It yields the following equations:

$$\nu_L = a_1 + a_2 P + a_3 T + a_4 T^2 \qquad \text{(A-2)}$$

$$C_{P,L} = b_1 + b_2 T + b_3 T^2 \qquad \text{(A-3)}$$

Similarly the corresponding vapor phase relations are defined as

$$\nu_V = \frac{RT}{P} + c_1 + \frac{c_2}{T^3} + \frac{c_3}{T^{11}} + \frac{c_4 P^2}{T^{11}} \qquad \text{(A-4)}$$

$$C_{P,V} = d_1 + d_2 T + d_3 T^2 \tag{A-5}$$

Application of the above-defined volume and heat capacity empirical relations to the integral form of Gibbs energy yields the following liquid and vapor phase equations in the reduced form.

For the liquid phase:

$$\begin{aligned} G_{r,L} = {} & H_{r,0,L} - T_r S_{r,0,L} + B_1\left(T_r - T_{r,0}\right) + \frac{B_2}{2}\left(T_r^2 - T_{r,0}^2\right) + \frac{B_3}{3}\left(T_r^3 - T_{r,0}^3\right) \\ & - B_1 T_r \ln\left(\frac{T_r}{T_{r,0}}\right) - B_2 T_r\left(T_r - T_{r,0}\right) - \frac{B_3}{2} T_r\left(T_r^2 - T_{r,0}^2\right) \\ & + \left(A_1 + A_3 T_r + A_4 T_r^2\right)\left(P_r - P_{r,0}\right) + \frac{A_2}{2}\left(P_r^2 - P_{r,0}^2\right) \end{aligned} \tag{A-6}$$

For the vapor phase:

$$\begin{aligned} G_{r,V} = {} & H_{r,0,V} - T_r S_{r,0,V} + D_1\left(T_r - T_{r,0}\right) + \frac{D_2}{2}\left(T_r^2 - T_{r,0}^2\right) + \frac{D_3}{3}\left(T_r^3 - T_{r,0}^3\right) \\ & - D_1 T_r \ln\left(\frac{T_r}{T_{r,0}}\right) - D_2 T_r\left(T_r - T_{r,0}\right) - \frac{D_3}{2} T_r\left(T_r^2 - T_{r,0}^2\right) + T_r \ln\left(\frac{P_r}{P_{r,0}}\right) \\ & + C_1\left(P_r - P_{r,0}\right) + C_2\left(\frac{P_r}{T_r^3} - 4\frac{P_{r,0}}{T_{r,0}^3} + 3\frac{P_{r,0}T_r}{T_{r,0}^4}\right) \\ & + C_3\left(\frac{P_r}{T_r^{11}} - 12\frac{P_{r,0}}{T_{r,0}^{11}} + 11\frac{P_{r,0}T_r}{T_{r,0}^{12}}\right) \\ & + \frac{C_4}{3}\left(\frac{P_r^3}{T_r^{11}} - 12\frac{P_{r,0}^3}{T_{r,0}^{11}} + 11\frac{P_{r,0}^3 T_r}{T_{r,0}^{12}}\right) \end{aligned} \tag{A-7}$$

The thermodynamic properties in the reduced form for the reference state of T_B = 100 K, P_B = 10 bar, and R = 8.314 kJ/kmole-K are defined as

$$T_r = \frac{T}{T_B} \tag{A-8}$$

$$P_r = \frac{P}{P_B} \tag{A-9}$$

$$G_r = \frac{MG}{RT_B} \tag{A-10}$$

$$H_r = \frac{MH}{RT_B} \tag{A-11}$$

$$S_r = \frac{MS}{R} \tag{A-12}$$

$$\nu_r = \frac{M\nu P_B}{RT_B} \tag{A-13}$$

The coefficients for empirical Gibbs energy equations are determined by fitting the experimental data and are listed in Table A-1.

Table A-1. Coefficients for the Gibbs energy relation

Coefficient	Ammonia	Water
A_1	3.971423×10^{-2}	2.748796×10^{-2}
A_2	-1.790557×10^{-5}	-1.016665×10^{-5}
A_3	-1.308905×10^{-2}	-4.452025×10^{-3}
A_4	3.752836×10^{-3}	8.389246×10^{-4}
B_1	$1.634519\times10^{+1}$	$1.214557\times10^{+1}$
B_2	-6.50812	-1.89807
B_3	1.448937	2.911966×10^{-1}
C_1	-1.049377×10^{-2}	2.136131×10^{-2}
C_2	-8.28822	$-3.169291\times10^{+1}$
C_3	$-6.647257\times10^{+2}$	$-4.634611\times10^{+4}$
C_4	$-3.04532\times10^{+3}$	0
D_1	3.673647	4.01917
D_2	9.989629×10^{-2}	-5.175550×10^{-2}
D_3	3.617622×10^{-2}	1.951939×10^{-2}
$H_{r,0,L}$	4.878576	21.82114
$H_{r,0,V}$	26.46887	60.96506
$S_{r,0,L}$	1.644773	5.733498

Table A-1 Continued

Coefficient	Ammonia	Water
Sr,0,V	8.339026	13.45343
Tr,0	3.2252	5.0705
Pr,0	2	3

(Ziegler and Trepp, 1984)

Maxwell relations are used to obtain other thermodynamic properties of the pure fluids, namely specific enthalpy, entropy, and volume. The relations are obtained by differentiating the reduced form of Gibbs energy function, and can be written as

$$H = -\frac{RT_B T_r^2}{M}\left[\frac{\partial}{\partial T_r}\left(\frac{G_r}{T_r}\right)\right]_{P_r} \tag{A-14}$$

$$S = -\frac{R}{M}\left[\frac{\partial G_r}{\partial T_r}\right]_{P_r} \tag{A-15}$$

$$\nu = \frac{RT_B}{MP_B}\left[\frac{\partial G_r}{\partial P_r}\right]_{T_r} \tag{A-16}$$

The above-mentioned equations are valid for pure fluids. The thermodynamic properties of a mixture deviate significantly from the ideal mixing behavior when a mixture undergoes a chemical reaction. To determine the properties of the ammonia-water gaseous mixture, the vapor mixture is assumed to behave ideally. The enthalpy, entropy and volume of the vapor mixture are computed by proportionally adding the corresponding pure component properties on the basis of their mole fraction. However, an extra entropic term S^{mix} accounts the entropy deviation from ideal mixing of the gaseous components.

$$H_{\text{aw}(V)} M_{\text{aw}(V)} = \tilde{y} H_{\text{NH}_3(V)} M_{\text{NH}_3} + \left(1 - \tilde{y}\right) H_{\text{H}_2\text{O}(V)} M_{\text{H}_2\text{O}} \tag{A-17}$$

$$S_{\text{aw}(V)} M_{\text{aw}(V)} = \tilde{y} S_{\text{NH}_3(V)} M_{\text{NH}_3} + \left(1 - \tilde{y}\right) S_{\text{H}_2\text{O}(V)} M_{\text{H}_2\text{O}} + S^{\text{mix}} M_{\text{aw}(V)} \tag{A-18}$$

$$\nu_{\mathrm{aw}(V)} M_{\mathrm{aw}(V)} = \tilde{y}\,\nu_{\mathrm{NH_3}(V)}\nu_{\mathrm{NH_3}} + \left(1-\tilde{y}\right)\nu_{\mathrm{H_2O}(V)} M_{\mathrm{H_2O}} \tag{A-19}$$

$$S^{\mathrm{mix}} = -\frac{R}{M_{\mathrm{aw}(V)}}\left\{\tilde{y}\ln\left(\tilde{y}\right)+\left(1-\tilde{y}\right)\ln\left(1-\tilde{y}\right)\right\} \tag{A-20}$$

For the liquid mixture, the deviation from ideal behavior is accounted by Gibbs excess energy G^E. Redlich and Kester proposed the correlation for Gibbs excess energy of the liquid mixture, and is expressed as (Ziegler and Trepp, 1984).

$$G_r^E = (1-\tilde{x})\left\{F_1 + F_2\left(2\tilde{x}-1\right) + F_3\left(2\tilde{x}-1\right)^2\right\} \tag{A-21}$$

where F_1, F_2, and F_3 are the functions of reduced pressure and temperature, and are defined as

$$F_1 = E_1 + E_2 P_r + \left(E_3 + E_4 P_r\right)T_r + \frac{E_5}{T_r} + \frac{E_6}{T_r^2} \tag{A-22}$$

$$F_2 = E_7 + E_8 P_r + \left(E_9 + E_{10} P_r\right)T_r + \frac{E_{11}}{T_r} + \frac{E_{12}}{T_r^2} \tag{A-23}$$

$$F_3 = E_{13} + E_{14} P_r + \frac{E_{15}}{T_r} + \frac{E_{16}}{T_r^2} \tag{A-24}$$

The constants E_1-E_{16} are determined by the regression analysis of experimental data, and are listed in Table A-2.

Table A-2. Coefficients for the Gibbs excess energy relation

E_1	-41.733398	E_9	0.387983
E_2	0.02414	E_{10}	-0.004772
E_3	6.702285	E_{11}	-4.648107
E_4	-0.011475	E_{12}	0.836376
E_5	63.608967	E_{13}	-3.553627
E_6	-62.490768	E_{14}	0.000904
E_7	1.761064	E_{15}	24.361723
E_8	0.008626	E_{16}	-20.736547

(Ibrahim and Klein, 1993)

Gibbs excess energy function can be then differentiated according to the previously mentioned Maxwell relations, to determine the excess specific enthalpy, entropy and volume. Therefore, liquid mixture properties can be obtained by the following equations.

$$H_{\mathrm{aw}(L)}M_{\mathrm{aw}(L)} = \tilde{x}\,H_{\mathrm{NH_3}(L)}M_{\mathrm{NH_3}} + \left(1-\tilde{x}\right)H_{\mathrm{H_2O}(L)}M_{\mathrm{H_2O}} + H^{E}M_{\mathrm{aw}(L)} \tag{A-25}$$

$$S_{\mathrm{aw}(L)}M_{\mathrm{aw}(L)} = \tilde{x}\,S_{\mathrm{NH_3}(L)}M_{\mathrm{NH_3}} + \left(1-\tilde{x}\right)S_{\mathrm{H_2O}(L)}M_{\mathrm{H_2O}} + S^{E}M_{\mathrm{aw}(L)} + S^{\mathrm{mix}}M_{\mathrm{aw}(L)} \tag{A-26}$$

$$\nu_{\mathrm{aw}(L)}M_{\mathrm{aw}(L)} = \tilde{x}\,\nu_{\mathrm{NH_3}(L)}M_{\mathrm{NH_3}} + \left(1-\tilde{x}\right)\nu_{\mathrm{H_2O}(L)}M_{\mathrm{H_2O}} + \nu^{E}M_{\mathrm{aw}(L)} \tag{A-27}$$

$$S^{\mathrm{mix}} = -\frac{R}{M_{\mathrm{aw}(L)}}\left\{\tilde{x}\ln\left(\tilde{x}\right)+\left(1-\tilde{x}\right)\ln\left(1-\tilde{x}\right)\right\} \tag{A-28}$$

Bubble and dew point temperatures are required to determine the phase equilibrium. Empirical correlations proposed by El-Sayed and Tribus (1985) are used to calculate the bubble and dew point temperatures of the ammonia-water mixture. The correlations can be expressed as

$$T_b = T_c - \sum_{i=1}^{7}\left(C_i + \sum_{j=1}^{10}C_{ij}x^{j}\right)\left[\ln\left(\frac{P_c}{P}\right)\right]^{i} \tag{A-29}$$

$$T_d = T_c - \sum_{i=1}^{6}\left\{A_i + \sum_{j=1}^{4}A_{ij}\left[\ln\left(1.0001-x\right)\right]^{j}\right\}\left[\ln\left(\frac{P_c}{P}\right)\right]^{i} \tag{A-30}$$

The critical temperature T_c and pressure P_c of the mixture are given by

$$T_c = T_{c,H_2O} - \sum_{i=1}^{4}a_i x^{i} \tag{A-31}$$

$$P_c = P_{c,H_2O} \exp\left(\sum_{i=1}^{8} b_i x^i \right) \tag{A-32}$$

The above equations yield bubble, dew and critical temperatures in °R and critical pressures in psia. The constants a_i, b_i, A_i, C_i, A_{ij}, and C_{ij} are listed in Table A-3.

Table A-3. Coefficients for the bubble, dew point and critical temperatures, and critical pressure correlations of the ammonia-water mixture

a_i	a_1	205.8889	a_2	280.930556
	a_3	-317.0138889	a_4	263.194444
A_i	A_1	153.170553460	A_2	-11.7705687461
	A_3	-1.78126355957	A_4	0.647385455059
	A_5	-0.0719950751898	A_6	0.00285423950786
A_{ij}	$A_{1,1}$	194.793913463	$A_{1,2}$	74.236124188
	$A_{1,3}$	9.84103819552	$A_{1,4}$	0.436843852745
	$A_{2,1}$	-74.3508283362	$A_{2,2}$	-33.2941879809
	$A_{2,3}$	-4.78866918581	$A_{2,4}$	-0.225416733476
	$A_{3,1}$	13.0175447367	$A_{3,2}$	6.1586564117
	$A_{3,3}$	0.789740337141	$A_{3,4}$	0.0321510834958
	$A_{4,1}$	-0.90857587517	$A_{4,2}$	-0.356752691147
	$A_{4,3}$	0.0238067275502	$A_{4,4}$	0.00495593933952
	$A_{5,1}$	-0.00071863574153	$A_{5,2}$	-0.0251026383533
	$A_{5,3}$	-0.0191664613304	$A_{5,4}$	-0.0017014253867
	$A_{6,1}$	0.00195441702983	$A_{6,2}$	0.00280533348937
	$A_{6,3}$	0.0013899436563	$A_{6,4}$	0.000116422611616
b_i	b_1	0.368105523897	b_2	-3.6679548875
	b_3	46.6000470809	b_4	-262.921061996
	b_5	732.99536936	b_6	-1076.0613489
	b_7	797.948078048	b_8	-235.903904222
C_i	C_1	153.634521459	C_2	-13.0305543892
	C_3	-1.14845282991	C_4	0.550358094447
	C_5	-0.0753450148427	C_6	0.0048111666267
	C_7	-0.000120433757177		
C_{ij}	$C_{1,1}$	-462.460321366	$C_{1,2}$	23739.9986309
	$C_{1,3}$	-194504.35292	$C_{1,4}$	639383.528867
	$C_{1,5}$	-523748.057636	$C_{1,6}$	-2328271.47551
	$C_{1,7}$	7562418.53499	$C_{1,8}$	-9668295.89504

Table A-3 Continued

$C_{1,9}$	5922081.87086	$C_{1,10}$	-1432405.52125
$C_{2,1}$	421.443122208	$C_{2,2}$	-14560.354925
$C_{2,3}$	53051.4495633	$C_{2,4}$	382763.793582
$C_{2,5}$	-3583589.86875	$C_{2,6}$	12243265.3815
$C_{2,7}$	-22307970.0156	$C_{2,8}$	22896656.8499
$C_{2,9}$	-12483324.8091	$C_{2,10}$	2813311.71633
$C_{3,1}$	-248.783804168	$C_{3,2}$	4807.07241098
$C_{3,3}$	13565.1003309	$C_{3,4}$	-466407.780832
$C_{3,5}$	2827083.44764	$C_{3,6}$	-8469715.15799
$C_{3,7}$	14459588.8962	$C_{3,8}$	-14281087.5331
$C_{3,9}$	7596403.59678	$C_{3,10}$	-1684002.64482
$C_{4,1}$	126.965580728	$C_{4,2}$	-2090.45270574
$C_{4,3}$	1993.17101166	$C_{4,4}$	100706.510396
$C_{4,5}$	-687388.808612	$C_{4,6}$	2132412.46959
$C_{4,7}$	-3699199.65914	$C_{4,8}$	3688365.22546
$C_{4,9}$	-1975122.39296	$C_{4,10}$	440201.446068
$C_{5,1}$	-33.5343446156	$C_{5,2}$	601.878586689
$C_{5,3}$	-3064.82070658	$C_{5,4}$	71.7954752052
$C_{5,5}$	51780.666659	$C_{5,6}$	-209714.899856
$C_{5,7}$	405011.985355	$C_{5,8}$	-428310.461566
$C_{5,9}$	238153.698326	$C_{5,10}$	-54497.0973336
$C_{6,1}$	3.97454953787	$C_{6,2}$	-77.026846469
$C_{6,3}$	541.19105807	$C_{6,4}$	-1696.60270972
$C_{6,5}$	1713.45942707	$C_{6,6}$	4019.01019872
$C_{6,7}$	-14844.7928004	$C_{6,8}$	19481.0094551
$C_{6,9}$	-12107.0794501	$C_{6,10}$	2966.92804386
$C_{7,1}$	-0.170806170177	$C_{7,2}$	3.48182859299
$C_{7,3}$	-27.7957587743	$C_{7,4}$	113.762064546
$C_{7,5}$	-258.750496922	$C_{7,6}$	311.002585218
$C_{7,7}$	-123.917993454	$C_{7,8}$	-123.480627492
$C_{7,9}$	154.375042114	$C_{7,10}$	-48.50838287

(El-Sayed and Tribus, 1985)

APPENDIX B
TRANSPORT PROPERTIES OF AMMONIA-WATER MIXTURE

In absorption, the diffusion coefficient of the solute in the solvent, thermal conductivity, and viscosity strongly influence the mass transfer process. Thermal conductivity and viscosity data for the liquid and vapor phases of the pure compounds have been compiled and correlated by Yaws (1995a & 1995b). The correlations are based on the regression analysis of the experimental and estimated values. The estimated values were obtained by using Chapman-Enskog and Reichenberg techniques.

For the liquid phase:

$$\lambda_{H_2O(L)} = -0.2758 + \left(4.612\times10^{-3}\right)T - \left(5.5391\times10^{-6}\right)T^2 \tag{B-1}$$

$$\lambda_{NH_3(L)} = 1.1606 - \left(2.284\times10^{-3}\right)T + \left(3.1245\times10^{-18}\right)T^2 \tag{B-2}$$

$$\log_{10}\mu_{H_2O(L)} = -10.2158 + \frac{\left(1.7925\times10^{3}\right)}{T} + \left(1.773\times10^{-2}\right)T - \left(1.2631\times10^{-5}\right)T^2 \tag{B-3}$$

$$\log_{10}\mu_{NH_3(L)} = -8.591 + \frac{\left(8.764\times10^{2}\right)}{T} + \left(2.681\times10^{-2}\right)T - \left(3.612\times10^{-5}\right)T^2 \tag{B-4}$$

For the vapor phase:

$$\lambda_{H_2O(V)} = 0.00053 + \left(4.7093\times10^{-5}\right)T + \left(4.9551\times10^{-8}\right)T^2 \tag{B-5}$$

$$\lambda_{NH_3(V)} = 0.00457 + \left(2.3239\times10^{-5}\right)T + \left(1.481\times10^{-7}\right)T^2 \tag{B-6}$$

$$\mu_{H_2O(V)} = -36.8255 + \left(4.2916\times10^{-1}\right)T - \left(1.624\times10^{-5}\right)T^2 \tag{B-7}$$

$$\mu_{NH_3(V)} = -7.8737 + \left(3.6745\times10^{-1}\right)T - \left(4.4729\times10^{-6}\right)T^2 \quad \text{(B-8)}$$

In the above relations, gas viscosity is in micropoise, liquid viscosity is in centipoise, thermal conductivity is in W/m-K and temperature is in Kelvin.

The following correlations were used to estimate the diffusion coefficient and viscosity of the ammonia-water liquid mixture (Frank et al., 1996). The correlations are not valid for pure water, as the dissociation of ammonia is large at low ammonia mass fractions. T (K) is the temperature, D_{aw} (m^2/s) is the diffusion coefficient, and μ_{aw} (Pa-s) is the dynamic viscosity.

$$\mu_{aw(L)} = \left\{\left(0.67 + 0.78\,\tilde{x}\right)\times10^{-6}\right\} e^{\frac{17900}{RT}} \quad \text{(B-9)}$$

$$D_{aw(L)} = \left\{\left(1.65 + 2.47\,\tilde{x}\right)\times10^{-6}\right\} e^{\frac{-16600}{RT}} \quad \text{(B-10)}$$

To determine the diffusion coefficient of the binary gaseous mixture, Fuller et al. (1965, 1969) has developed a correlation that retains the general form of the equation originally derived by Chapman-Enskog, with empirical constants based on the experimental data.

$$D_{aw(V)} = \frac{0.00143T^{1.75}}{PM_{12}^{1/2}\left[\left(\Sigma_v\right)_1^{1/3} + \left(\Sigma_v\right)_2^{1/3}\right]^2} \quad \text{(B-11)}$$

with M_{12} being $M_{12} = 2\left[\left(1/M_1\right) + \left(1/M_2\right)\right]^{-1}$ (B-12)

where

D_{aw} = Diffusion coefficients, cm^2/s

T = Temperature, K

P = Pressure, bar

M_1, M_2 = Molecular weight of ammonia and water, kg/kmole

Σ_V is determined by adding the atomic diffusion volumes of the basic elements.

$$\left(\Sigma_V\right)_{H_2O} = 20.7 \tag{B-13}$$

$$\left(\Sigma_V\right)_{NH_3} = 13.1 \tag{B-14}$$

Wilke (1950) method is used to compute the viscosity of the gaseous mixture. He employed the simplified approach of Chapman-Enskog's kinetic theory by neglecting the second order effect of the gaseous constituents. The viscosity correlation for the binary system is given by

$$\mu_{aw(V)} = \left[\frac{\tilde{y}_1 \mu_1}{\tilde{y}_1 + \tilde{y}_2 \phi_{12}} + \frac{\tilde{y}_2 \mu_2}{\tilde{y}_2 + \tilde{y}_1 \phi_{21}}\right] \tag{B-15}$$

$$\text{with } \phi_{12} = \frac{\left[1 + \left(\mu_1 / \mu_2\right)^{1/2} \left(M_2 / M_1\right)^{1/4}\right]^2}{\left[8\left(1 + M_1 / M_2\right)\right]^{1/2}} \tag{B-16}$$

$$\phi_{21} = \phi_{12} \frac{\mu_2 M_1}{\mu_1 M_2} \tag{B-17}$$

where μ is the viscosity, M is the molecular weight, and $\tilde{y}$ is the mole fraction of the components in mixture.

The Jamieson et al. (1975) method is adapted to estimate the thermal conductivity of the binary liquid mixtures.

$$\lambda_{aw(L)} = x_1\lambda_1 + x_2\lambda_2 - \alpha\left(\lambda_2 - \lambda_1\right)\left[1 - x_2^{1/2}\right]x_2 \tag{B-18}$$

with x_1, x_2 the mass fraction and λ_1, λ_2 the thermal conductivity of 1 and 2 components. In the correlation, the components are chosen such that $\lambda_2 \geq \lambda_1$. α is the characteristic parameter of the binary mixture and can be taken as unity if the experimental data are unavailable for the regression analysis.

An analogous form to the theoretical relation for viscosity of a gaseous mixture is used to estimate the thermal conductivity of a multi-component gaseous mixture (Reid et al., 1987).

$$\lambda_{aw(V)} = \left[\frac{\tilde{y}_1\lambda_1}{\tilde{y}_1 + \tilde{y}_2 A_{12}} + \frac{\tilde{y}_2\lambda_2}{\tilde{y}_2 + \tilde{y}_1 A_{21}}\right] \tag{B-19}$$

with λ the thermal conductivity, n the number of components, and $\tilde{y}$ the mole fraction of the components in mixture. A_{12} is determined by the following correlation (Mason and Saxena, 1958)

$$A_{12} = \frac{\varepsilon\left[1 + \left(\lambda_{tr1}/\lambda_{tr2}\right)^{1/2}\left(M_1/M_2\right)^{1/4}\right]}{\left[8\left(1 + M_1/M_2\right)\right]^{1/2}} \tag{B-20}$$

where

M = Molecular weight, kg/kmole

λ_t= Translational thermal conductivity

ε = 1.065

The ratio of translational thermal conductivity can be determined by

$$\frac{\lambda_{tr1}}{\lambda_{tr2}} = \frac{\Psi_2}{\Psi_1}\left[\frac{\exp\left(0.0464T_{r1}\right)-\exp\left(-0.2412T_{r1}\right)}{\exp\left(0.0464T_{r2}\right)-\exp\left(-0.2412T_{r2}\right)}\right] \tag{B-21}$$

where Ψ is the reduced inverse thermal conductivity and is given by

$$\Psi = 210\left(\frac{T_c M^3}{P_c^4}\right)^{1/6} \tag{B-22}$$

T_r is the reduced temperature, P_c (bar) is the critical pressure, and T_c (K) is the critical temperature. The temperature in reduced form T_r is defined as

$$T_r = \left(\frac{T}{T_c}\right) \tag{B-23}$$

APPENDIX C
EXPERIMENTAL DETAILS

This appendix provides the instrumentation details of the experimental setup. The basic operational principle of each instrument is followed by its specification, calibration technique, and measurement uncertainty. The appendix later presents the uncertainty of the derived measurements.

Specification and Uncertainty of Direct Measurements

The following table lists the specification of various measurement instruments as provided by the manufacturer.

Table C-1. Specification of the instruments used in the experimental setup

Component	Part Number/Model	Manufacturer	Specifications
Data Acquisition PC Interface	DaqBook 200	IOtech, Inc.	16-bit resolution analog to digital converter; 100 kHz sampling rate
Data Acquisition Software	LabVIEW	National Instruments	Version 7.0
Current/Voltage Measurement Card	DBK 15	IOtech, Inc.	16 channels; measures 4 – 20 mA as well as voltage up to ±30 V
Thermocouple Measurement Card	DBK 82	IOtech, Inc.	14 channels; 200 kHz maximum scan rate; measures thermocouple of type J, K, S, T, E, B, R, and N as well as voltage up to ± 100 mV, accuracy ±0.5 °C
Pressure Transducer (Absorber strong exit)	Model 68073-04	Cole Parmer Instrument Company	Range -14.7 – 60 psig; output 4 – 20 mA; input 24 VDC; accuracy ±0.13% full scale
Pressure Transducer (Absorber weak inlet)	Model 68073-06	Cole Parmer Instrument Company	Range -14.7 – 100 psig; output 4 – 20 mA; input 24 VDC; accuracy ±0.13% full scale

Table C-1 Continued

Component	Part Number/Model	Manufacturer	Specifications
Pressure Transducer (Absorber)	Model 68070-02	Cole Parmer Instrument Company	Range 0 – 50 psig; output 4 – 20 mA; input 24 VDC; accuracy ±0.13% full scale
Pressure Transducer (Absorber vapor inlet)	Model 07356-13	Cole Parmer Instrument Company	Range -14.7 – 60 psig; output 4 – 20 mA; input 24 VDC; accuracy ±0.4% full scale
Pressure Transducer (Boiler exit)	Model 256	Setra Systems, Inc.	Range 0 – 250 psig; output 4 – 20 mA; input 24 VDC; accuracy ±0.13% full scale
Differential Pressure Transducer (Absorber coolant)	Model 68071-58	Cole Parmer Instrument Company	Range 0 – 10 psid; output 4 – 20 mA; input 24 VDC ; accuracy ±0.25% full scale
Thermocouples	Model TMQSS	Omega Engineering, Inc.	T-type Copper-Constantan; ungrounded junction; 304 SS sheath; sheath diameter 0.125 inches; accuracy ±1°C
Flow Meter (Absorber coolant)	Model A1	Great Plains Industries, Inc.	Paddlewheel flow meter; range 0.3 – 3 gpm; accuracy ±1% full scale
Flow Meter (Strong solution)	Model 1110	Brooks Instrument	Variable area flow meter; range 0.11 – 1.11 gpm; accuracy ±1% full scale; calibrated at 0.833 sg and 1.08 cP
Flow Meter (Weak solution)	Model 1110	Brooks Instrument	Variable area flow meter; range 0.08 – 0.84 gpm; accuracy ±1% full scale; calibrated at 0.88 sg and 1.08 cP
Flow Meter (Vapor)	Model HO3/4X3/4	Hoffer Flow Controls, Inc.	Turbine flow meter; range 1.25 – 25 m3/hr; accuracy ±1% of reading
Gas Chromatograph	Model 8610-50	SRI Instruments	Thermal conductivity detector; column type HAYSEP T
Thermopile (Absorber coolant)		Made by myself	15 T-type junctions; thermocouple wire: Model TT-T-30 (Omega Engineering, Inc.)

This section also provides details of the calibration scheme used in the current experimental work. An instrument is usually not individually calibrated by the manufacture, rather a sample size of instruments are tested to obtain a generalized calibration curve. The variation among the sample size is overlapped by having a larger uncertainty band to eliminate the tedious and expensive calibration of individual instruments. Measurement inaccuracies are further increased by the introduction of external factors, such as installation, noise and environmental effects. Thus, the individual calibration of instruments is desired to ensure and improve the accuracy of a measurement. An effort was made to test the instruments for the validity of their measurement accuracy, and incorporate a correction factor to further improve their precision. Though most of the instruments are calibrated in the laboratory, the error of instruments as reported by the manufacturer is still used for the experimental analysis. Numerous unaccountable errors like installation, noise and environmental effects make it infeasible to predict the actual error of the device after calibration. The purpose of calibration was to improve the precision of instruments, and to ascertain that the error is within the uncertainty bands as mentioned by the manufacturer.

Thermocouple

Thermocouple is the most widely used temperature sensor as it is inexpensive, rugged and stable. It consists of two dissimilar metals joined together at one end by twisting, soldering or welding. It is based on the Seebeck effect; that is a temperature difference across the junction of dissimilar metals generates an electrical potential. The amount of voltage produced depends on the characteristics of both metals, and is proportional to the temperature difference. The induced voltage can thus be used to estimate the temperature difference across the junction. The reference junction was

traditionally kept in an ice bath. However, being inpractical for some conditions, the temperature of the reference junction was measured by a RTD/thermistor temperature sensor.

The current experimental system uses T-type thermocouples (copper-constantan junction) to measure the temperature at various state points. These measurements are recorded in a real time manner with the help of a temperature measurement card (DBK 82, IOtech, Inc.) and a PC data acquisition interface (DaqBook 200, IOtech, Inc.). A two-point calibration was performed on all the thermocouples by using melting ice and boiling water at atmospheric pressure as the reference temperatures. It yields a linear correction equation for the operating range of temperature considered in this experimental analysis. De-ionized water was used to achieve freezing and boiling points of water, and thereby, avoiding the effect of salts on the freezing and boiling points. All the vessels and thermocouple probes were also thoroughly rinsed with de-ionized water. Ice bath was prepared by putting slurry of crushed ice in a Dewar flask. Similarly, boiling point was achieved by boiling de-ionized water in an electric pot. Measurements were made after a period of 5-10 minutes of the immersion of probes into ice and boiling baths; it ensures a thermal equilibrium of probes with respect to the bath. The measurement readings at ice point and boiling point were an average of the multiple readings recorded at a sampling rate of 100 Hz for a period of 10 sec.

Thermopile

A thermopile is used to directly and precisely measure the temperature difference. It is constructed by connecting a number of thermocouples in series, and is represented in Figure C-1. As many thermocouples are connected in series, the total voltage across the thermopile is a sum of voltages produced by individual thermocouple pairs. Thermopiles

are inexpensive, rugged and stable; the characteristics inherited from thermocouples. A set of several thermocouple junctions being connected in series magnifies the voltage signal, and make thermopiles more sensitive and accurate than thermocouples.

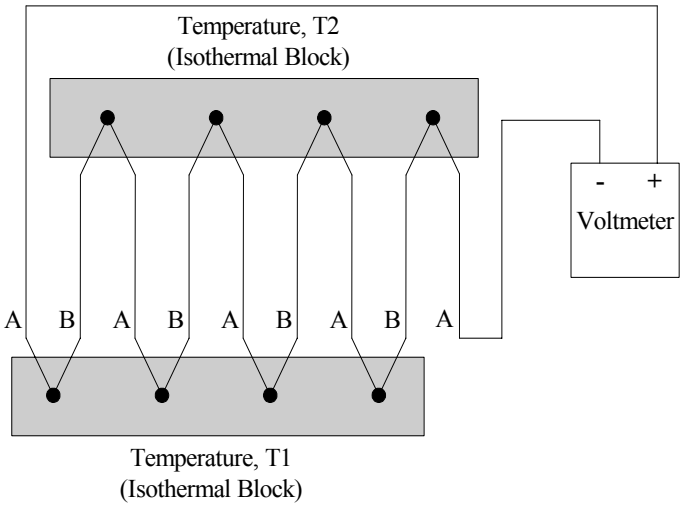

Figure C-1. A thermopile circuit with 4 thermocouple junctions

In the experimental setup for the thermodynamic cycle, a thermopile is used to measure the difference in temperature between the inlet and outlet flow streams of the coolant. The number of thermocouples to be connected in series is based on the accuracy of voltage measurement device and the desired accuracy of differential temperature. In the current experimental study, 15 thermocouple junctions were chosen to be connected in series. Thermocouple wire used for the purpose was a high grade copper-constantan with PFA sheath (TT-T-30, Omega Engineering Company). Thermocouple junctions were made by soldering the ends of dissimilar metals i.e. copper and constantan with tin/lead alloy. The wires were twisted around one another, and bonded with a very fine layer of tin-lead alloy to insure perfect thermal contact and minimal thermal effects of soldering alloy. In addition, a conventional thermocouple junction was also installed to measure the approximate temperature at each probe. All thermocouple junctions on both ends of thermopile were then packed in a Polyvinyl Chloride (PVC) housing of 5/8

inches in diameter, and were leak tightened with an epoxy. It allowed the installation of thermopile ends into standard Swagelok® tube fittings.

Thermopile needs to be calibrated to determine the relation between temperature difference and corresponding generation of emf *E(T)*. It is accomplished by measuring the Seebeck voltage produced at the known temperature difference across the two junctions. In this regard, one end of the thermopile is immersed in an ice bath, whereas another end is immersed in a constant temperature bath (Model 9501, PolyScience). The non-uniformity in temperature across the constant temperature bath is less than ±0.01°C. A high precision thermistor sensor (Model 4400, Ever Ready Thermometer Company, Inc.) having an uncertainty of ±0.015°C is used to measure the temperature of constant temperature bath. The temperature of constant temperature bath was then varied from 10 to 40°C at incremental steps of 0.5°C. The output of thermopile at all incremental steps of temperature was recorded by a voltage measurement card (DBK 15, IOtech, Inc.) having an accuracy of ±50μV. The regression of calibration data yields the following empirical correlations:

$$\begin{aligned} E(T) = {} & -2.35\times10^{-12}T^9 + 4.28\times10^{-10}T^8 - 3.11\times10^{-8}T^7 + 1.07\times10^{-6}T^6 \\ & -1.18\times10^{-5}T^5 - 3.73563\times10^{-4}T^4 + 0.015847801T^3 - 0.247202292T^2 \\ & +2.415909564T - 5.202883565 \end{aligned} \tag{C-1}$$

and

$$\begin{aligned} T(E) = {} & 1.87\times10^{-10}E^9 - 1.54\times10^{-8}E^8 + 2.74\times10^{-7}E^7 + 1.43\times10^{-5}E^6 \\ & -0.000843485T^5 + 0.019658477T^4 - 0.252258166T^3 + 1.850683238T^2 \\ & -5.531541618T + 11.47394167 \end{aligned} \tag{C-2}$$

Following procedure is then used to determine the temperature difference (Huang, 1990):

1. Measure the approximate temperatures at each probe, T_1 and T_2.

2. Calculate the average temperature, $T_{avg} = (T_1+T_2)/2$.

3. Determine the corresponding emf E_{avg} for T_{avg} using Eq. C-1.

4. Measure the induced Seebeck voltage across the thermopile ΔE.

5. Calculate E (= E_{avg} + $\Delta E/2$) and E' (= E_{avg} – $\Delta E/2$).

6. Determine the corresponding temperature, T and T' for the respective emf values, E and E' using Eq. C.2.

7. Calculate the desired temperature difference, $\Delta T = (T\text{-}T')$.

The sources of uncertainty in thermopile measurements are calibration uncertainties and uncertainties in the determination of average temperature T_{avg} and Seebeck voltage ΔE. The calibration error is due to the non-uniformity of ±0.01 °C across the constant temperature bath, uncertainty of ±0.015 °C in temperature measurement, and uncertainty of ±0.005 °C in representing experimental results with an empirical correlation. Thus, the combined uncertainty due to calibration is given by

$$\delta_{cal} = \left(0.01^2 + 0.015^2 + 0.005^2\right)^{1/2} = \pm 0.0187 \text{ °C} \tag{C-3}$$

The error in thermopile measurement due to the uncertainty in voltage measurement is given by

$$\left(\frac{\partial \Delta T}{\partial \Delta E}\right)\delta_{\Delta E} = 1.65\frac{\text{°C}}{\text{mV}} \times 0.05\text{mV} = \pm 0.0825 \text{ °C} \tag{C-4}$$

As T-type thermocouples approximately exhibit a linear increase in voltage with temperature, $\partial\Delta T/\partial\Delta E$ is equated to the average slope of emf-T calibration curve. Similarly, thermopile error due to the uncertainty in determining the average temperature is given by

$$\left[\left(\frac{\partial \Delta T}{\partial T_1}\right)^2 \delta_{T_1}^2 + \left(\frac{\partial \Delta T}{\partial T_2}\right)^2 \delta_{T_2}^2\right]^{1/2} = \pm 0.0061 \text{ °C} \quad \text{(C-5)}$$

where the sensitivity of thermocouple uncertainty on thermopile measurements is computed by forward difference scheme. It was computed for the baseline experimental conditions at which the inlet and outlet temperature of the coolant is about 27 °C and 37 °C, respectively. The overall uncertainty in thermopile measurements is then represented as root sum square of uncertainties by all the above mentioned sources, and is given by

$$\delta_{\Delta T} = \left[\delta_{cal}^2 + \left(\frac{\partial \Delta T}{\partial \Delta E}\right)^2 \delta_{\Delta E}^2 + \left(\frac{\partial \Delta T}{\partial T_1}\right)^2 \delta_{T_1}^2 + \left(\frac{\partial \Delta T}{\partial T_2}\right)^2 \delta_{T_2}^2\right]^{1/2} = \pm 0.085 \text{ °C} \quad \text{(C-6)}$$

Pressure Transducer

The most common type of pressure transducer consists of a pressure sensing diaphragm, preferably made up of stainless steel to protect the inner electrical circuit from the pressurized media. The deflection in diaphragm caused by an application of pressure is sensed by a sensor to estimate the applied pressure. A variety of sensors are universally used to measure the deflection of the diaphragm; the most common among them being strain gauge, capacitance and piezoelectric sensors. Pressure transducers used in the experimental setup of thermodynamic cycle contain capacitance type sensors. A capacitor is an electric charge storage device consisting of two metallic plates separated by an electrical insulator. The diaphragm is located either between the two metallic plates or on one of the metallic plates, depending on the configuration of capacitance sensor. The deflection of diaphragm changes the capacitance value which is detected by an electrical circuit. The transducers are configured depending on the type of pressure measuring requirements: absolute, gauge or differential pressure. In the case of gauge

pressure transducer, the reference side of diaphragm is vented to the local atmosphere, whereas, differential transducer usually contains two diaphragms both having their reference sides at a common atmosphere.

All pressure transducers in the current experimental setup require an electrical input of about 24 V, and provide an output current signal of the range 4-20 mA. They were calibrated with a precision pressure calibrator (Model HL-24, Ametek Calibration Instruments). The calibration was done at 5 points equidistant in the pressure range of transducers, and it was followed with determination of the correction curve by linear regression.

Variable Area Flow Meter (Rotameter)

Rotameter is the most common type of flow meter consisting of a uniformly tapered flow passage and a float. It is installed vertically along the length of the tapered tube with larger diameter end at the top. The fluid enters the tapered flow path from the bottom end, and it causes a resultant pressure differential across the float. The imbalance in vertical forces across the float causes it to rise in the tapered flow passage. The flow passage being tapered, the rise of the float increases the flow area and thus reduces the differential pressure. The float rises until a balance between the forces of gravity, buoyancy and upward differential pressure is achieved. The stable position of the float is indicative of the flow rate. The range of a rotameter for a given process fluid can be changed by changing the float density. Thus, they provide an economical, reliable and simple solution to a wide range of flow measuring requirements.

The weak and strong solution flow rates are measured with variable area flow meters. The material of the float in both rotameters is SS 316 (density 8016 kg/m^3). The weak and strong solution flow meters were calibrated for fluids having specific gravity of

0.88 and 0.833, respectively. Thus, a correction factor is required to account for the difference in densities of actual and calibration fluids. The relation between the actual and measured volumetric flow rates is given by

$$V_{\text{actual}} = V_{\text{measured}} \left[\frac{\rho_{\text{cal}} \left(\rho_{\text{float}} - \rho_{\text{actual}} \right)}{\rho_{\text{actual}} \left(\rho_{\text{float}} - \rho_{\text{cal}} \right)} \right]^{1/2} \tag{C-7}$$

Turbine Flow Meter

Turbine flow meter consists of a rotor having an axis of rotation perpendicular to the flow stream. The multi-bladed rotor is suspended in the flow path. The fluid flow causes the spinning of rotor, and its rotational speed is proportional to the flow rate. The rotational speed of rotor is measured by mechanical, optical or electrical sensors. Vapor flow rate in the current experimental study is measured with the help of a turbine flow meter. The rotational speed of the rotor is sensed by a magnetic pickup coil. The signal is processed by the turbine transmitter (Model HIT-2A, Hoffer Flow Controls, Inc.), and its output is a 4-20 mA linearized signal proportional to the volumetric flow rate. The flow meter was calibrated for ammonia gas by the manufacturer, and the reported uncertainty is ±1% of the reading. The knowledge of temperature, pressure and concentration of the vapor phase then yields the mass flow rate from volumetric flow rate.

Paddlewheel Flow Meter

Paddlewheel flow meter is a variation of the turbine flow meter, where the rotor has an axis of rotation parallel to the fluid flow. The coolant flow rate for both absorber designs were measured with a paddlewheel flow meter. The flow meter was tested for its accuracy by measuring the amount of water collected in a given period of time. However, the flow meter was not calibrated, and no correction factor was applied to the readings.

Gas Chromatograph (GC)

Gas Chromatography is an analytical technique used to qualitatively and quantitatively identify the volatile substances in a mixture. It works on the principle that selective adsorption/desorption rate of volatile compounds over an adsorbent separates the volatile mixture into its individual constituents. The major components of a gas chromatograph include a carrier gas, an oven, a separation column and a detector. A carrier gas which is usually an inert gas, such as helium, argon or nitrogen, is used to move the sample through the separation column. The sample of mixture to be analyzed is injected into the column through an injection port. The separation column is kept inside an oven, and the column temperature is maintained above the boiling point of the least volatile constituent in the sample. The sample thus vaporizes, and continues to flow through the column. The column is either coated or packed with an adsorbent material. The varying affinity of different constituents towards adsorbent results in their partitioning as they flow through the separation column. The amount of time taken by a volatile constituent to pass through the column is called its retention time. Several operating parameters, like adsorbent material, column length and temperature are selected in a manner that each constituent in a mixture eludes through the column at different time. The sample thus separates into individual constituents, and the components are separately analyzed by the detector. The selection of detectors depends on the type of substance to be analyzed. The wide range of detectors include the flame ionization detector (FID), thermal conductivity detector (TCD), electron capture detector (ECD), photoionization detector (PID), flame photometric detector (FPD) and thermionic detector. The signal generated by the detector is later processed and plotted with respect to time. The components then appear as peaks on a time dependent chart. The retention

time identifies the constituent, whereas, the area under the peak represents its concentration in the sample.

The concentration of the ammonia-water binary solution was measured by a Gas Chromatograph having thermal conductivity detector (TCD). Samples of the binary mixture were collected in a syringe through septum ports installed in the experimental setup. The syringe was pre-cooled before analyzing a liquid mixture to prevent the boiling of the liquid sample in the syringe. In the case of vapor samples, it was found that some vapor was getting condensed on the surface of the syringe. The syringe therefore needs to be pre-heated to a temperature higher than the vapor sample. The temperature of the vapor to be analyzed was more than 75°C in all the operating conditions, which made this option difficult. Thus, sampling through a syringe was considered unsuitable for determining the concentration of vapor. The vapor concentration was estimated by measuring the temperature and pressure of the vapor phase, and then applying the vapor-liquid equilibrium correlations.

The following equation is used to estimate the liquid concentration by Gas Chromatography. x is the ammonia mass fraction in the sample, and A_{NH3} is the ratio of area under ammonia peak to area under all the peaks.

$$A_{NH_3} = \frac{Cx}{(C-1)x+1} \tag{C-8}$$

In the above equation, C is the calibration constant which was determined by a single point calibration of GC with a standard ammonia-water liquid mixture at 28.76% of ammonia mass fraction. The equation used to calculate the value of C is given by

$$C = \left(\frac{1 - x_{\text{cal}}}{x_{\text{cal}}} \right) \left(\frac{A_{\text{NH}_3}\big|_{x=x_{\text{cal}}}}{1 - A_{\text{NH}_3}\big|_{x=x_{\text{cal}}}} \right) \tag{C-9}$$

A total of 15 measurements were made for the standard sample, and the average value of C was 0.9794. The uncertainty for the corresponding measurements was ±0.015 with 95% confidence.

Uncertainty Analysis of Derived Measurements

This section presents the details of uncertainties in indirect measurements to obtain a level of confidence in the experimental analysis. The basic quantities which define the state of a fluid are temperature, pressure, composition and volumetric flow rate. These basic properties are much easier to measure, and are directly determined with the help of instruments. Other properties like heat duty, size and mass flow rate are theoretically related to the basic properties. Thus, uncertainties of these derived properties are also directly dependent on uncertainties of instruments used to measure basic properties.

The overall uncertainty of derived measurements was determined by ascertaining the sensitivity of various dependent parameters through perturbation method. Consider a generalized derived measurement R as a function of several primary measurements r_i

$$R = f\left(r_1, r_2, ...r_j\right) \tag{C-10}$$

The uncertainty of the derived measurement y is dependent on the uncertainties of primary measurements and their individual sensitivity over the derived measurement. It can be expressed as

$$\delta_R^2 = \left(\frac{\partial R}{\partial r_1} \right)^2 \delta_{r_1}^2 + \left(\frac{\partial R}{\partial r_2} \right)^2 \delta_{r_2}^2 + ... + \left(\frac{\partial R}{\partial r_j} \right)^2 \delta_{r_j}^2 \tag{C-11}$$

where the $\delta_R,\ \delta_{r_1},\ \delta_{r_2}, ...\delta_{r_j}$ are the overall uncertainties of derived and primary

measurements, respectively. ∂r_i is the finite perturbation in the value of primary measurement. The partial differential of R with respect to r_i, $\partial R / \partial r_i$ represents the sensitivity of a finite perturbation of r_i over R, and can be computed with forward difference scheme.

$$\frac{\partial R}{\partial r_i} = \lim_{\Delta r_i \to 0} \left[\frac{R(r_i + \Delta r_i) - R(r_i)}{\Delta r_i} \right] \approx \frac{R(r_i + \delta r_i) - R(r_i)}{\delta r_i} \tag{C-12}$$

The derived measurements in the current experimental investigation include the determination of coolant differential temperature, vapor concentration, mass flow rates of various streams, absorber heat duty and absorber size. In the current investigation of uncertainty analysis, it is assumed that the thermodynamic and thermophysical properties of ammonia and water binary mixture are well established, and uncertainty associated with them is neglected.

Vapor Concentration

As mentioned in the earlier section, the measurement of the vapor composition by GC was unsuitable with the current configuration of sampling through a syringe. The vapor phase being at saturation state, it was decided to estimate its concentration by the application of vapor-liquid equilibrium correlations on the measured temperature and pressure of vapor stream. Thus, the uncertainty in determining the vapor concentration is directly related to the uncertainty of temperature and pressure measurements, and is of the form

$$\delta_y^2 = \left(\frac{\partial y}{\partial T} \right)^2 \delta_T^2 + \left(\frac{\partial y}{\partial P} \right)^2 \delta_P^2 \tag{C-13}$$

Mass Flow Rate

The variable flow meters and the turbine flow meter utilized in the current experimental investigation measures volumetric flow rate. The weak and strong solution flow rates are measured through a variable flow meter, whereas the vapor flow rate is determined by a turbine flow meter. These measurements are converted into the mass flow rate with the multiplication of density, and are given by

$$m_{L,V} = \rho V \tag{C-14}$$

Thermodynamic properties are used to compute the density of liquid and vapor phases at the given temperature, pressure and concentration. It should be noted that the concentration of vapor phase is determined from the temperature and pressure measurements. It yields

$$m_L = \rho\left(T, P, x\right)V \tag{C-15}$$

and

$$m_V = \rho\left(T, P\right)V \tag{C-16}$$

Thus, the uncertainty in determining the mass flow rate is directly related to the uncertainty in volumetric flow, temperature, pressure and concentration measurements, and is of the form

$$\delta_{m_L}^2 = \left(\frac{V\partial\rho}{\partial T}\right)^2 \delta_T^2 + \left(\frac{V\partial\rho}{\partial P}\right)^2 \delta_P^2 + \left(\frac{V\partial\rho}{\partial x}\right)^2 \delta_x^2 + \left(\rho\right)^2 \delta_V^2 \tag{C-17}$$

and

$$\delta_{m_V}^2 = \left(\frac{V\partial\rho}{\partial T}\right)^2 \delta_T^2 + \left(\frac{V\partial\rho}{\partial P}\right)^2 \delta_P^2 + \left(\rho\right)^2 \delta_V^2 \tag{C-18}$$

Absorber Heat Duty (Coolant Side)

Absorber heat duty is the total amount of heat rejected to the coolant medium, and is a function of coolant volumetric flow rate, density, specific heat and temperature difference. The expression of absorber heat duty is

$$Q = (\rho V) C_p \Delta T \tag{C-19}$$

The coolant is expected to be in the temperature range of 20 to 40 °C, and thus density and specific heat are assumed to be constant in the given operating range. The uncertainty of absorber heat duty can be written as

$$\begin{aligned} \delta_Q^2 &= \left(\frac{\partial Q}{\partial V}\right)^2 \delta_V^2 + \left(\frac{\partial Q}{\partial \Delta T}\right)^2 \delta_{\Delta T}^2 \\ &= \left(\rho C_p \Delta T\right)^2 \delta_V^2 + \left(\rho V C_p\right)^2 \delta_{\Delta T}^2 \end{aligned} \tag{C-20}$$

Absorber Heat Duty (Solution Side)

Heat rejected to the coolant medium can also be determined by conducting an energy balance over the binary fluid mixture. It requires the knowledge of enthalpy and mass flow rate of the binary fluids which are entering and exiting the absorber, namely, vapor, weak solution and strong solution. It yields the following expression

$$Q = m_V H_V + m_{L,W} H_{L,W} - m_{L,S} H_{L,S} \tag{C-21}$$

The mass flow rate and enthalpy of a binary fluid are computed by the application of thermodynamic property correlations. The volumetric flow rate of vapor is measured at the exit of the separator, and thus, the temperature and pressure at the separator exit are required to determine the vapor mass flow produced in the separator. The vapor then flows through the flow meter and the throttle valve into the absorber. The concentration of vapor at the absorber inlet was also determined by using thermodynamic correlations.

The individual species balance was done at the separator exit and absorber inlet, and it was noticed that a very small fraction of vapor, ≈1% condenses before it enters the absorber. The amount of vapor condensed is also taken into consideration to determine the actual mass flow rate of vapor entering the absorber. It yields

$$\begin{aligned} Q = {} & m_V\left(T_{V,\text{abs,inlet}}, T_{V,\text{rec,exit}}, P_{\text{abs}}, P_{\text{boil}}\right) H_V\left(T_{V,\text{abs,inlet}}, P_{\text{abs}}\right) \\ & + m_W\left(T_{W,\text{abs,inlet}}, P_{\text{boil}}, x_{W,\text{abs,inlet}}\right) H_W\left(T_{W,\text{abs,inlet}}, P_{\text{abs}}, x_{W,\text{abs,inlet}}\right) \\ & - m_S\left(T_{S,\text{abs,exit}}, P_{\text{boil}}, x_{S,\text{abs,exit}}\right) H_S\left(T_{S,\text{abs,exit}}, P_{\text{abs}}, x_{S,\text{abs,exit}}\right) \end{aligned} \tag{C-22}$$

The uncertainty in estimating the solution side heat duty is given by

$$\begin{aligned} \delta_{m_V}^2 = {} & \left(\frac{H_V \partial m_V}{\partial T_{V,\text{abs,inlet}}}\right)^2 \delta_{T_{V,\text{abs,exit}}}^2 + \left(\frac{H_V \partial m_V}{\partial T_{V,\text{rec,exit}}}\right)^2 \delta_{T_{V,\text{rec,exit}}}^2 + \left(\frac{H_V \partial m_V}{\partial P_{\text{abs}}}\right)^2 \delta_{P_{\text{abs}}}^2 \\ & + \left(\frac{H_V \partial m_V}{\partial P_{\text{boil}}}\right)^2 \delta_{P_{\text{boil}}}^2 + \left(\frac{m_V \partial H_V}{\partial P_{\text{abs}}}\right)^2 \delta_{P_{\text{abs}}}^2 + \left(\frac{m_V \partial H_V}{\partial T_{V,\text{abs,inlet}}}\right)^2 \delta_{T_{V,\text{abs,inlet}}}^2 \\ & + \left(\frac{m_W \partial H_W}{\partial T_{W,\text{abs,inlet}}}\right)^2 \delta_{T_{W,\text{abs,inlet}}}^2 + \left(\frac{m_W \partial H_W}{\partial P_{\text{abs}}}\right)^2 \delta_{P_{\text{abs}}}^2 + \left(\frac{m_W \partial H_W}{\partial x_{W,\text{abs,inlet}}}\right)^2 \delta_{x_{W,\text{abs,inlet}}}^2 \\ & + \left(\frac{H_W \partial m_W}{\partial T_{W,\text{abs,inlet}}}\right)^2 \delta_{T_{W,\text{abs,inlet}}}^2 + \left(\frac{H_W \partial m_W}{\partial P_{\text{boil}}}\right)^2 \delta_{P_{\text{boil}}}^2 + \left(\frac{H_W \partial m_W}{\partial x_{W,\text{abs,inlet}}}\right)^2 \delta_{x_{W,\text{abs,inlet}}}^2 \\ & + \left(\frac{m_S \partial H_S}{\partial T_{S,\text{abs,inlet}}}\right)^2 \delta_{T_{S,\text{abs,inlet}}}^2 + \left(\frac{m_S \partial H_S}{\partial P_{\text{abs}}}\right)^2 \delta_{P_{\text{abs}}}^2 + \left(\frac{m_S \partial H_S}{\partial x_{S,\text{abs,exit}}}\right)^2 \delta_{x_{S,\text{abs,exit}}}^2 \\ & + \left(\frac{H_S \partial m_S}{\partial T_{S,\text{abs,exit}}}\right)^2 \delta_{T_{S,\text{abs,exit}}}^2 + \left(\frac{H_S \partial m_S}{\partial P_{\text{boil}}}\right)^2 \delta_{P_{\text{boil}}}^2 + \left(\frac{H_{L,S} \partial m_{L,S}}{\partial x_{S,\text{abs,exit}}}\right)^2 \delta_{x_{S,\text{abs,exit}}}^2 \end{aligned} \tag{C-23}$$

Finite Difference Model

A finite difference model is developed to predict the minimum size of falling film absorber required to accomplish the vapor absorption in the weak solution. The amount of heat rejected to the coolant is also computed for the minimum absorber size. The absorber size and heat duty are dependent on several operating and dimensional parameters. Uncertainties in dimensional parameters are quite small, and their effect on

overall uncertainty in predicting the absorber size and heat duty was found to be negligible. However, uncertainties in the measurement of temperature, pressure, concentration and flow of weak solution, vapor and coolant do incorporate an overall uncertainty when the experimental results are compared with the theoretical model. Thus, uncertainty analysis was also performed on the theoretical model to assess the effect of measurement uncertainties. The size and heat duty of absorber can be expressed in terms of parameters which are associated with measurement uncertainties, and are required as an input to the finite difference model.

$$\text{Size} = f\begin{pmatrix} T_{W,\text{abs,inlet}}, T_{V,\text{abs,inlet}}, T_{C,\text{inlet}}, P_{\text{abs}}, m_{W,\text{abs,inlet}}, m_{V,\text{abs,inlet}}, m_C, x_{W,\text{abs,inlet}} \\ , T_{V,\text{rec,exit}}, P_{\text{boil}} \end{pmatrix} \tag{C-24}$$

$$Q = f\begin{pmatrix} T_{W,\text{abs,inlet}}, T_{V,\text{abs,inlet}}, T_{C,\text{inlet}}, P_{\text{abs}}, m_{W,\text{abs,inlet}}, m_{V,\text{abs,inlet}}, m_C, x_{W,\text{abs,inlet}} \\ , T_{V,\text{rec,exit}}, P_{\text{boil}} \end{pmatrix} \tag{C-25}$$

where $T_{W,\text{abs,inlet}}$, $T_{V,\text{abs,inlet}}$ and $T_{C,\text{inlet}}$ are inlet temperatures of the weak solution, vapor and coolant; P_{abs} the absorber pressure; $m_{W,\text{abs,inlet}}$, $m_{V,\text{abs,inlet}}$ and m_C are inlet volumetric flow rates of the weak solution, vapor and coolant; $x_{W,\text{abs,inlet}}$ is the concentration of weak solution at inlet to the absorber. It should be noted that the volumetric flow of vapor is measured at the separator exit, and its mass flow rate is derived from the thermodynamic property correlations. Thus, error due to vapor's temperature, $T_{V,\text{rec,exit}}$ and pressure, P_{boil} at the exit of seperator are also the input to the model. Therefore, the uncertainty in size due to the experimental uncertainties can be expressed as

$$\begin{aligned}\delta_{\text{Size}}^2 = &\left(\frac{\partial f}{\partial T_{W,\text{abs,inlet}}}\right)^2 \delta_{T_{W,\text{abs,inlet}}}^2 + \left(\frac{\partial f}{\partial T_{V,\text{abs,inlet}}}\right)^2 \delta_{T_{V,\text{abs,inlet}}}^2 + \left(\frac{\partial f}{\partial T_{C,\text{inlet}}}\right)^2 \delta_{T_{C,\text{inlet}}}^2 \\ &+ \left(\frac{\partial f}{\partial P_{\text{abs}}}\right)^2 \delta_{P_{\text{abs}}}^2 + \left(\frac{\partial f}{\partial m_{W,\text{abs,inlet}}}\right)^2 \delta_{m_{W,\text{abs,inlet}}}^2 + \left(\frac{\partial f}{\partial m_{V,\text{abs,inlet}}}\right)^2 \delta_{m_{V,\text{abs,inlet}}}^2 \\ &+ \left(\frac{\partial f}{\partial m_C}\right)^2 \delta_{m_C}^2 + \left(\frac{\partial f}{\partial x_{W,\text{abs,inlet}}}\right)^2 \delta_{x_{W,\text{abs,inlet}}}^2 + \left(\frac{\partial f}{\partial T_{V,\text{rec,exit}}}\right)^2 \delta_{T_{V,\text{rec,exit}}}^2 \\ &+ \left(\frac{\partial f}{\partial P_{\text{boil}}}\right)^2 \delta_{P_{\text{boil}}}^2\end{aligned} \tag{C-26}$$

Similarly, the uncertainty in the heat duty of the absorber is given by

$$\begin{aligned}\delta_Q^2 = &\left(\frac{\partial f}{\partial T_{W,\text{abs,inlet}}}\right)^2 \delta_{T_{W,\text{abs,inlet}}}^2 + \left(\frac{\partial f}{\partial T_{V,\text{abs,inlet}}}\right)^2 \delta_{T_{V,\text{abs,inlet}}}^2 + \left(\frac{\partial f}{\partial T_{C,\text{inlet}}}\right)^2 \delta_{T_{C,\text{inlet}}}^2 \\ &+ \left(\frac{\partial f}{\partial P_{\text{abs}}}\right)^2 \delta_{P_{\text{abs}}}^2 + \left(\frac{\partial f}{\partial m_{W,\text{abs,inlet}}}\right)^2 \delta_{m_{W,\text{abs,inlet}}}^2 + \left(\frac{\partial f}{\partial m_{V,\text{abs,inlet}}}\right)^2 \delta_{m_{V,\text{abs,inlet}}}^2 \\ &+ \left(\frac{\partial f}{\partial m_C}\right)^2 \delta_{m_C}^2 + \left(\frac{\partial f}{\partial x_{W,\text{abs,inlet}}}\right)^2 \delta_{x_{W,\text{abs,inlet}}}^2 + \left(\frac{\partial f}{\partial T_{V,\text{rec,exit}}}\right)^2 \delta_{T_{V,\text{rec,exit}}}^2 \\ &+ \left(\frac{\partial f}{\partial P_{\text{boil}}}\right)^2 \delta_{P_{\text{boil}}}^2\end{aligned} \tag{C-27}$$

The finite difference model was individually executed for small perturbations in each parameter to find the respective change in absorber size and heat duty. It enabled us to find the sensitivity of every input measurement on the finite difference model.

The details of individual contribution of measurements and overall uncertainty of the derived measurements for conventional and proposed design are listed in Tables C-2 and C-3, respectively. Due to the limitation of space, only the details of uncertainty analysis for the baseline operating condition are presented.

Table C-2. Uncertainty of derived measurements for the microchannel falling film absorber (baseline operating condition)

Derived measurement, R	Dependent measurements, r_i				Overall uncertainty, δ_R
	Parameter	Evaluated at	Uncertainty, δ_{r_i}	Uncertainty Contribution, $\left(\partial R/\partial r_i\right)\delta_{r_i}$	
Vapor concentration (Absorber inlet)	P	0.279 MPa	±0.00206 MPa	±0.00041 kg/kg	±0.00148 kg/kg
	T	330.2 K	±0.5 K	±0.00142 kg/kg	
Vapor concentration (Rectifier outlet)	P	0.469 MPa	±0.00224 MPa	±0.0003 kg/kg	±0.0014 kg/kg
	T	343.6 K	±0.5 K	±0.00139 kg/kg	
Absorber heat duty (Coolant Side)	V	88.7 cm^3/s	±1.7 cm^3/s	±65 W	±72 W
	ΔT	9.14 K	±0.0825 K	±31 W	
Absorber heat duty (Solution Side)	$V_{S,\text{abs,exit}}$	18.9 cm^3/s	±0.631 cm^3/s	±23 W	±127 W
	$V_{W,\text{abs,inlet}}$	16.4 cm^3/s	±0.479 cm^3/s	±1.7 W	
	$V_{V,\text{rec,exit}}$	633.4 cm^3/s	±6.334 cm^3/s	±27 W	
	P_{abs}	0.279 MPa	±0.00206 MPa	±0.02 W	
	P_{boil}	0.469 MPa	±0.00224 MPa	±1.2 W	
	$T_{W,\text{abs,inlet}}$	316.2 K	±0.5 K	±31 W	
	$T_{S,\text{abs,exit}}$	313.1 K	±0.5 K	±35 W	
	$T_{V,\text{abs,inlet}}$	330. 2 K	±0.5 K	±2 W	
	$T_{V,\text{rec,exit}}$	343.6 K	±0.5 K	±0.9 W	
	$x_{W,\text{abs,inlet}}$	0.3 kg/kg	±0.015 kg/kg	±92 W	
	$x_{S,\text{abs,exit}}$	0.37 kg/kg	±0.015 kg/kg	±65 W	
Weak solution mass flow	V	16.4 cm^3/s	±0.479 cm^3/s	±0.422 g/s	±0.424 g/s
	P	0.469 MPa	±0.00103 MPa	±3.4x10^{-6} g/s	
	T	316.2 K	±0.5 K	±0.0024 g/s	
	x	0.3 kg/kg	±0.015 kg/kg	±0.0352 g/s	

Table C-2 Continued

Derived measurement, R	Dependent measurements, r_i				Overall uncertainty, δ_R
	Parameter	Evaluated at	Uncertainty, δ_{r_i}	Uncertainty Contribution, $\left(\partial R / \partial r_i\right)\delta_{r_i}$	
Strong solution mass flow	V	18.93 cm^3/s	±0.631 cm^3/s	±0.534 g/s	±0.535 g/s
	P	0.469 MPa	±0.00067 MPa	$\pm 2.5 \times 10^{-6}$ g/s	
	T	313.1 K	±0.5 K	±0.0029 g/s	
	x	0.37 kg/kg	±0.015 kg/kg	±0.0352 g/s	
Vapor mass flow (Rectifier outlet)	V	633.3 cm^3/s	±6.334 cm^3/s	±0.0183 g/s	±0.021 g/s
	P	0.469 MPa	±0.00224 MPa	±0.009 g/s	
	T	343.6 K	±0.5 K	±0.0027 g/s	
Absorber size Prediction	$T_{W,\text{abs,inlet}}$	316.2 K	±0.5 K	±0.0 tubes	±12.3 tubes
	$T_{V,\text{abs,inlet}}$	330.2 K	±0.5 K	±0.0 tubes	
	T_C	300.2 K	±0.5 K	±2 tubes	
	P_{abs}	0.279 MPa	±0.00045 MPa	±0.45 tubes	
	$V_{W,\text{abs,inlet}}$	16.4 cm3/s	±0.479 cm3/s	±0.96 tubes	
	$V_{V,\text{rec,exit}}$	633.3 cm^3/s	±6.334 cm^3/s	±1.27 tubes	
	V_C	88.7 cm^3/s	±1.7 cm^3/s	±0.85 tubes	
	$x_{W,\text{abs,inlet}}$	0.3 kg/kg	±0.015 kg/kg	±12 tubes	
	P_{boil}	0.469 MPa	±0.00224 MPa	±0.0 tubes	
	$T_{V,\text{rec,exit}}$	343.6 K	±0.5 K	±0.0 tubes	

Table C-2 Continued

Derived measurement, R	Dependent measurements, r_i				Overall uncertainty, δ_R
	Parameter	Evaluated at	Uncertainty, δ_{r_i}	Uncertainty Contribution, $\left(\partial R / \partial r_i\right)\delta_{r_i}$	
Absorber size heat duty prediction	$T_{W,\text{abs,inlet}}$	316.2 K	±0.5 K	±24.8 W	±63.8 W
	$T_{V,\text{abs,inlet}}$	330.2 K	±0.5 K	±3.3 W	
	T_C	300.2 K	±0.5 K	±12.8 W	
	P_{abs}	0.279 MPa	±0.00045 MPa	±8.1 W	
	$V_{W,\text{abs,inlet}}$	16.4 cm3/s	±0.479 cm3/s	±8.6 W	
	$V_{V,\text{rec,exit}}$	633.3 cm^3/s	±6.334 cm^3/s	±36.8 W	
	V_C	88.7 cm^3/s	±1.7 cm^3/s	±15.8 W	
	$x_{W,\text{abs,inlet}}$	0.3 kg/kg	±0.015 kg/kg	±39.2 W	
	P_{boil}	0.469 MPa	±0.00224 MPa	±0.03 W	
	$T_{V,\text{rec,exit}}$	343.6 K	±0.5 K	±0.12 W	

Table C-3. Uncertainty of derived measurements for the proposed falling film absorber (baseline operating condition)

Derived measurement, R	Dependent measurements, r_i				Overall uncertainty, δ_R
	Parameter	Evaluated at	Uncertainty, δ_{r_i}	Uncertainty Contribution, $\left(\partial R/\partial r_i\right)\delta_{r_i}$	
Vapor concentration (Absorber inlet)	P	0.279 MPa	±0.00206 MPa	±0.00053 kg/kg	±0.00181 kg/kg
	T	332.5 K	±0.5 K	±0.00173 kg/kg	
Vapor concentration (Rectifier outlet)	P	0.462 MPa	±0.00224 MPa	±0.00035 kg/kg	±0.0016 kg/kg
	T	344.8 K	±0.5 K	±0.00156 kg/kg	
Absorber heat duty (Coolant Side)	V	88.7 cm^3/s	±1.7 cm^3/s	±78 W	±84 W
	ΔT	11.0 K	±0.0825 K	±31 W	
Absorber heat duty (Solution Side)	$V_{S,\text{abs,exit}}$	19.6 cm^3/s	±0.631 cm^3/s	±25 W	±127 W
	$V_{W,\text{abs,inlet}}$	16.4 cm^3/s	±0.479 cm^3/s	±1.3 W	
	$V_{V,\text{rec,exit}}$	730.5 cm^3/s	±7.305 cm^3/s	±30 W	
	P_{abs}	0.279 MPa	±0.00206 MPa	±0.02 W	
	P_{boil}	0.462 MPa	±0.00224 MPa	±1.4 W	
	$T_{W,\text{abs,inlet}}$	316.4 K	±0.5 K	±31 W	
	$T_{S,\text{abs,exit}}$	312.8 K	±0.5 K	±36 W	
	$T_{V,\text{abs,inlet}}$	332.5 K	±0.5 K	±2.4 W	
	$T_{V,\text{rec,exit}}$	344.8 K	±0.5 K	±0.7 W	
	$x_{W,\text{abs,inlet}}$	0.3 kg/kg	±0.015 kg/kg	±92 W	
	$x_{S,\text{abs,exit}}$	0.38 kg/kg	±0.015 kg/kg	±61 W	
Weak solution mass flow	V	16.4 cm^3/s	±0.479 cm^3/s	±0.422 g/s	±0.424 g/s
	P	0.462 MPa	±0.00103 MPa	$\pm 3.4 \times 10^{-6}$ g/s	
	T	316.4 K	±0.5 K	±0.0024 g/s	
	x	0.3 kg/kg	±0.015 kg/kg	±0.0352 g/s	

Table C-3 Continued

Derived measurement, R	Dependent measurements, r_i				Overall uncertainty, δ_R
	Parameter	Evaluated at	Uncertainty, δ_{r_i}	Uncertainty Contribution, $\left(\partial R / \partial r_i\right)\delta_{r_i}$	
Strong solution mass flow	V	19.6 cm^3/s	±0.631 cm^3/s	±0.534 g/s	±0.535 g/s
	P	0.462 MPa	±0.00067 MPa	±2.5x10^{-6} g/s	
	T	312.8 K	±0.5 K	±0.0029 g/s	
	x	0.38 kg/kg	±0.015 kg/kg	±0.0352 g/s	
Vapor mass flow (Rectifier outlet)	V	730.5 cm^3/s	±6.334 cm^3/s	±0.0183 g/s	±0.021 g/s
	P	0.462 MPa	±0.00224 MPa	±0.009 g/s	
	T	344.8 K	±0.5 K	±0.0027 g/s	
Absorber size Prediction	$T_{W,\text{abs,inlet}}$	316.4 K	±0.5 K	±0.0 tubes	±12.34 tubes
	$T_{V,\text{abs,inlet}}$	332.5 K	±0.5 K	±0.0 tubes	
	T_C	300.1 K	±0.5 K	±2 tubes	
	P_{abs}	0.279 MPa	±0.00045 MPa	±0.45 tubes	
	$V_{W,\text{abs,inlet}}$	16.4 cm3/s	±0.479 cm3/s	±0.96 tubes	
	$V_{V,\text{rec,exit}}$	730.5 cm^3/s	±7.305 cm^3/s	±1.46 tubes	
	V_C	88.7 cm^3/s	±1.7 cm^3/s	±0.85 tubes	
	$x_{W,\text{abs,inlet}}$	0.3 kg/kg	±0.015 kg/kg	±12 tubes	
	P_{boil}	0.462 MPa	±0.00224 MPa	±0.0 tubes	
	$T_{V,\text{rec,exit}}$	344.8 K	±0.5 K	±0.5 tubes	

Table C-3 Continued

Derived measurement, R	Dependent measurements, r_i				Overall uncertainty, δ_R
	Parameter	Evaluated at	Uncertainty, δ_{r_i}	Uncertainty Contribution, $\left(\partial R / \partial r_i\right)\delta_{r_i}$	
Absorber size heat duty prediction	$T_{W,\text{abs,inlet}}$	316.4 K	±0.5 K	±23 W	±82 W
	$T_{V,\text{abs,inlet}}$	332.5 K	±0.5 K	±3.75 W	
	T_C	300.1 K	±0.5 K	±13 W	
	P_{abs}	0.279 MPa	±0.00045 MPa	±9.2 W	
	$V_{W,\text{abs,inlet}}$	16.4 cm3/s	±0.479 cm3/s	±3.3 W	
	$V_{V,\text{rec,exit}}$	730.5 cm^3/s	±7.305 cm^3/s	±47 W	
	V_C	88.7 cm^3/s	±1.7 cm^3/s	±8 W	
	$x_{W,\text{abs,inlet}}$	0.3 kg/kg	±0.015 kg/kg	±58.5 W	
	P_{boil}	0.462 MPa	±0.00224 MPa	±0.04 W	
	$T_{V,\text{rec,exit}}$	344.8 K	±0.5 K	±16 W	

APPENDIX D
COMPUTER PROGRAM

The computational language C++ was used to numerically model the conventional horizontal tube type absorber and the proposed design. A separate routine was also written to determine the thermodynamic and transport properties of the ammonia-water mixture. The property evaluation code is titled as “property.c”. The values of various coefficients required by the property routine are in “property.h” header file. The main program which solves the numerical model is named as “tube.cpp” for the proposed absorber design. The numerical code developed to model the proposed design is also utilized to model the microchannel absorber design (i.e. an absorber without mesh) by assuming the length of mesh to be equal to zero. The program calls the property evaluation rotuine to determine the properties of ammonia-water mixture.

Property Evaluation Code

property.h

```
double h2o_a1 = 2.748796e-2, h2o_a2 = -1.016665e-5, h2o_a3 = -4.452025e-3,
h2o_a4 = 8.389246e-4;

double h3n_a1 = 3.971423e-2, h3n_a2 = -1.790557e-5, h3n_a3 = -1.308905e-2,
h3n_a4 = 3.752836e-3;

double h2o_b1 = 12.14557, h2o_b2 = -1.898065, h2o_b3 = 0.2911966;

double h3n_b1 = 16.34519, h3n_b2 = -6.508119, h3n_b3 = 1.448937;

double h2o_c1 = 2.136131e-2, h2o_c2 = -31.69291, h2o_c3 = -4.634611e+4, h2o_c4
= 0.0;
```

```
        double h3n_c1 = -1.049377e-2, h3n_c2 = -8.288224, h3n_c3 = -6.647257e+2,
h3n_c4 = -3.045352e+3;
        double h2o_d1 = 4.019170, h2o_d2 = -5.175550e-2, h2o_d3 = 1.951939e-2;
        double h3n_d1 = 3.673647, h3n_d2 = 9.989629e-2, h3n_d3 = 3.617622e-2;
        double h2ohl_ro = 21.821141, h2ohg_ro = 60.965058;
        double h3nhl_ro = 4.878573, h3nhg_ro = 26.468873;
        double h2osl_ro = 5.733498, h2osg_ro = 13.453430;
        double h3nsl_ro = 1.644773, h3nsg_ro = 8.339026;
        double h2oT_ro = 5.0705, h2oP_ro = 3.0000;
        double h3nT_ro = 3.2252, h3nP_ro = 2.0000;
        double Tb = 100., Pb = 10.;
        double e1 = -41.733398;
        double e2 = 0.02414;
        double e3 = 6.702285;
        double e4 = -0.011475;
        double e5 = 63.608967;
        double e6 = -62.490768;
        double e7 = 1.761064;
        double e8 = 0.008626;
        double e9 = 0.387983;
        double e10 = -0.004772;
        double e11 = -4.648107;
        double e12 = 0.836376;
```

```
double e13 = -3.553627;

double e14 = 0.000904;

double e15 = 24.3616723;

double e16 = -20.736547;

double c1 = 153.634521459;

double c2 = -13.0305543892;

double c3 = -1.14845282991;

double c4 = .550358094447;

double c5 = -.0753450148427;

double c6 = .0048111666267;

double c7 = -.000120433757177;

double c11 = -462.460321366;

double c12 = 23739.9986309;

double c13 = -194504.35292;

double c14 = 639383.528867;

double c15 = -523748.057636;

double c16 = -2328271.47551;

double c17 = 7562418.53499;

double c18 = -9668295.89504;

double c19 = 5922081.87086;

double c110 = -1432405.52125;

double c21 = 421.443122208;

double c22 = -14560.354925;
```

```
double c23 = 53051.4495633;

double c24 = 382763.793582;

double c25 = -3583589.86875;

double c26 = 12243265.3815;

double c27 = -22307970.0156;

double c28 = 22896656.8499;

double c29 = -12483324.8091;

double c210 = 2813311.71633;

double c31 = -248.783804168;

double c32 = 4807.07241098;

double c33 = 13565.1003309;

double c34 = -466407.780832;

double c35 = 2827083.44764;

double c36 = -8469715.15799;

double c37 = 14459588.8962;

double c38 = -14281087.5331;

double c39 = 7596403.59678;

double c310 = -1684002.64482;

double c41 = 126.965580728;

double c42 = -2090.45270574;

double c43 = 1993.17101166;

double c44 = 100706.510396;

double c45 = -687388.808612;
```

```
double c46 = 2132412.46959;

double c47 = -3699199.65914;

double c48 = 3688365.22546;

double c49 = -1975122.39296;

double c410 = 440201.446068;

double c51 = -33.5343446156;

double c52 = 601.878586689;

double c53 = -3064.82070658;

double c54 = 71.7954752052;

double c55 = 51780.666659;

double c56 = -209714.899856;

double c57 = 405011.985355;

double c58 = -428310.461566;

double c59 = 238153.698326;

double c510 = -54497.0973336;

double c61 = 3.97454953787;

double c62 = -77.026846469;

double c63 = 541.19105807;

double c64 = -1696.60270972;

double c65 = 1713.45942707;

double c66 = 4019.01019872;

double c67 = -14844.7928004;

double c68 = 19481.0094551;
```

```
double c69 = -12107.0794501;

double c610 = 2966.92804386;

double c71 = -.170806170177;

double c72 = 3.48182859299;

double c73 = -27.7957587743;

double c74 = 113.762064546;

double c75 = -258.750496922;

double c76 = 311.002585218;

double c77 = -123.917993454;

double c78 = -123.480627492;

double c79 = 154.375042114;

double c710 = -48.5083828701;

static double a1 = 205.8889;

static double a2 = 280.930556;

static double a3 = -317.0138889;

static double a4 = 263.194444;

double b1 = .368105523897;

double b2 = -3.6679548875;

double b3 = 46.6000470809;

double b4 = -262.921061996;

double b5 = 732.99536936;

double b6 = -1076.0613489;

double b7 = 797.948078048;
```

```
double b8 = -235.903904222;

double al1 = 153.17055346;

double al2 = -11.7705687461;

double al3 = -1.78126355957;

double al4 = .647385455059;

double al5 = -.0719950751898;

double al6 = .00285423950786;

double a11 = 194.793913463;

double a12 = 74.236124188;

double a13 = 9.84103819552;

double a14 = .436843852745;

double a21 = -74.3508283362;

double a22 = -33.2941879809;

double a23 = -4.78866918581;

double a24 = -.225416733476;

double a31 = 13.0175447367;

double a32 = 6.1586564117;

double a33 = .789740337141;

double a34 = .0321510834958;

double a41 = -.90857587517;

double a42 = -.356752691147;

double a43 = .0238067275502;

double a44 = .00495593933952;
```

```
double a51 = -.00071863574153;

double a52 = -.0251026383533;

double a53 = -.0191664613304;

double a54 = -.0017014253867;

double a61 = .00195441702983;

double a62 = .00280533348937;

double a63 = .0013899436563;

double a64 = .000116422611616;

double tc1 = 647.3, tc2 = 405.5;

double pc1 = 221.2, pc2 = 113.5;

double wm1 = 18.015, wm2 = 17.031;

double trf1 = 273.15, trf2 = .01;

static double r = 8.3144;

double tb, tb1, tb2, tb3, tb4, tb5, tb6, tb7;

double td, td1, td2, td3, td4, td5, td6;

double tc_h2o = 647.3, tc_nh3 = 405.5,tr_h2o,tr_nh3;

double pc_h2o = 221.2, pc_nh3 = 113.5;

double mw_h2o = 18.015, mw_nh3 = 17.031, mw_mix;

double h_h2ol, h_h2ov, cp_h2oL, cp_h2oV, s_h2ol, s_h2ov, v_h2ol, v_h2ov;

double h_h3nl, h_h3nv, cp_h3nl, cp_h3nv, s_h3nl, s_h3nv, v_h3nl, v_h3nv;

double gamma_h2ol,gamma_nh3l;

double he, cpe, se, ve;

double Tr, Pr;
```

```
double lamda_h2ol,lamda_h2ov,lamda_nh3l,lamda_nh3v;
double mu_h2ol,mu_h2ov,mu_nh3l,mu_nh3v;
```

property.c

```
#include <math.h>
#include "propertyv6.h"
/*Originally coded by Feng Xu
Modified By Sanjay Vijayaraghavan to correct error in specific volume computation
Mar 2002
Last Modified By Nitin Goel to incorporate Cp and transport properties of
ammonia-water mixture. Replaced the units of H, Cp, S in mix_l,mix_v
to kJ/kmole. Also included mix_l_ph() and mix_v_ph() functions
Dec 2002*/

// h, s, are in kJ/kmole for steam_l,steam_v,ammonia_l,ammonia_v,mix_l,mix_v
// cp are in kJ/kmole.K for steam_l,steam_v,ammonia_l,ammonia_v,mix_l,mix_v
// v is specific volume and is in m3/kmole
// x is mass fraction
// THERMODYNAMIC PROPERTIES VALID FOR 0.2 TO 110 BAR AND 230
TO 630 K
// T in K, lamda in W/mK
// mu in N.s/m2
// Diffusion coefficient is in 10^9*m2/s
// lamda is in W/m.K
void tsteam_l(double t, double *lamda_h2ol, double *mu_h2ol)
```

```
{
// mu_h2ol is in N.s/m2 and valid for 273-643 Kelvin
// lamda_h2ol is in W/m.K and valid for 273-633 Kelvin
  *lamda_h2ol=-0.2758+4.612e-3*t-5.5391e-6*pow(t,2);
  *mu_h2ol= pow(10,-3)*pow(10,-10.2158+(1.7925e+3)/t+(1.773e-2)*t-(1.2631e-
5)*pow(t,2));
}
void tsteam_v(double t, double *lamda_h2ov, double *mu_h2ov)
{
// mu_h2ov is in N.s/m2 and valid for 280-1073 Kelvin
// lamda_h2ov is in W/m.K and valid for 275-1073 Kelvin
  *lamda_h2ov=0.00053+4.7093e-5*t+4.9551e-8*pow(t,2);
  *mu_h2ov=pow(10,-7)*(-36.8255+(4.2916e-1)*t-(1.624e-5)*pow(t,2));
}
void tammonia_l(double t, double *lamda_nh3l, double *mu_nh3l)
{
// mu_nh3l is in N.s/m2 and valid for 195-406 Kelvin
// lamda_nh3l is in W/m.K and valid for 220-400 Kelvin
  *lamda_nh3l=1.1606-2.284e-3*t+3.1245e-18*pow(t,2);
  *mu_nh3l=pow(10,-3)*pow(10,-8.591+(8.764e+2)/t+(2.681e-2)*t-(3.612e-
5)*pow(t,2));
}
void tammonia_v(double t, double *lamda_nh3v, double *mu_nh3v)
```

```
{
// mu_nh3v is in N.s/m2 and valid for 195-1000 Kelvin
// lamda_nh3v is in W/m.K and valid for 200-700 Kelvin
  *lamda_nh3v=0.00457+2.3239e-5*t+1.481e-7*pow(t,2);
  *mu_nh3v=pow(10,-7)*(-7.8737+(3.6745e-1)*t-(4.4729e-6)*pow(t,2));
}
void tmix_l(double t, double p, double x,  double *lamda_mixl, double *d_mixl,
double *mu_mixl)
{
  double frmolw,frmola;
// Diffusivity and viscosity is valid for 293-333 K and 0-0.312 mole fraction of
ammonia
// Viscoity is in N.s/m2
// Diffusion coefficient is in 10^9*m2/s
  frmolw = ((1 - x)/mw_h2o)/((1 - x)/mw_h2o + x/mw_nh3);
  frmola = 1 - frmolw;
  *mu_mixl=(0.67+0.78*frmola)*pow(10,-6)*exp(17900/(r*t));
  *d_mixl=(1.65+2.47*frmola)*pow(10,-6)*exp(-16600/(r*t))*pow(10,9);
  tsteam_l(t,&lamda_h2ol,&mu_h2ol);
  tammonia_l(t,&lamda_nh3l,&mu_nh3l);
// Thermal conductivity is not valid below 270 Kelvin
  *lamda_mixl=x*lamda_nh3l+(1-x)*lamda_h2ol-(lamda_h2ol-lamda_nh3l)*(1-
pow(1-x,0.5))*(1-x);
```

```
}
void tmix_v(double t, double p, double x, double *lamda_mixv, double *d_mixv,
double *mu_mixv)
{
 double a21,a12,b12,b21,m12,f_h2o,f_nh3,lamda_tr_ratio12,lamda_tr_ratio21;
 double frmolw,frmola;
// subscript 1 signifies h2o
 tsteam_v(t,&lamda_h2ov,&mu_h2ov);
 tammonia_v(t,&lamda_nh3v,&mu_nh3v);
 frmolw = ((1 - x)/mw_h2o)/((1 - x)/mw_h2o + x/mw_nh3);
 frmola = 1 - frmolw;
// d_mixv is in 10^9*m2/s
 m12=2*pow(1/mw_h2o+1/mw_nh3,-1);
 *d_mixv=pow(10,5)*((0.00143*pow(t,7./4))/(p*pow(m12,0.5)*pow(pow(20.7,1./3
)+pow(13.1,1./3),2)));
 b12=pow(1+pow(mu_h2ov/mu_nh3v,0.5)*pow(mw_nh3/mw_h2o,0.25),2)/pow(8*
(1+mw_h2o/mw_nh3),0.5);
 b21=b12*(mu_nh3v*mw_h2o)/(mu_h2ov*mw_nh3);
 *mu_mixv=((frmolw*mu_h2ov)/(frmolw+frmola*b12)+(frmola*mu_nh3v)/(frmol
a+frmolw*b21));
 f_h2o=210*pow(tc_h2o*pow(mw_h2o,3)/pow(pc_h2o,4),1./6);
 f_nh3=210*pow(tc_nh3*pow(mw_nh3,3)/pow(pc_nh3,4),1./6);
```

```
        tr_h2o=t/tc_h2o;
        tr_nh3=t/tc_nh3;
        lamda_tr_ratio12=(f_nh3*(exp(0.0464*tr_h2o)-exp(-
0.2412*tr_nh3)))/(f_h2o*(exp(0.0464*tr_nh3)-exp(-0.2412*tr_h2o)));
        lamda_tr_ratio21=(f_h2o*(exp(0.0464*tr_nh3)-exp(-
0.2412*tr_h2o)))/(f_nh3*(exp(0.0464*tr_h2o)-exp(-0.2412*tr_nh3)));
        a12=pow(1+pow(lamda_tr_ratio12,0.5)*pow(mw_nh3/mw_h2o,0.25),2)/pow(8*(1
+mw_h2o/mw_nh3),0.5);
        a21=pow(1+pow(lamda_tr_ratio21,0.5)*pow(mw_h2o/mw_nh3,0.25),2)/pow(8*(1
+mw_nh3/mw_h2o),0.5);
        *lamda_mixv=(frmolw*lamda_h2ov)/(frmolw+frmola*a12)+(frmola*lamda_nh3v)
/(frmola+frmolw*a21);
      }
      void steam_l(double t, double p, double *h_h2ol, double *s_h2ol, double *v_h2ol)
      {
       double h, s, v;
       Tr = t/Tb;
       Pr = p/Pb;
       h = -h2ohl_ro + h2o_b1*h2oT_ro + h2o_b2/2*(h2oT_ro*h2oT_ro + Tr*Tr)
       + h2o_b3/3*(h2oT_ro*h2oT_ro*h2oT_ro - Tr*Tr*Tr) - h2o_b1*Tr
       - h2o_b2*Tr*Tr + (h2o_a4*Tr*Tr - h2o_a1)*(Pr - h2oP_ro)
       - h2o_a2/2*(Pr*Pr - h2oP_ro*h2oP_ro);
```

```
  *h_h2ol = -r*Tb*h;


  s = -h2osl_ro - h2o_b1*log(Tr/h2oT_ro) + h2o_b2*(h2oT_ro - Tr)
  + h2o_b3/2*(h2oT_ro*h2oT_ro - Tr*Tr) + (h2o_a3 + 2*h2o_a4*Tr)*(Pr -
h2oP_ro);
  *s_h2ol = -r*s;
  v = h2o_a1 + h2o_a2*Pr + h2o_a3*Tr + h2o_a4*Tr*Tr;
  *v_h2ol = (r*Tb/Pb*v)/100;
 }
 void steam_v(double t, double p, double *h_h2ov, double *s_h2ov, double *v_h2ov)
 {
  double h, s, v;
  Tr = t/Tb;
  Pr = p/Pb;
  h = -h2ohg_ro + h2o_d1*h2oT_ro + h2o_d2/2*(h2oT_ro*h2oT_ro + Tr*Tr)
  + h2o_d3/3*(h2oT_ro*h2oT_ro*h2oT_ro - Tr*Tr*Tr) - h2o_d1*Tr
  - h2o_d2*Tr*Tr - h2o_c1*(Pr - h2oP_ro)
  + h2o_c2*4*(h2oP_ro*pow(h2oT_ro,-3) - Pr*pow(Tr,-3))
  + h2o_c3*12*(h2oP_ro*pow(h2oT_ro,-11) - Pr*pow(Tr,-11))
  + h2o_c4*4*(pow(h2oP_ro,3)*pow(h2oT_ro,-11) - pow(Pr,3)*pow(Tr,-11));
  *h_h2ov = -r*Tb*h;
  s = -h2osg_ro - h2o_d1*log(Tr/h2oT_ro) + h2o_d2*(h2oT_ro - Tr)
  + h2o_d3/2*(h2oT_ro*h2oT_ro - Tr*Tr) + log(Pr/h2oP_ro)
```

```
        + 3*h2o_c2*(h2oP_ro*pow(h2oT_ro,-4) - Pr*pow(Tr,-4))
        + 11*h2o_c3*(h2oP_ro*pow(h2oT_ro,-12) - Pr*pow(Tr,-12))
        + (11./3)*h2o_c4*(pow(h2oP_ro,3)*pow(h2oT_ro,-12) - pow(Pr,3)*pow(Tr,-12));
        *s_h2ov = -r*s;
        v = Tr/Pr + h2o_c1 + h2o_c2*pow(Tr,-3) + pow(Tr,-11)*(h2o_c3 +
h2o_c4*Pr*Pr);
        *v_h2ov = (r*Tb/Pb*v)/100;
       }
       void ammonia_l(double t, double p, double *h_h3nl, double *s_h3nl, double
*v_h3nl)
       {
        double h, s, v;
        Tr = t/Tb;
        Pr = p/Pb;
        h = -h3nhl_ro + h3n_b1*h3nT_ro + h3n_b2/2*(h3nT_ro*h3nT_ro + Tr*Tr)
        + h3n_b3/3*(h3nT_ro*h3nT_ro*h3nT_ro - Tr*Tr*Tr) - h3n_b1*Tr
        - h3n_b2*Tr*Tr + (h3n_a4*Tr*Tr - h3n_a1)*(Pr - h3nP_ro)
        - h3n_a2/2*(Pr*Pr - h3nP_ro*h3nP_ro);
        *h_h3nl = -r*Tb*h;
         s = -h3nsl_ro - h3n_b1*log(Tr/h3nT_ro) + h3n_b2*(h3nT_ro - Tr)
        + h3n_b3/2*(h3nT_ro*h3nT_ro - Tr*Tr) + (h3n_a3 + 2*h3n_a4*Tr)*(Pr -
h3nP_ro);
        *s_h3nl = -r*s;
```

```
  v = h3n_a1 + h3n_a2*Pr + h3n_a3*Tr + h3n_a4*Tr*Tr;
  *v_h3nl = (r*Tb/Pb*v)/100;
 }
 void ammonia_v(double t, double p, double *h_h3nv, double *s_h3nv, double
*v_h3nv)
 {
  double h, s, v;
  Tr = t/Tb;
  Pr = p/Pb;
  h = -h3nhg_ro + h3n_d1*h3nT_ro + h3n_d2/2*(h3nT_ro*h3nT_ro + Tr*Tr)
  + h3n_d3/3*(h3nT_ro*h3nT_ro*h3nT_ro - Tr*Tr*Tr) - h3n_d1*Tr
  - h3n_d2*Tr*Tr - h3n_c1*(Pr - h3nP_ro)
  + h3n_c2*4*(h3nP_ro*pow(h3nT_ro,-3) - Pr*pow(Tr,-3))
  + h3n_c3*12*(h3nP_ro*pow(h3nT_ro,-11) - Pr*pow(Tr,-11))
  + h3n_c4*4*(pow(h3nP_ro,3)*pow(h3nT_ro,-11) - pow(Pr,3)*pow(Tr,-11));
    *h_h3nv = -r*Tb*h;
  s = -h3nsg_ro - h3n_d1*log(Tr/h3nT_ro) + h3n_d2*(h3nT_ro - Tr)
  + h3n_d3/2*(h3nT_ro*h3nT_ro - Tr*Tr) + log(Pr/h3nP_ro)
  + 3*h3n_c2*(h3nP_ro*pow(h3nT_ro,-4) - Pr*pow(Tr,-4))
  + 11*h3n_c3*(h3nP_ro*pow(h3nT_ro,-12) - Pr*pow(Tr,-12))
  + (11./3)*h3n_c4*(pow(h3nP_ro,3)*pow(h3nT_ro,-12) - pow(Pr,3)*pow(Tr,-12));
  *s_h3nv = -r*s;
```

```
    v = Tr/Pr + h3n_c1 + h3n_c2*pow(Tr,-3) + pow(Tr,-11)*(h3n_c3 +
h3n_c4*Pr*Pr);
    *v_h3nv = (r*Tb/Pb*v)/100;
  }
  void excess(double t, double p, double x, double *he, double *se, double *ve)
  {
   double f1, f2, f3;
   x = (x/wm2)/((1 - x)/wm1 + x/wm2);
   Tr = t/Tb;
   Pr = p/Pb;
   f1 = e1 + e2*Pr + 2*e5/Tr +3*e6/(Tr*Tr);
   f2 = e7 + e8*Pr + 2*e11/Tr +3*e12/(Tr*Tr);
   f3 = e13 + e14*Pr + 2*e15/Tr +3*e16/(Tr*Tr);
   *he = r*Tb*(f1 + f2*(2*x - 1) + f3*(2*x - 1)*(2*x - 1))*(1 - x)*x;
   f1 = e3 + e4*Pr - e5/(Tr*Tr) - 2*e6/(Tr*Tr*Tr);
   f2 = e9 + e10*Pr - e11/(Tr*Tr) - 2*e12/(Tr*Tr*Tr);
   f3 = -e15/(Tr*Tr) - 2*e16/(Tr*Tr*Tr);
   *se = -r*(f1 + f2*(2*x - 1) + f3*(2*x - 1)*(2*x - 1))*(1 - x)*x;
   *ve = (r*Tb/Pb*(e2 + e4*Tr +(e8 + e10*Tr)*(2*x - 1)
    + e14*(2*x - 1)*(2*x - 1))*(1 - x)*x)/100;
  }
```

```
double bubble(double p, double xf)
{
  double tcw, tcb, pcb, pcw;
  double pz;
  tcw = (tc1 - 273.15)*1.8 + 32;
  pcw = pc1 * 14.50377;
  tcb = tcw - (a1*xf + a2*pow(xf,2) + a3*pow(xf,3) + a4*pow(xf,4));
  pcb = pcw*exp(b1*xf + b2*pow(xf,2) + b3*pow(xf,3) + b4*pow(xf,4)
    + b5*pow(xf,5) + b6*pow(xf,6) + b7*pow(xf,7) + b8*pow(xf,8));
  pz = log(pcb/(p*14.50377));
  tb1 = (c1 + (c11*xf + c12*pow(xf,2) + c13*pow(xf,3) + c14*pow(xf,4)
    + c15*pow(xf,5) + c16*pow(xf,6) + c17*pow(xf,7) + c18*pow(xf,8)
    + c19*pow(xf,9) + c110*pow(xf,10)))*pow(pz,1);
  tb2 = (c2 + (c21*xf + c22*pow(xf,2) + c23*pow(xf,3) + c24*pow(xf,4)
    + c25*pow(xf,5) + c26*pow(xf,6) + c27*pow(xf,7) + c28*pow(xf,8)
    + c29*pow(xf,9) + c210*pow(xf,10)))*pow(pz,2);
  tb3 = (c3 + (c31*xf + c32*pow(xf,2) + c33*pow(xf,3) + c34*pow(xf,4)
    + c35*pow(xf,5) + c36*pow(xf,6) + c37*pow(xf,7) + c38*pow(xf,8)
    + c39*pow(xf,9) + c310*pow(xf,10)))*pow(pz,3);
  tb4 = (c4 + (c41*xf + c42*pow(xf,2) + c43*pow(xf,3) + c44*pow(xf,4)
    + c45*pow(xf,5) + c46*pow(xf,6) + c47*pow(xf,7) + c48*pow(xf,8)
    + c49*pow(xf,9) + c410*pow(xf,10)))*pow(pz,4);
```

```
  tb5 = (c5 + (c51*xf + c52*pow(xf,2) + c53*pow(xf,3) + c54*pow(xf,4)
    + c55*pow(xf,5) + c56*pow(xf,6) + c57*pow(xf,7) + c58*pow(xf,8)
    + c59*pow(xf,9) + c510*pow(xf,10)))*pow(pz,5);
  tb6 = (c6 + (c61*xf + c62*pow(xf,2) + c63*pow(xf,3) + c64*pow(xf,4)
    + c65*pow(xf,5) + c66*pow(xf,6) + c67*pow(xf,7) + c68*pow(xf,8)
    + c69*pow(xf,9) + c610*pow(xf,10)))*pow(pz,6);
  tb7 = (c7 + (c71*xf + c72*pow(xf,2) + c73*pow(xf,3) + c74*pow(xf,4)
    + c75*pow(xf,5) + c76*pow(xf,6) + c77*pow(xf,7) + c78*pow(xf,8)
    + c79*pow(xf,9) + c710*pow(xf,10)))*pow(pz,7);
  tb = tcb - (tb1 + tb2 + tb3 + tb4 + tb5 + tb6 + tb7);
  return tb = (tb - 32)/1.8 + 273.15;
}
double dew(double p, double xg)
{
  double tcw, pcw, px, aa, s1, s2;
  double pc, tc;
  tcw = (tc1 - 273.15)*1.8 + 32;
  tc = tcw - (a1*xg + a2*pow(xg,2) + a3*pow(xg,3) + a4*pow(xg,4));
  pcw = pc1*14.50377;
  s1 = b1*xg + b2*pow(xg,2) + b3*pow(xg,3) + b4*pow(xg,4);
  s2 = b5*pow(xg,5) + b6*pow(xg,6) + b7*pow(xg,7) + b8*pow(xg,8);
  pc = pcw*exp(s1 + s2);
  px = log(pc/(p*14.50377));
```

```
        aa = log(1.0001 - xg);
        td1 = (al1 + (a11*aa + a12*pow(aa,2) + a13*pow(aa,3) +
a14*pow(aa,4)))*pow(px,1);
        td2 = (al2 + (a21*aa + a22*pow(aa,2) + a23*pow(aa,3) +
a24*pow(aa,4)))*pow(px,2);
        td3 = (al3 + (a31*aa + a32*pow(aa,2) + a33*pow(aa,3) +
a34*pow(aa,4)))*pow(px,3);
        td4 = (al4 + (a41*aa + a42*pow(aa,2) + a43*pow(aa,3) +
a44*pow(aa,4)))*pow(px,4);
        td5 = (al5 + (a51*aa + a52*pow(aa,2) + a53*pow(aa,3) +
a54*pow(aa,4)))*pow(px,5);
        td6 = (al6 + (a61*aa + a62*pow(aa,2) + a63*pow(aa,3) +
a64*pow(aa,4)))*pow(px,6);
        td = tc - (td1 + td2 + td3 + td4 + td5 + td6);
        return td = (td - 32)/1.8 + 273.15;
      }
      void amm_fraction(double t, double p, double *xf, double *xg)
      {
       double err, xf1, xf2, xfold, xg1, xg2, xgold;
         xf1=0.0;  xf2=1.0;
       *xf=0.0;
       do
        {
```

```
  xfold=*xf;
  *xf=(xf1+xf2)/2.;
  tb=bubble(p,*xf);
  if(tb<t) xf2=*xf;
  else xf1=*xf;
  err=fabs(*xf-xfold);
 }while(err>1.0e-20);
 xg1=0.0;  xg2=1.0;
 *xg=0.0;
 do
 {
  xgold=*xg;
  *xg=(xg1+xg2)/2.;
  td=dew(p,*xg);
  if(td<t) xg2=*xg;
  else xg1=*xg;
  err=fabs(*xg-xgold);
 }while(err>1.0e-20);
}
void mix_l(double t, double p, double x, double *hmix, double *smix, double *vmix)
{
 double frmolw, frmola;
 double wm;
```

```
        steam_l(t,p,&h_h2ol,&s_h2ol,&v_h2ol);
        ammonia_l(t, p,&h_h3nl,&s_h3nl,&v_h3nl);
        excess(t, p, x, &he, &se, &ve);
        frmolw = ((1 - x)/wm1)/((1 - x)/wm1 + x/wm2);
        frmola = 1 - frmolw;
        wm = frmolw * wm1 + frmola * wm2;
        *hmix = h_h2ol*frmolw + h_h3nl*frmola + he;
       if(frmola == 0. || frmolw == 0.)
          *smix = s_h2ol*frmolw + s_h3nl*frmola;
       else
          *smix = s_h2ol*frmolw + s_h3nl*frmola + se - r*(frmola*log(frmola) +
frmolw*log(frmolw));
        *vmix = v_h2ol*frmolw + v_h3nl*frmola + ve;
        *hmix = *hmix;
        *smix = *smix;
        *vmix = *vmix;
      }
      void mix_v(double t, double p, double x, double *hmix, double *smix, double
*vmix)
      {
        double frmolw, frmola;
```

```
        double wm;


        steam_v(t,p,&h_h2ov,&s_h2ov,&v_h2ov);
        ammonia_v(t, p,&h_h3nv,&s_h3nv,&v_h3nv);
        frmolw = ((1 - x)/wm1)/((1 - x)/wm1 + x/wm2);
        frmola = 1 - frmolw;
        wm = frmolw * wm1 + frmola * wm2;
        *hmix = h_h2ov*frmolw + h_h3nv*frmola;
        if(frmola == 0. || frmolw == 0.)
          *smix = s_h2ov*frmolw + s_h3nv*frmola;
        else
          *smix = s_h2ov*frmolw + s_h3nv*frmola - r*(frmola*log(frmola) +
frmolw*log(frmolw));
        *vmix = v_h2ov*frmolw + v_h3nv*frmola;
        *hmix = *hmix;
        *smix = *smix;
        *vmix = *vmix;
      }
      void mix_equ(double t, double p, double x, double *hmix, double *smix, double
*vmix)
      {
        double amv, aml;
        double h2omfv, h2omfl, h3nmfv, h3nmfl;
```

```
double xs, xf, xg, xfw, xgw, wml, wmv;
double hmixl, hmixv, smixl, smixv, vmixl, vmixv;
steam_l(t,p,&h_h2ol,&s_h2ol,&v_h2ol);
ammonia_l(t, p,&h_h3nl,&s_h3nl,&v_h3nl);
steam_v(t,p,&h_h2ov,&s_h2ov,&v_h2ov);
ammonia_v(t, p,&h_h3nv,&s_h3nv,&v_h3nv);
amm_fraction(t, p, &xf, &xg);
xfw = 1 - xf;
xgw = 1 - xg;
xs = x;
amv = (xs - xf)/(xg - xf);
aml = (xg - xs)/(xg - xf);
h2omfv = (amv*xgw/wm1)/(amv*xgw/wm1 + amv*xg/wm2);
h2omfl = (aml*xfw/wm1)/(aml*xfw/wm1 + aml*xf/wm2);
h3nmfv = 1 - h2omfv;
h3nmfl = 1 - h2omfl;
wml = h2omfl * wm1 + h3nmfl * wm2;
wmv = h2omfv * wm1 + h3nmfv * wm2;
excess(t, p, xf, &he, &se, &ve);
hmixl = h_h2ol*h2omfl + h_h3nl*h3nmfl + he;
if(h3nmfl == 0. || h2omfl == 0.)
   smixl = s_h2ol*h2omfl + s_h3nl*h3nmfl;
else
```

```
            smixl = s_h2ol*h2omfl + s_h3nl*h3nmfl + se - r*(h3nmfl*log(h3nmfl) +
h2omfl*log(h2omfl));
            vmixl = v_h2ol*h2omfl + v_h3nl*h3nmfl + ve;
            hmixl = hmixl;
            smixl = smixl;
            vmixl = vmixl;
            hmixv = h_h2ov*h2omfv + h_h3nv*h3nmfv;
           if(h3nmfv == 0. || h2omfv == 0.)
             smixv = s_h2ov*h2omfv + s_h3nv*h3nmfv;
           else
             smixv = s_h2ov*h2omfv + s_h3nv*h3nmfv - r*(h3nmfv*log(h3nmfv) +
h2omfv*log(h2omfv));
            vmixv = v_h2ov*h2omfv + v_h3nv*h3nmfv;
            hmixv = hmixv;
            smixv = smixv;
            vmixv = vmixv;
            *hmix = amv * hmixv + aml * hmixl;
            *smix = amv * smixv + aml * smixl;
            *vmix = amv * vmixv + aml * vmixl;
          }
```

```
void property(double t, double p, double x, double *hmix, double *smix, double
*vmix)
{
  td = dew(p, x);
  tb = bubble(p, x);
  if (t <= tb)       mix_l(t, p, x, hmix, smix, vmix);
  else if (t >= td)  mix_v(t, p, x, hmix, smix, vmix);
  else               mix_equ(t, p, x, hmix, smix, vmix);
}
void property_s_t(double p, double s_st, double x, double *hmixs, double *tts,
double *vmixs)
{
  double tt1, tt2, ttsold, err, *smixs, hercules;
  double hb, sb, vb;
  double hd, sd, vd;
  td = dew(p, x);
  tb = bubble(p, x);
  mix_l(tb, p, x, &hb, &sb, &vb);
  mix_v(td, p, x, &hd, &sd, &vd);
  *tts=0.;
  *hmixs=0.;
  hercules=0.;
  smixs=&hercules;
```

```
*vmixs=0.;
if(s_st <= sb)
 {
 tt1=200.;
 tt2=tb;
  do{
     ttsold=*tts;
     *tts = (tt1 + tt2)/2.;
     mix_l(*tts, p, x, hmixs, smixs, vmixs);
     if (*smixs > s_st) tt2 = *tts;
    else              tt1 = *tts;
    err = fabs(*tts - ttsold);
 }while(err > 1.0e-20);
 }
 else if(s_st >= sd)
 {
 tt1=td;
 tt2=700.;
  do{
     ttsold=*tts;
     *tts = (tt1 + tt2)/2.;
     mix_v(*tts, p, x, hmixs, smixs, vmixs);
```

```
            if (*smixs > s_st) tt2 = *tts;
           else              tt1 = *tts;
           err = fabs(*tts - ttsold);
        }while(err > 1.0e-20);
        }
      else
       {
        tt1=tb;
        tt2=td;
         do{
            ttsold=*tts;
            *tts = (tt1 + tt2)/2.;
            mix_equ(*tts, p, x, hmixs, smixs, vmixs);
            if (*smixs > s_st) tt2 = *tts;
            else              tt1 = *tts;
           err = fabs(*tts - ttsold);
        }while(err > 1.0e-20);
        }
    }
    void property_h_t(double p, double h_st, double x, double *tth, double *smixh,
double *vmixh)
    {
     double tt1, tt2, tthold, err, *hmixh, hercules;
```

```
double hb, sb, vb;
double hd, sd, vd;
td = dew(p, x);
tb = bubble(p, x);
mix_l(tb, p, x, &hb, &sb, &vb);
mix_v(td, p, x, &hd, &sd, &vd);
*tth=0.;
hercules=0.;
hmixh=&hercules;
*smixh=0.;
*vmixh=0.;
if(h_st <= hb)
  {
   tt1=200.;
   tt2=tb;
   do{
      tthold=*tth;
      *tth = (tt1 + tt2)/2.;
      mix_l(*tth, p, x, hmixh, smixh, vmixh);
      if (*hmixh > h_st) tt2 = *tth;
     else              tt1 = *tth;
     err = fabs(*tth - tthold);
  }while(err > 1.0e-20);
```

```
  }
  else if(h_st >= hd)
  {
   tt1=td;
   tt2=700.;
   do{
      tthold=*tth;
      *tth = (tt1 + tt2)/2.;
      mix_v(*tth, p, x, hmixh, smixh, vmixh);
     if (*hmixh > h_st) tt2 = *tth;
    else              tt1 = *tth;
    err = fabs(*tth - tthold);
  }while(err > 1.0e-20);
  }
else
  {
   tt1=tb;
   tt2=td;
   do{
      tthold=*tth;
      *tth = (tt1 + tt2)/2.;
      mix_equ(*tth, p, x, hmixh, smixh, vmixh);
```

```
        if (*hmixh > h_st) tt2 = *tth;
       else              tt1 = *tth;
       err = fabs(*tth - tthold);
    }while(err > 1.0e-20);
   }
}
double sat_con(double p,double t)
{
  double x, x1, x2, xold, tt, err;
  x=0.;
  x1=0.;
  x2=1.;
  do
  {
    xold=x;
    x=(x1+x2)/2;
  tt=bubble(p,x);
  if(t>tt) x2=x;
  else     x1=x;
  err=fabs(x-xold);
  }while(err>1.0e-20);
  return x;
}
```

```
double h2o_sat_p(double t)
{
  double f[10] = {0.0, -7.691234564, -2.608023696e1, -1.681706546e2,
                  6.423285504e1, -1.189646225e2, 4.16711732,
                                 2.09750676e1, 1.0e9, 6.0};
  double zt, ztt, pk, psk;
  int i;
  zt = t / 647.3;
  ztt = 1. - zt;
  pk = 0.;
  for(i = 5; i >= 0; i--) pk = pk * ztt + f[i];
  pk = pk / (zt * (1. + f[6] * ztt + f[7] * ztt * ztt));
  pk = pk - ztt / (f[8] * ztt * ztt + f[9]);
  psk = exp(pk) * 221.20;
  return psk;
}
void steam_l_ph(double p, double h, double *t_h2ol, double *s_h2ol, double
*v_h2ol)
{
  double tt1=265, tt2=500, tt, ttold;
  double hh, ss, vv;
```

```
        double err;
          tt=hh=ss=vv=0;
        do
        {
                ttold=tt;
                tt=(tt1+tt2)/2;
                steam_l(tt, p, &hh, &ss, &vv);
          if(hh>h) tt2=tt;
          else     tt1=tt;
          err=fabs(tt-ttold);
         }while(err>1.0e-20);
         *t_h2ol=tt;
         *s_h2ol=ss;
         *v_h2ol=vv;
       }
       void mix_l_ph(double p, double h, double x, double *t_mixl, double *s_mixl, double
*v_mixl)
       {
         double tt1=265, tt2=500, tt, ttold;
         double hh, ss, vv;
         double err;
          tt=hh=ss=vv=0;
         do
```

```
 {
        ttold=tt;
        tt=(tt1+tt2)/2;
        mix_l(tt, p, x, &hh, &ss, &vv);
  if(hh>h) tt2=tt;
  else     tt1=tt;
  err=fabs(tt-ttold);
 }while(err>1.0e-20);
 *t_mixl=tt;
 *s_mixl=ss;
 *v_mixl=vv;
}
void mix_v_ph(double p, double h, double x, double *t_mixv, double *s_mixv,
double *v_mixv)
{
 double tt1=265, tt2=500, tt, ttold;
 double hh, ss, vv;
 double err;
   tt=hh=ss=vv=0;
 do
 {
        ttold=tt;
        tt=(tt1+tt2)/2;
```

```
            mix_v(tt, p, x, &hh, &ss, &vv);
   if(hh>h) tt2=tt;
   else     tt1=tt;
   err=fabs(tt-ttold);
  }while(err>1.0e-20);
  *t_mixv=tt;
  *s_mixv=ss;
  *v_mixv=vv;
}
double sat_p(double t, double x)
{
  double p, p1, p2, pold, tt, err;
            p=0;
            p1=0;
            p2=115;
  do
  {
            pold=p;
            p=(p1+p2)/2;
            tt=bubble(p,x);
            if(t<tt) p2=p;
            else     p1=p;
            err=fabs(p-pold);
```

```
  }while(err>1.0e-20);
  return p;
}
double dew_p(double t, double x)
{
  double p, p1, p2, pold, tt, err;
            p=0;
            p1=0;
            p2=115;
  do
  {
            pold=p;
            p=(p1+p2)/2;
            tt=dew(p,x);
            if(t<tt) p2=p;
            else     p1=p;
            err=fabs(p-pold);
  }while(err>1.0e-20);
  return p;
}
void steamcp_l(double t, double p, double *cp_h2oL)
{
  double cp;
```

```
  Tr = t/Tb;
  Pr = p/Pb;
  cp =  h2o_b2*Tr - h2o_b3*Tr*Tr - h2o_b1 - 2*h2o_b2*Tr + 2*h2o_a4*Tr*(Pr -
h2oP_ro);
  *cp_h2oL = -r*cp;
// cp in kJ/Kmole-K
}
void steamcp_v(double t, double p, double *cp_h2oV)
{
 double cp;
  Tr = t/Tb;
  Pr = p/Pb;
  cp =  h2o_d2*Tr - h2o_d3*Tr*Tr - h2o_d1 - 2*h2o_d2*Tr +
    h2o_c2*12*Pr*pow(Tr,-4)
  + h2o_c3*12*11*Pr*pow(Tr,-12)
  + h2o_c4*44*pow(Pr,3)*pow(Tr,-12);
  *cp_h2oV = -r*cp;
// cp in kJ/Kmole-K
}
void ammoniacp_l(double t, double p, double *cp_h3nl)
{
 double cp;
```

```
  Tr = t/Tb;
  Pr = p/Pb;
  cp = h3n_b2*Tr - h3n_b3*Tr*Tr - h3n_b1 - h3n_b2*2*Tr
    + h3n_a4*2*Tr*(Pr - h3nP_ro);
  *cp_h3nl = -r*cp;
// cp in kJ/Kmole-K
}
void ammoniacp_v(double t, double p, double *cp_h3nv)
{
  double cp;
  Tr = t/Tb; Pr = p/Pb;
  cp = h3n_d2*Tr - h3n_d3*Tr*Tr - h3n_d1 - 2*h3n_d2*Tr +
    h3n_c2*12*Pr*pow(Tr,-4)
  + h3n_c3*132*Pr*pow(Tr,-12)
  + h3n_c4*44*pow(Pr,3)*pow(Tr,-12);
    *cp_h3nv = -r*cp;
// cp in kJ/Kmole-K
}
void excesscp(double t, double p, double x, double *cpe)
{
  double f1, f2, f3;
  f1 = -2*e5/(Tr*Tr) - 6*e6/(Tr*Tr*Tr);
  f2 = -2*e11/(Tr*Tr) - 6*e12/(Tr*Tr*Tr);
```

```
  f3 = -2*e15/(Tr*Tr) - 6*e16/(Tr*Tr*Tr);
    *cpe = r*(f1 + f2*(2*x - 1) + f3*(2*x - 1)*(2*x - 1))*(1 - x)*x;
  }
void mixcp_l(double t, double p, double x, double *cpmix)
{
  double frmolw, frmola;
  double cp_h2oL,cp_h3nl;
  double wm;
  steamcp_l(t,p,&cp_h2oL);
  ammoniacp_l(t, p,&cp_h3nl);
  excesscp(t, p, x, &cpe);
  frmolw = ((1 - x)/wm1)/((1 - x)/wm1 + x/wm2);
  frmola = 1 - frmolw;
  wm = frmolw * wm1 + frmola * wm2;
  *cpmix = cp_h2oL*frmolw + cp_h3nl*frmola + cpe;
}
void mixcp_v(double t, double p, double x, double *cpmix)
{
  double frmolw, frmola;
  double cp_h2oV,cp_h3nv;
  double wm;
  steamcp_v(t,p,&cp_h2oV);
  ammoniacp_v(t, p,&cp_h3nv);
```

```
  frmolw = ((1 - x)/wm1)/((1 - x)/wm1 + x/wm2);
  frmola = 1 - frmolw;
  wm = frmolw * wm1 + frmola * wm2;
  *cpmix = cp_h2oV*frmolw + cp_h3nv*frmola;
}
void tension_h2o(double t, double *gamma_h2ol)
{
  double tu;
  tu=1-t/647.096;
  *gamma_h2ol=235.8*(1-0.625*tu)*pow(tu,1.256);
}
void tension_nh3(double t, double *gamma_nh3l)
{
  double tu;
  tu=1-t/647.096;
  *gamma_nh3l=91.2*pow(tu,1.1028);
}
void tension_mix(double t, double x, double *gamma_mix)
{
  double f,tu;
  tu=1-t/647.096;
  tension_h2o(t,&gamma_h2ol);
  tension_nh3(t,&gamma_nh3l);
```

```
  f=1.442*(1-x)*(1-exp(-2.5*x*x*x*x))+1.106*x*(1-exp(-2.5*pow(1-x,6)));
  *gamma_mix=x*gamma_nh3l+(1-x)*gamma_h2ol-(gamma_h2ol-gamma_nh3l)*f;
}
```

Numerial Model Evaluation Code - tube.cpp

```
#include <stdio.h>
#include <stdlib.h>
#include <math.h>
#include <time.h>
#include "propertyv10.c"
#include <iostream.h>
#include <fstream.h>
#include <iomanip.h>
// T in K
// H, s, are in kJ/kmole for steam_l,steam_v,ammonia_l,ammonia_v,mix_l,mix_v
// cp are in kJ/kmole.K for steam_l,steam_v,ammonia_l,ammonia_v,mix_l,mix_v
// v is specific volume and is in m3/kmole
// x is mass fraction
// xm is mole fraction
// mu in N.s/m2
// diffusion coefficient is in 10^9*m2/s
// k is in W/m.K
// mw is molecular weight in kg/kmole
  double Sc(double,double,double,double);
  double Prandtl(double,double,double,double);
```

```
        double Re_ci(double,double,double);
        double Re_co(double,double,double);
        double Re_l(double,double,double);
        double Re_v(double,double,double,double,double);
        double h_ci(double,double,double,double);
        double h_co(double,double,double,double,double,double);
        double K_l(double,double,double,double,double);
        double h_l(double,double,double,double,double);
        double
h_v1(double,double,double,double,double,double,double,double,double,double);
        double h_v2(double,double,double,double,double,double,double,double,double);
        double
K_v1(double,double,double,double,double,double,double,double,double,double);
        double K_v2(double,double,double,double,double,double,double,double,double);
        double
U(double,double,double,double,double,double,double,double,double,double,double);
        double Pressure(double,double,double,double,double,double);
        double d_o,d_i,k_t,L,n1,n2,B,b,l,P,P_c;
        double M_l,m_l,x_l,x,x_sat,xm,T_l,t_l;
        double M_v,m_v,y_v,y,y_sat,ym,T_v,t_v;
        double M_c,m_c,T_c,t_c,newt_c;
        double T_i,newT_i,x_i,xm_i,y_i,ym_i,newz,z,latentheat_h2oi,latentheat_nh3i;
        double cp_h2ol,cp_h2ov;
```

```
double cp_nh3l,cp_nh3v;
double H_h2oli,s_h2oli,v_h2oli,H_h2ovi,s_h2ovi,v_h2ovi;
double H_nh3li,s_nh3li,v_nh3li,H_nh3vi,s_nh3vi,v_nh3vi;
double H_l,s_l,v_l;
double H_v,s_v,v_v;
double H_c,s_c,v_c;
double mw_mixl,mw_mixv,newmw_mixl,newmw_mixv;
double moleabsorbl,dm_nh3,dm_h2o,dx,dy,dH_l,dH_v,dA;
double h_loverall,h_voverall,h_ltmp,h_vtmp,C_ol,C_ov;
double Tc[100],Tm_c,newTm_c,dH_c,Q_c,dQ_c;
double delta,delta1,delta2,deltaP;
int     incr1,incr2,try1;
double m_vtmp,t_vtmp,y_tmp;
int counter_tmp;



double accuracy;
int
value,datafeed,wait1,wait2,checkz,checkTm_c,checkT_i,iteration,counter,counter1,counter
2,counter3,counter4,counter5,search,searchnode,done,constraint;
double temp,temp11,temp22,temp33,temp44,temp55,temp66,temp77;
double data[10000][15],predata[10000][15];
int N,Np;
```

```
  double deltaM, deltaE, accuracyM, accuracyE;
  double M_li,xi,xmi,t_li;
  double M_lo,xo,xmo,t_lo;
  double M_vi,yi,ymi,t_vi;
  double M_vo,yo,ymo,t_vo;
  double t_ci,t_co;
  double H_li,s_li,v_li;
  double H_vi,s_vi,v_vi;
  double H_ci,s_ci,v_ci;
  double H_lo,s_lo,v_lo;
  double H_vo,s_vo,v_vo;
  double H_co,s_co,v_co;
  double mw_mixli,mw_mixvi,mw_mixlo,mw_mixvo;
  double P_v,P_rec,M_vrec,M_vliq,T_vrec,y_vrec,x_vliq;
  double xm_vliq,mw_mix_vliq,H_vliq,s_vliq,v_vliq;
  double deltaT_c,T_loexp,cp_c,Q_cexp,Q_sexp,Q_s;

void main()
{
        value=-1;
        done=0;
// here N is number of tubes
        N=80;
```

```
        ofstream ofile("results.xls");
        printf("The simulation code for a Falling Film Absorber \n");
        printf("\n\nConditions of the absorber entered in the code are as
following:\n");
        printf("N: %d\n",N);
        P=2.835;
    //Inlet Conditions of the liquid
      M_l=0.014474;
      x_l=0.29444804651456;
      T_l=273.15+42.20;
    //Inlet Conditions of the vapor
      P_rec=4.716;
      M_vrec=0.0023344;
      T_vrec=273.15+72.10;
      amm_fraction(T_vrec,P_rec,&x_i,&y_vrec);
      P_v=2.918;
      T_v=273.15+59.88;
      M_vliq=0.0;
      M_v=M_vrec;
      amm_fraction(T_v,P_v,&x_vliq,&y_v);
      if ((M_vrec-M_vrec*(x_vliq-y_vrec)/(x_vliq-y_v))>0)
      {     M_v=M_vrec*(x_vliq-y_vrec)/(x_vliq-y_v);
            M_vliq=M_vrec-M_v;
```

```
}
else
        y_v=y_vrec;
//Inlet Conditions of the coolant
M_c=0.088705;
T_c=273.15+25.99;
P_c=1;
        printf("\n System pressure, P (bar): %lf",P);
        printf("\n Inlet Conditions of the weak solution:");
        printf("\n \t Mass flow rate, M_l (kg/s): %lf",M_l);
        printf("\n \t Concentration, x : %lf",x_l);
        printf("\n \t Temperature, T_l (K): %lf",T_l);
        printf("\n Inlet Conditions of the vapor:");
        printf("\n \t Mass flow rate, M_v (kg/s): %lf",M_v);
        printf("\n \t Concentration, y : %lf",y_v);
        printf("\n \t Temperature, T_v (K): %lf",T_v);
        printf("\n Inlet Conditions of the coolant:");
        printf("\n \t Mass flow rate, M_c (kg/s): %lf",M_c);
        printf("\n \t Pressure, P_c (bar): %lf",P_c);
        printf("\n \t Temperature, T_c (K): %lf",T_c);
        datafeed=0;
        printf("\n \n If you want to give your own conditions, press 1 otherwise
press anyother key:");
```

```
scanf("%d",&datafeed);
if (datafeed==1)
{
        printf("\n\n Enter the system pressure, P (bar):");
        scanf("%lf",&P);
        printf("\n Enter the Inlet Conditions of the weak solution:");
        printf("\n \t Mass flow rate, M_l (kg/s):");
        scanf("%lf",&M_l);
        printf("\n \t Concentration, x:");
        scanf("%lf",&x_l);
        printf("\n \t Temperature, T_l:");
        scanf("%lf",&T_l);
        printf("\n Enter the Inlet Conditions of the vapor:");
        printf("\n \t Mass flow rate, M_v (kg/s):");
        scanf("%lf",&M_v);
        printf("\n \t Concentration, y:");
        scanf("%lf",&y_v);
        printf("\n \t Temperature, T_v (K):");
        scanf("%lf",&T_v);
        printf("\n Enter the Inlet Conditions of the coolant:");
        printf("\n \t Mass flow rate, M_c (kg/s):");
        scanf("%lf",&M_c);
        printf("\n \t Pressure, P_c (bar):");
```

```
scanf("%lf",&P_c);
printf("\n \t Temperature, T_c (K):");
scanf("%lf",&T_c);
printf("\n\n You entered:\n");
printf("\n System pressure, P (bar): %lf",P);
printf("\n Inlet Conditions of the weak solution:");
printf("\n \t Mass flow rate, M_l (kg/s): %lf",M_l);
printf("\n \t Concentration, x : %lf",x_l);
printf("\n \t Temperature, T_l (K): %lf",T_l);
printf("\n Inlet Conditions of the vapor:");
printf("\n \t Mass flow rate, M_v (kg/s): %lf",M_v);
printf("\n \t Concentration, y : %lf",y_v);
printf("\n \t Temperature, T_v (K): %lf",T_v);
printf("\n Inlet Conditions of the coolant:");
printf("\n \t Mass flow rate, M_c (kg/s): %lf",M_c);
printf("\n \t Pressure, P_c (bar): %lf",P_c);
printf("\n \t Temperature, T_c (K): %lf\n\n",T_c);
}
//Number of coolant tubes in parallel (should not more than 100, if required change
array size)
n1=15;
d_o=3.175e-3;
d_i=2.286e-3;
```

```
        k_t=16.3;
//  B is the tube length
        B=0.0978;
//Number of coolant tubes in a row
        n2=4;
//  vertical tube spacing (center to center spacing)
        l=7.62e-3;
//  horizontal tube spacing (center to center spacing)
        b=15.875e-3;
        delta=0.5e-3;
        incr1=int(d_o/delta);
        delta1=(d_o/incr1);
        incr2=int((l-d_o)/delta);
        //incr2=0;
        delta2=((l-d_o)/incr2);
        m_c=M_c/(n1*n2);

// Variables which needs to be updated
        ofile << "System pressure, P (bar)" << '\t' << P << endl;
        ofile << "Inlet Conditions of the weak solution" << endl;
        ofile << '\t' << "Mass flow rate (kg/s)" << '\t' << M_l << endl;
        ofile << '\t' << "Concentration" << '\t' << x_l << endl;
        ofile << '\t' << "Temperature" << '\t' << T_l << endl;
```

```
            ofile << "Inlet Conditions of the vapor" << endl;
            ofile << '\t' << "Mass flow rate (kg/s)" << '\t' << M_v << endl;
            ofile << '\t' << "Concentration" << '\t' << y_v << endl;
            ofile << '\t' << "Temperature" << '\t' << T_v << endl;
            ofile << "Inlet Conditions of the coolant" << endl;
            ofile << '\t' << "Mass flow rate (kg/s)" << '\t' << M_c << endl;
            ofile << '\t' << "Pressure (bar)" << '\t' << P_c << endl;
            ofile << '\t' << "Temperature" << '\t' << T_c << endl;
            ofile << endl;
            ofile << "Geometric Dimensions" << endl;
            ofile << '\t' << "Number of coolant tubes in parallel" << '\t' << n1 << endl;
            ofile << '\t' << "Number in tubes in a row" << '\t' << n2 << endl;
            ofile << '\t' << "Inner diameter of the tube" << '\t' << d_i << endl;
            ofile << '\t' << "Outer diameter of the tube" << '\t' << d_o << endl;
            ofile << '\t' << "Thermal conductivity" << '\t' << k_t << endl;
            ofile << '\t' << "Tube length" << '\t' << B << endl;
            ofile << '\t' << "Vertical tube spacing" << '\t' << l << endl;
            ofile << '\t' << "Horizontal tube spacing" << '\t' << b << endl;
            ofile << endl;
            wait1 = 1;
while (wait1 != 0)
{
  // initialized the data array
```

```
  for (counter1 = 0 ; counter1 <= (N*(incr1+incr2)-1); ++counter1)
{
        data[counter1][0]=0.0;
        data[counter1][1]=0.0;
        data[counter1][2]=0.0;
        data[counter1][3]=0.0;
        data[counter1][4]=0.0;
        data[counter1][5]=T_v;
        data[counter1][6]=y_v;
        data[counter1][7]=M_v;
        data[counter1][8]=T_c;
        data[counter1][9]=0.0;
        data[counter1][10]=0.0;
        data[counter1][11]=0.0;
        data[counter1][12]=0.0;
        data[counter1][13]=0.0;
        data[counter1][14]=0.0;
        predata[counter1][0]=0.0;
        predata[counter1][1]=0.0;
        predata[counter1][2]=0.0;
        predata[counter1][3]=0.0;
        predata[counter1][4]=0.0;
        predata[counter1][5]=0.0;
```

```
            predata[counter1][6]=0.0;
            predata[counter1][7]=0.0;
            predata[counter1][8]=0.0;
            predata[counter1][9]=0.0;
            predata[counter1][10]=0.0;
            predata[counter1][11]=0.0;
            predata[counter1][12]=0.0;
            predata[counter1][13]=0.0;
            predata[counter1][14]=0.0;
}
  iteration=1;
  wait2 = 1;
while (wait2 != 0)
{
  for (counter5 = 0 ; counter5 <= 3; ++counter5)
{
  m_l=M_l/(n2);
  t_l=T_l;
  x=x_l;
//now moving from top to bottom for liquid
  printf("\n Working on liquid side \n");
  counter=0;
  for (counter1 = 0 ; counter1 <= (N-1); ++counter1)
```

```
{
//  "For loop" for the tube side simulation
        for (counter2 = 1 ; counter2 <= incr1; ++counter2)
        {
                t_v=data[counter][5];
                y=data[counter][6];
                m_v=data[counter][7]/n2;
                t_c=data[counter][8];
                steam_l(t_c,P_c,&H_c,&s_c,&v_c);
                xm=(x/mw_nh3)/((1-x)/mw_h2o+x/mw_nh3);
                ym=(y/mw_nh3)/((1-y)/mw_h2o+y/mw_nh3);
                mw_mixl=(1-xm)*mw_h2o+xm*mw_nh3;
                mw_mixv=(1-ym)*mw_h2o+ym*mw_nh3;
                mix_l(t_l,P,x,&H_l,&s_l,&v_l);
                mix_v(t_v,P,y,&H_v,&s_v,&v_v);

                h_ltmp=h_l(m_l,d_o,t_l,P,x);
                steamcp_l(t_l,P,&cp_h2ol);
                ammoniacp_l(t_l,P,&cp_nh3l);
                h_vtmp=h_v1(m_l,m_v,b,B,d_o,t_l,t_v,P,x,y);
                steamcp_v(t_v,P,&cp_h2ov);
                ammoniacp_v(t_v,P,&cp_nh3v);
```

```
dA=2*B*(d_o/2)*fabs((asin(2*fabs(d_o/2-counter2*delta1)/d_o)-
asin(2*fabs(d_o/2-(counter2-1)*delta1)/d_o)));
// Guess interface temperature
T_i=t_l;
checkT_i=0;
// "While loop" for T_i interation
while (checkT_i != 1)
{
amm_fraction(T_i,P,&x_i,&y_i);
xm_i=(x_i/mw_nh3)/((1-x_i)/mw_h2o+x_i/mw_nh3);
ym_i=(y_i/mw_nh3)/((1-y_i)/mw_h2o+y_i/mw_nh3);
// Guess value z
checkz=0;
z=1.1;
// "While loop" for z interation
while (checkz == 0)
{
moleabsorbl=K_l(m_l,d_o,t_l,P,x)*log(fabs(((z-
xm)/(z-xm_i))));
newz=(ym_i-
ym*exp(moleabsorbl/K_v1(m_l,m_v,b,B,d_o,t_l,t_v,P,x,y)))/(1-
exp(moleabsorbl/K_v1(m_l,m_v,b,B,d_o,t_l,t_v,P,x,y)));
if (fabs(moleabsorbl)<1.0e-7)
```

```
{       printf(",(Saturation: %d),",counter);
        moleabsorbl=0;
        h_loverall=h_ltmp;
        h_voverall=h_vtmp;
        dm_nh3=0;
        dm_h2o=0;
        goto a;
}
if ((z-newz)<=1.0e-5 && (-z+newz)<=1.0e-5)
        checkz=1;
else
        z=(z+newz)/2;
} // End of "While loop" for z interation
dm_nh3=dA*moleabsorbl*z*mw_nh3;
dm_h2o=dA*moleabsorbl*(1-z)*mw_h2o;
steam_l(T_i,P,&H_h2oli,&s_h2oli,&v_h2oli);
steam_v(T_i,P,&H_h2ovi,&s_h2ovi,&v_h2ovi);
latentheat_h2oi=H_h2ovi-H_h2oli;
ammonia_l(T_i,P,&H_nh3li,&s_nh3li,&v_nh3li);
ammonia_v(T_i,P,&H_nh3vi,&s_nh3vi,&v_nh3vi);
latentheat_nh3i=H_nh3vi-H_nh3li;
C_ol=((dm_h2o*cp_h2ol*1000)/(mw_h2o*dA) +
(dm_nh3*cp_nh3l*1000)/(mw_nh3*dA))/h_ltmp;
```

```
                    h_loverall=(h_ltmp*C_ol)/(1-exp(-C_ol));
                    C_ov=((dm_h2o*cp_h2ov*1000)/(mw_h2o*dA) +
(dm_nh3*cp_nh3v*1000)/(mw_nh3*dA))/h_vtmp;
                    h_voverall=(h_vtmp*C_ov)/(1-exp(-C_ov));
        newT_i=(h_voverall*dA*t_v+h_loverall*dA*t_l+dm_nh3*(1000*latentheat_nh3i/
mw_nh3)+dm_h2o*(1000*latentheat_h2oi/mw_h2o))/(h_loverall*dA+h_voverall*dA);
                    if ((T_i-newT_i)<=1.0e-5 && (-T_i+newT_i)<=1.0e-5)
                        checkT_i=1;
                    else
                    T_i=(T_i+newT_i)/2;

                } // End of "While loop" for T_i interation
      a:

                    dQ_c=dA*U(d_o,d_i,B,k_t,m_c,t_c,P_c,m_l,t_l,P,x)*(t_l-t_c);
                    data[counter][0]=counter;
                    data[counter][1]=t_l;
                    data[counter][2]=x;
                    data[counter][3]=m_l*n2;
                    data[counter][4]=T_i;
                    data[counter][9]=z;
                    data[counter][10]=1.0;
                    data[counter][11]=x_i;
```

```
                    data[counter][12]=y_i;
                    counter=counter+1;

                    // Updating x,y
                    x=(m_l*x+dm_nh3)/(m_l+dm_nh3+dm_h2o);
                    xm=(x/mw_nh3)/((1-x)/mw_h2o+x/mw_nh3);
                    newmw_mixl=(1-xm)*mw_h2o+xm*mw_nh3;
                    dH_l=((newmw_mixl)*(-
m_l*(H_l/mw_mixl)+(h_loverall/1000)*dA*(T_i-
t_l)+dm_nh3*(H_nh3li/mw_nh3)+dm_h2o*(H_h2oli/mw_h2o)-dQ_c/1000))/(m_l-
dm_nh3-dm_h2o)+H_l;

                    // Updating T_l,T_v
                    H_l=H_l+dH_l;
                    mix_l_ph(P,H_l,x,&t_l,&s_l,&v_l);

                    // Updating m_v,m_l
                    m_l=m_l+dm_nh3+dm_h2o;

                } // End of "For loop" for tube side simulation

        // this is for mesh side
        for (counter2 = 1 ; counter2 <= incr2; ++counter2)
```

```
{
        t_v=data[counter][5];
        y=data[counter][6];
        m_v=data[counter][7]/n2;

        xm=(x/mw_nh3)/((1-x)/mw_h2o+x/mw_nh3);
        ym=(y/mw_nh3)/((1-y)/mw_h2o+y/mw_nh3);
        mw_mixl=(1-xm)*mw_h2o+xm*mw_nh3;
        mw_mixv=(1-ym)*mw_h2o+ym*mw_nh3;
        mix_l(t_l,P,x,&H_l,&s_l,&v_l);
        mix_v(t_v,P,y,&H_v,&s_v,&v_v);

        h_ltmp=h_l(m_l,d_o,t_l,P,x);
        steamcp_l(t_l,P,&cp_h2ol);
        ammoniacp_l(t_l,P,&cp_nh3l);
        h_vtmp=h_v2(m_l,m_v,b,B,t_l,t_v,P,x,y);
        steamcp_v(t_v,P,&cp_h2ov);
        ammoniacp_v(t_v,P,&cp_nh3v);

        dA=2*B*delta2;

        // Guess interface temperature
        T_i=t_l;
```

```
checkT_i=0;

// "While loop" for T_i interation
while (checkT_i != 1)
{
        amm_fraction(T_i,P,&x_i,&y_i);
        xm_i=(x_i/mw_nh3)/((1-x_i)/mw_h2o+x_i/mw_nh3);
        ym_i=(y_i/mw_nh3)/((1-y_i)/mw_h2o+y_i/mw_nh3);

        // Guess value z
        checkz=0;
        z=1.1;

        // "While loop" for z interation
        while (checkz == 0)
        {
                moleabsorbl=K_l(m_l,d_o,t_l,P,x)*log(fabs(((z-
xm)/(z-xm_i))));
                newz=(ym_i-
ym*exp(moleabsorbl/K_v2(m_l,m_v,b,B,t_l,t_v,P,x,y)))/(1-
exp(moleabsorbl/K_v2(m_l,m_v,b,B,t_l,t_v,P,x,y)));
                if (fabs(moleabsorbl)<1.0e-7)
                {       printf(",(Saturation: %d),",counter);
```

```
                moleabsorbl=0;
                h_loverall=h_ltmp;
                h_voverall=h_vtmp;
                dm_nh3=0;
                dm_h2o=0;
                goto b;
        }
        if ((z-newz)<=1.0e-5 && (-z+newz)<=1.0e-5)
                checkz=1;
        else
                z=(z+newz)/2;


} // End of "While loop" for z interation

dm_nh3=dA*moleabsorbl*z*mw_nh3;
dm_h2o=dA*moleabsorbl*(1-z)*mw_h2o;

steam_l(T_i,P,&H_h2oli,&s_h2oli,&v_h2oli);
steam_v(T_i,P,&H_h2ovi,&s_h2ovi,&v_h2ovi);
latentheat_h2oi=H_h2ovi-H_h2oli;

ammonia_l(T_i,P,&H_nh3li,&s_nh3li,&v_nh3li);
```

```
                ammonia_v(T_i,P,&H_nh3vi,&s_nh3vi,&v_nh3vi);
                latentheat_nh3i=H_nh3vi-H_nh3li;

                C_ol=((dm_h2o*cp_h2ol*1000)/(mw_h2o*dA) +
(dm_nh3*cp_nh3l*1000)/(mw_nh3*dA))/h_ltmp;
                h_loverall=(h_ltmp*C_ol)/(1-exp(-C_ol));

                C_ov=((dm_h2o*cp_h2ov*1000)/(mw_h2o*dA) +
(dm_nh3*cp_nh3v*1000)/(mw_nh3*dA))/h_vtmp;
                h_voverall=(h_vtmp*C_ov)/(1-exp(-C_ov));

        newT_i=(h_voverall*dA*t_v+h_loverall*dA*t_l+dm_nh3*(1000*latentheat_nh3i/
mw_nh3)+dm_h2o*(1000*latentheat_h2oi/mw_h2o))/(h_loverall*dA+h_voverall*dA);
                if ((T_i-newT_i)<=1.0e-5 && (-T_i+newT_i)<=1.0e-5)
                        checkT_i=1;
                else
                T_i=(T_i+newT_i)/2;
        } // End of "While loop" for T_i interation
    b:
                data[counter][0]=counter;
                data[counter][1]=t_l;
                data[counter][2]=x;
```

```
data[counter][3]=m_l*n2;
data[counter][4]=T_i;
data[counter][8]=0;
data[counter][9]=z;
data[counter][10]=0.0;
data[counter][11]=x_i;
data[counter][12]=y_i;
counter=counter+1;

// Updating x,y
x=(m_l*x+dm_nh3)/(m_l+dm_nh3+dm_h2o);
xm=(x/mw_nh3)/((1-x)/mw_h2o+x/mw_nh3);
newmw_mixl=(1-xm)*mw_h2o+xm*mw_nh3;
dH_l=((newmw_mixl)*(-
m_l*(H_l/mw_mixl)+(h_loverall/1000)*dA*(T_i-
t_l)+dm_nh3*(H_nh3li/mw_nh3)+dm_h2o*(H_h2oli/mw_h2o)))/(m_l-dm_nh3-
dm_h2o)+H_l;

// Updating T_l,T_v
H_l=H_l+dH_l;
mix_l_ph(P,H_l,x,&t_l,&s_l,&v_l);
// Updating m_v,m_l
m_l=m_l+dm_nh3+dm_h2o;
```

```
            } // End of "For loop" for mesh side simulation
            printf("%d,", counter1);
} // End of counter

//now moving from bottom to top for vapor and coolant
  printf("\n Working on vapor side \n");
  counter=N*(incr1+incr2)-1;
  t_c=T_c;
  t_v=T_v;
  y=y_v;
  m_v=M_v/(n2);

  for (counter1 = (N-1) ; counter1 >= 0; --counter1)
{

// this is for mesh side
for (counter2 = 1 ; counter2 <= incr2; ++counter2)
            {
                  t_l=data[counter][1];
                  x=data[counter][2];
                  m_l=data[counter][3]/n2;
```

```
xm=(x/mw_nh3)/((1-x)/mw_h2o+x/mw_nh3);
ym=(y/mw_nh3)/((1-y)/mw_h2o+y/mw_nh3);
mw_mixl=(1-xm)*mw_h2o+xm*mw_nh3;
mw_mixv=(1-ym)*mw_h2o+ym*mw_nh3;
mix_l(t_l,P,x,&H_l,&s_l,&v_l);
mix_v(t_v,P,y,&H_v,&s_v,&v_v);

h_ltmp=h_l(m_l,d_o,t_l,P,x);
steamcp_l(t_l,P,&cp_h2ol);
ammoniacp_l(t_l,P,&cp_nh3l);
h_vtmp=h_v2(m_l,m_v,b,B,t_l,t_v,P,x,y);
steamcp_v(t_v,P,&cp_h2ov);
ammoniacp_v(t_v,P,&cp_nh3v);

dA=2*B*delta2;

// Guess interface temperature
T_i=t_l;
checkT_i=0;

// "While loop" for T_i interation
while (checkT_i != 1)
```

```
{
        amm_fraction(T_i,P,&x_i,&y_i);
        xm_i=(x_i/mw_nh3)/((1-x_i)/mw_h2o+x_i/mw_nh3);
        ym_i=(y_i/mw_nh3)/((1-y_i)/mw_h2o+y_i/mw_nh3);

        // Guess value z
        checkz=0;
        z=1.1;

        // "While loop" for z interation
        while (checkz == 0)
        {
                moleabsorbl=K_l(m_l,d_o,t_l,P,x)*log(fabs(((z-
xm)/(z-xm_i))));
                newz=(ym_i-
ym*exp(moleabsorbl/K_v2(m_l,m_v,b,B,t_l,t_v,P,x,y)))/(1-
exp(moleabsorbl/K_v2(m_l,m_v,b,B,t_l,t_v,P,x,y)));
                if (fabs(moleabsorbl)<1.0e-7)
                {       printf(",(Saturation: %d),",counter);
                        moleabsorbl=0;
                        h_loverall=h_ltmp;
                        h_voverall=h_vtmp;
                        dm_nh3=0;
```

```
                dm_h2o=0;
                goto d;
        }
        if ((z-newz)<=1.0e-5 && (-z+newz)<=1.0e-5)
                checkz=1;
        else
                z=(z+newz)/2;


} // End of "While loop" for z interation

dm_nh3=dA*moleabsorbl*z*mw_nh3;
dm_h2o=dA*moleabsorbl*(1-z)*mw_h2o;

steam_l(T_i,P,&H_h2oli,&s_h2oli,&v_h2oli);
steam_v(T_i,P,&H_h2ovi,&s_h2ovi,&v_h2ovi);
latentheat_h2oi=H_h2ovi-H_h2oli;

ammonia_l(T_i,P,&H_nh3li,&s_nh3li,&v_nh3li);
ammonia_v(T_i,P,&H_nh3vi,&s_nh3vi,&v_nh3vi);
latentheat_nh3i=H_nh3vi-H_nh3li;
```

```
                    C_ol=((dm_h2o*cp_h2ol*1000)/(mw_h2o*dA) +
(dm_nh3*cp_nh3l*1000)/(mw_nh3*dA))/h_ltmp;
                    h_loverall=(h_ltmp*C_ol)/(1-exp(-C_ol));

                    C_ov=((dm_h2o*cp_h2ov*1000)/(mw_h2o*dA) +
(dm_nh3*cp_nh3v*1000)/(mw_nh3*dA))/h_vtmp;
                    h_voverall=(h_vtmp*C_ov)/(1-exp(-C_ov));

      newT_i=(h_voverall*dA*t_v+h_loverall*dA*t_l+dm_nh3*(1000*latentheat_nh3i/
mw_nh3)+dm_h2o*(1000*latentheat_h2oi/mw_h2o))/(h_loverall*dA+h_voverall*dA);
                    if ((T_i-newT_i)<=1.0e-5 && (-T_i+newT_i)<=1.0e-5)
                        checkT_i=1;
                    else
                    T_i=(T_i+newT_i)/2;
                } // End of "While loop" for T_i interation
    d:
                    data[counter][4]=T_i;
                    data[counter][5]=t_v;
                    data[counter][6]=y;
                    data[counter][7]=m_v*n2;
                    data[counter][8]=0;
                    data[counter][9]=z;
```

```
                    data[counter][10]=0.0;
                    data[counter][11]=x_i;
                    data[counter][12]=y_i;
                    counter=counter-1;

                    // Updating x,y
                    y=(m_v*y-dm_nh3)/(m_v-dm_nh3-dm_h2o);
                    ym=(y/mw_nh3)/((1-y)/mw_h2o+y/mw_nh3);
                    newmw_mixv=(1-ym)*mw_h2o+ym*mw_nh3;
                    dH_v=((newmw_mixv)*(-
m_v*(H_v/mw_mixv)+(h_voverall/1000)*dA*(t_v-
T_i)+dm_nh3*(H_nh3vi/mw_nh3)+dm_h2o*(H_h2ovi/mw_h2o)))/(m_v-dm_nh3-
dm_h2o)+H_v;

                    // Updating T_l,T_v
                    H_v=H_v-dH_v;
                    mix_v_ph(P,H_v,y,&t_v,&s_v,&v_v);

                    // Updating m_v,m_l
                    m_v=m_v-dm_nh3-dm_h2o;

                } // End of "For loop" for mesh side simulation
```

```
Tm_c=t_c;
checkTm_c=0;
while (checkTm_c!=1)
{
        counter_tmp=counter;
        m_vtmp=m_v;
        t_vtmp=t_v;
        y_tmp=y;
        steam_l(t_c,P_c,&H_c,&s_c,&v_c);

//  "For loop" for the tube side simulation
        for (counter2 = 1 ; counter2 <= incr1; ++counter2)
        {
                t_l=data[counter_tmp][1];
                x=data[counter_tmp][2];
                m_l=data[counter_tmp][3]/n2;

                xm=(x/mw_nh3)/((1-x)/mw_h2o+x/mw_nh3);
                ym=(y_tmp/mw_nh3)/((1-y_tmp)/mw_h2o+y_tmp/mw_nh3);
                mw_mixl=(1-xm)*mw_h2o+xm*mw_nh3;
                mw_mixv=(1-ym)*mw_h2o+ym*mw_nh3;
                mix_l(t_l,P,x,&H_l,&s_l,&v_l);
                mix_v(t_vtmp,P,y_tmp,&H_v,&s_v,&v_v);
```

```
h_ltmp=h_l(m_l,d_o,t_l,P,x);
steamcp_l(t_l,P,&cp_h2ol);
ammoniacp_l(t_l,P,&cp_nh3l);

h_vtmp=h_v1(m_l,m_vtmp,b,B,d_o,t_l,t_vtmp,P,x,y_tmp);
steamcp_v(t_vtmp,P,&cp_h2ov);
ammoniacp_v(t_vtmp,P,&cp_nh3v);

dA=2*B*(d_o/2)*fabs((asin(2*fabs(d_o/2-counter2*delta1)/d_o)-
asin(2*fabs(d_o/2-(counter2-1)*delta1)/d_o)));

// Guess interface temperature
T_i=t_l;
checkT_i=0;

// "While loop" for T_i interation
while (checkT_i != 1)
{
        amm_fraction(T_i,P,&x_i,&y_i);
        xm_i=(x_i/mw_nh3)/((1-x_i)/mw_h2o+x_i/mw_nh3);
        ym_i=(y_i/mw_nh3)/((1-y_i)/mw_h2o+y_i/mw_nh3);
```

```
// Guess value z
checkz=0;
z=1.1;

// "While loop" for z interation
while (checkz == 0)
{
        moleabsorbl=K_l(m_l,d_o,t_l,P,x)*log(fabs(((z-xm)/(z-xm_i))));
        newz=(ym_i-ym*exp(moleabsorbl/K_v1(m_l,m_vtmp,b,B,d_o,t_l,t_vtmp,P,x,y_tmp)))/(1-exp(moleabsorbl/K_v1(m_l,m_vtmp,b,B,d_o,t_l,t_vtmp,P,x,y_tmp)));
        if (fabs(moleabsorbl)<1.0e-7)
        {       printf(",(Saturation: %d),",counter_tmp);
                moleabsorbl=0;
                h_loverall=h_ltmp;
                h_voverall=h_vtmp;
                dm_nh3=0;
                dm_h2o=0;
                goto c;
        }
        if ((z-newz)<=1.0e-5 && (-z+newz)<=1.0e-5)
                checkz=1;
```

```
else
        z=(z+newz)/2;


} // End of "While loop" for z interation

dm_nh3=dA*moleabsorbl*z*mw_nh3;
dm_h2o=dA*moleabsorbl*(1-z)*mw_h2o;

steam_l(T_i,P,&H_h2oli,&s_h2oli,&v_h2oli);
steam_v(T_i,P,&H_h2ovi,&s_h2ovi,&v_h2ovi);
latentheat_h2oi=H_h2ovi-H_h2oli;

ammonia_l(T_i,P,&H_nh3li,&s_nh3li,&v_nh3li);
ammonia_v(T_i,P,&H_nh3vi,&s_nh3vi,&v_nh3vi);
latentheat_nh3i=H_nh3vi-H_nh3li;

C_ol=((dm_h2o*cp_h2ol*1000)/(mw_h2o*dA) +
(dm_nh3*cp_nh3l*1000)/(mw_nh3*dA))/h_ltmp;
h_loverall=(h_ltmp*C_ol)/(1-exp(-C_ol));

C_ov=((dm_h2o*cp_h2ov*1000)/(mw_h2o*dA) +
(dm_nh3*cp_nh3v*1000)/(mw_nh3*dA))/h_vtmp;
```

```
                h_voverall=(h_vtmp*C_ov)/(1-exp(-C_ov));


        newT_i=(h_voverall*dA*t_vtmp+h_loverall*dA*t_l+dm_nh3*(1000*latentheat_n
h3i/mw_nh3)+dm_h2o*(1000*latentheat_h2oi/mw_h2o))/(h_loverall*dA+h_voverall*dA)
;
                if ((T_i-newT_i)<=1.0e-5 && (-T_i+newT_i)<=1.0e-5)
                        checkT_i=1;
                else
                T_i=(T_i+newT_i)/2;

        } // End of "While loop" for T_i interation
    c:
                dQ_c=dA*U(d_o,d_i,B,k_t,m_c,Tm_c,P_c,m_l,t_l,P,x)*(t_l-Tm_c);
                dH_c=(dQ_c*mw_h2o)/(m_c*1000);
                H_c=H_c+dH_c;

                data[counter_tmp][4]=T_i;
                data[counter_tmp][5]=t_vtmp;
                data[counter_tmp][6]=y_tmp;
                data[counter_tmp][7]=m_vtmp*n2;
                data[counter_tmp][8]=Tm_c;
                data[counter_tmp][9]=z;
```

```
data[counter_tmp][10]=1.0;
data[counter_tmp][11]=x_i;
data[counter_tmp][12]=y_i;
data[counter_tmp][13]=t_c;
counter_tmp=counter_tmp-1;


// Updating x,y
y_tmp=(m_vtmp*y_tmp-dm_nh3)/(m_vtmp-dm_nh3-dm_h2o);
ym=(y_tmp/mw_nh3)/((1-y_tmp)/mw_h2o+y_tmp/mw_nh3);
newmw_mixv=(1-ym)*mw_h2o+ym*mw_nh3;
dH_v=((newmw_mixv)*(-
m_vtmp*(H_v/mw_mixv)+(h_voverall/1000)*dA*(t_vtmp-
T_i)+dm_nh3*(H_nh3vi/mw_nh3)+dm_h2o*(H_h2ovi/mw_h2o)))/(m_vtmp-dm_nh3-
dm_h2o)+H_v;

// Updating T_l,T_v
H_v=H_v-dH_v;
mix_v_ph(P,H_v,y_tmp,&t_vtmp,&s_v,&v_v);

// Updating m_v,m_l
m_vtmp=m_vtmp-dm_nh3-dm_h2o;
```

```
        } // End of "For loop" for tube side simulation


        // Updating T_c
        steam_l_ph(P_c,H_c,&newt_c,&s_c,&v_c);
        newTm_c=(t_c+newt_c)/2;


        if ((Tm_c-newTm_c)<=1.0e-5 && (-Tm_c+newTm_c)<=1.0e-5)
        {
                checkTm_c=1;
        }
        else
                Tm_c=(Tm_c+newTm_c)/2;


        data[counter_tmp+1][14]=newt_c;
} // End of "While loop" for checkTm_c .


        if ((N-counter1-n1*int((N-counter1)/n1))==0)
        {
                t_c=newt_c;
                for (counter3 = 0 ; counter3 <= n1-2; ++counter3)
                t_c=t_c+Tc[counter3];
                t_c=t_c/n1;
        }
```

```
                else
                        Tc[int(N-counter1-n1*int((N-counter1)/n1))-1]=newt_c;
                        try1=int(N-counter1-n1*int((N-counter1)/n1))-1;

                counter=counter_tmp;
                m_v=m_vtmp;
                t_v=t_vtmp;
                y=y_tmp;
                printf("%d,", counter1);
        } // End of counter1

        } // End of counter5 it makes the program to run four times before deciding on the
length

        //if ( ((iteration/10.0)-floor(iteration/10))==0)

          ofile << iteration << endl;

        for (counter3 = 0 ; counter3 <= (N*(incr1+incr2)-1); ++counter3)
        {

                        ofile << data[counter3][0] << '\t' << setprecision(20) <<
data[counter3][1] << '\t'
```

```
                        << data[counter3][2] << '\t' << data[counter3][3] << '\t' <<
                        data[counter3][4] << '\t' << data[counter3][5] << '\t' <<
data[counter3][6] <<
                        '\t' << data[counter3][7] << '\t' << data[counter3][8] <<'\t' <<
data[counter3][9] <<
                        '\t' << data[counter3][10] << '\t' << data[counter3][11] <<'\t'
                        << data[counter3][12] << '\t' << data[counter3][13] <<'\t' <<
data[counter3][14] << endl;
        }

                ofile << endl;

        printf("\n\n NUMBER OF TIMES ITERATION HAS BEEN DONE: %d\n",
iteration);

          searchnode=-1;
          search=0;
          counter1=0;

          if (done == 0)
          {       while ( (counter1 <= (N*(incr1+incr2)-1)) && (search == 0))
                  {       if ( data[counter1][7] < 0 && data[counter1+1][7] > 0)
                          {       search=1;
```

```
                    searchnode=int(counter1/(incr1+incr2))+1;
                }
                counter1++;
        }

if ( value == 0 && searchnode == -1)
        {       N=N;
                done=1;
        }
if ( value == 1 && searchnode > 0)
{       N=N-1;
        done=1;
}

if ( searchnode == -1 && done== 0)
//      need to increase the length of absorber
{       printf("\n\n Need to increase the length of the absorber");
        printf("\n Currently it has %d nodes", N);
        if ( data[0][7] > 1e-2 )
                N=N+10;
        else if ( data[0][7] > 1e-3 )
                N=N+5;
        else if ( data[0][7] > 1e-4 )
```

```
                N=N+2;
        else
        {       N=N+1;
                value=1;        }
                printf("\n Increasing the length to %d nodes\n", N);
                ofile << endl;
                ofile << "Increasing the node value to:" << '\t' << N << endl;
        }
        else if ( searchnode > 0 && done==0)
//      need to decrease the length of absorber
        {       printf("\n\n Need to decrease the length of the absorber");
                printf("\n Currently it has %d nodes", N);
                N=N-searchnode;
                value=0;
                printf("\n Decreasing the length to %d nodes\n", N);
                ofile << endl;
                ofile << "Decreasing the node value to:" << '\t' << N << endl;
        }
        else
// continue on iteration
        {       wait1=3;
                done=1;
                ofile << endl;
```

```
                    ofile << "Continuing on iteration" << '\t' << iteration << endl;
            }
        }
        else if ( data[0][7] < 0 )
        {       N=N-1;
                printf("\n \n After doing iteration, it was found that mass flow rate of vapor was negative at the exit. So, length of the absorber is decreased by 1 node and the interation is started again. \n");
                wait1=2;
                ofile << endl;
                ofile << "Restarting iteration with N:" << '\t' << N << endl;
        }
        else if ( data[0][7] > 0 )
        {       wait1=3;
                ofile << endl;
                ofile << "Continuing on iteration" << '\t' << iteration<< endl;
        }


        if ( wait1 == 3)
        {       printf("\n\n NUMBER OF TIMES ITERATION HAS BEEN DONE: %d\n", iteration);
                constraint=1;
```

```
accuracy=1e-7;
for (counter1 = 0 ; counter1 <= (N-1); ++counter1)
{
        if (fabs(data[counter1][0]-predata[counter1][0]) > accuracy)
                constraint=0;
        if (fabs(data[counter1][1]-predata[counter1][1]) > accuracy)
                constraint=0;
        if (fabs(data[counter1][2]-predata[counter1][2]) > accuracy)
                constraint=0;
        if (fabs(data[counter1][3]-predata[counter1][3]) > accuracy)
                constraint=0;
        if (fabs(data[counter1][4]-predata[counter1][4]) > accuracy)
                constraint=0;
        if (fabs(data[counter1][5]-predata[counter1][5]) > accuracy)
                constraint=0;
        if (fabs(data[counter1][6]-predata[counter1][6]) > accuracy)
                constraint=0;
        if (fabs(data[counter1][7]-predata[counter1][7]) > accuracy)
                constraint=0;
        if (fabs(data[counter1][8]-predata[counter1][8]) > accuracy)
                constraint=0;
        if (fabs(data[counter1][9]-predata[counter1][9]) > accuracy)
                constraint=0;
```

```
        if (fabs(data[counter1][11]-predata[counter1][11]) > accuracy)
                constraint=0;
        if (fabs(data[counter1][12]-predata[counter1][12]) > accuracy)
                constraint=0;
}

for (counter1 = 0 ; counter1 <= (N-1); ++counter1)
{
        predata[counter1][0]=data[counter1][0];
        predata[counter1][1]=data[counter1][1];
        predata[counter1][2]=data[counter1][2];
        predata[counter1][3]=data[counter1][3];
        predata[counter1][4]=data[counter1][4];
        predata[counter1][5]=data[counter1][5];
        predata[counter1][6]=data[counter1][6];
        predata[counter1][7]=data[counter1][7];
        predata[counter1][8]=data[counter1][8];
        predata[counter1][9]=data[counter1][9];
        predata[counter1][11]=data[counter1][11];
        predata[counter1][12]=data[counter1][12];
}

if ( constraint == 1)
```

```
                    {       wait1=0;        wait2=0;        }
                    iteration++;
  }
  else
          wait2=0;

} // end of wait2 while loop
} // end of wait1 while loop

  t_li=data[0][1];
  xi=data[0][2];
  M_li=data[0][3];
  t_vo=data[0][5];
  yo=data[0][6];
  M_vo=data[0][7];
  t_co=data[0][8];

  t_lo=data[N*(incr1+incr2)-1][1];
  xo=data[N*(incr1+incr2)-1][2];
  M_lo=data[N*(incr1+incr2)-1][3];
  t_vi=data[N*(incr1+incr2)-1][5];
  yi=data[N*(incr1+incr2)-1][6];
  M_vi=data[N*(incr1+incr2)-1][7];
```

```
t_ci=data[N*(incr1+incr2)-1-incr2][13];

xmi=(xi/mw_nh3)/((1-xi)/mw_h2o+xi/mw_nh3);
ymi=(yi/mw_nh3)/((1-yi)/mw_h2o+yi/mw_nh3);
mw_mixli=(1-xmi)*mw_h2o+xmi*mw_nh3;
mw_mixvi=(1-ymi)*mw_h2o+ymi*mw_nh3;
steam_l(t_ci,P_c,&H_ci,&s_ci,&v_ci);
mix_l(t_li,P,xi,&H_li,&s_li,&v_li);
mix_v(t_vi,P,yi,&H_vi,&s_vi,&v_vi);

xmo=(xo/mw_nh3)/((1-xo)/mw_h2o+xo/mw_nh3);
ymo=(yo/mw_nh3)/((1-yo)/mw_h2o+yo/mw_nh3);
mw_mixlo=(1-xmo)*mw_h2o+xmo*mw_nh3;
mw_mixvo=(1-ymo)*mw_h2o+ymo*mw_nh3;
steam_l(t_co,P_c,&H_co,&s_co,&v_co);
mix_l(t_lo,P,xo,&H_lo,&s_lo,&v_lo);
mix_v(t_vo,P,yo,&H_vo,&s_vo,&v_vo);

deltaE=M_c*(H_ci-H_co)/mw_h2o+M_li*(H_li/mw_mixli)-
M_lo*(H_lo/mw_mixlo)+M_vi*(H_vi/mw_mixvi)-M_vo*(H_vo/mw_mixvo);
deltaM=M_li+M_vi-M_lo-M_vo;
Q_s=M_li*(H_li/mw_mixli)-M_lo*(H_lo/mw_mixlo)+M_vi*(H_vi/mw_mixvi)-
M_vo*(H_vo/mw_mixvo);
```

```
    accuracyM=100-fabs((deltaM/(M_li+M_vi))*100);
    accuracyE=100-fabs((deltaE/(M_c*(H_ci-H_co)/mw_h2o))*100);
    ofile << "deltaM" << '\t' << deltaM << endl << "accuracyM" << '\t' << accuracyM
<< endl << "deltaE" << '\t' << deltaE << endl << "accuracyE" << '\t' << accuracyE << endl
<< "E" << '\t' << Q_s << endl;

  }


  double Sc(double mu_temp, double v_temp, double x_temp, double D_temp )
  {  double xm_temp,mw_mix_temp,temp;

    xm_temp = (x_temp/mw_nh3)/((1 - x_temp)/mw_h2o + x_temp/mw_nh3);
    mw_mix_temp = (1-xm_temp) * mw_h2o + xm_temp * mw_nh3;
    temp=(mu_temp*v_temp)/(pow(10,-9)*D_temp*mw_mix_temp);
    return temp;
  }

  double Prandtl(double mu_temp, double cp_temp, double x_temp, double k_temp )
  {  double xm_temp,mw_mix_temp,temp;

    xm_temp = (x_temp/mw_nh3)/((1 - x_temp)/mw_h2o + x_temp/mw_nh3);
```

```
  mw_mix_temp = (1-xm_temp) * mw_h2o + xm_temp * mw_nh3;
  temp=(mu_temp*cp_temp)/(pow(10,-3)*k_temp*mw_mix_temp);
  return temp;
}


double Re_ci(double m_temp, double d_temp, double mu_temp )
{  double temp;

  // Assuming that coolant passes through only only row at a time
  // Source: page 494 of incropera
  temp=(4*m_temp)/(3.1416*d_temp*mu_temp);
  return temp;
}


double Re_co(double m_temp, double B_temp, double mu_temp )
{  double temp;

// Source: Garemilla paper m_temp is the mass flow rate per tube length. Thats why it is divided by B. It can also be seen from dimensions
  temp=(4*m_temp)/(2*B_temp*mu_temp);
  return temp;
```

```
}


double Re_v(double v_temp, double y_temp, double u_temp, double Dh_temp,
double mu_temp )
{  double ym_temp,mw_mix_temp,temp;

// Source: page 419 of incropera
  ym_temp = (y_temp/mw_nh3)/((1 - y_temp)/mw_h2o + y_temp/mw_nh3);
  mw_mix_temp = (1-ym_temp) * mw_h2o + ym_temp * mw_nh3;
  temp=(mw_mix_temp*u_temp*Dh_temp)/(v_temp*mu_temp);
  return temp;
}

double h_ci(double m_temp, double d_temp, double Tc_temp, double P_c )
{  double
muc_temp,kc_temp,cpc_temp,Re_temp,Prandtl_temp,temp,f,Bstar,Gz,sum;
   int count;

  tsteam_l(Tc_temp,&kc_temp,&muc_temp);
  steamcp_l(Tc_temp,P_c,&cpc_temp);
  Re_temp=Re_ci(m_temp,d_temp,muc_temp);
  Prandtl_temp=Prandtl(muc_temp,cpc_temp,0,kc_temp);
```

```
// Source: page 491, equation 8.60 of incropera
// above source should not be used but it is valid only for Re>10000 whereas our Re is around 1540
// it should be 3.66 but is increasing our problem
//temp1=0.023*pow(1540,0.8)*pow(Prandtl_temp,0.4);

  if (Re_temp<3000)
  {       sum=0;
          for (count = 1 ; count <= 1000; ++count)
          {       Bstar=(B/1000)*count/(Prandtl_temp*d_temp*Re_temp);
                  Gz=3.1415926/(4*Bstar);

  sum=sum+5.364*pow(1+pow(Gz/55,1.1112),0.3)*pow(1+pow(Gz/(28.8*pow(1+pow((Prandtl_temp/0.0207),0.6667),0.5)*pow(1+pow(Gz/55,1.1112),0.6)),1.6667),0.3)-1;
          }
          temp=(sum/1000)*(kc_temp/d_temp);
  }
  else
// Source: Gnielinski equation page 492, equation 8.63 of incropera
// above source should not be used but it is valid only for 3000<Re<500000
  {
          f=pow(0.79*log(Re_temp)-1.64,-2);
```

```
                temp=(kc_temp/d_temp)*((f/8)*(Re_temp-
1000)*Prandtl_temp)/(1+12.7*pow(f/8,0.5)*(pow(Prandtl_temp,0.6667)-1));
        }
        temp11=temp;
        return temp;
      }


      double h_co(double m_temp, double B_temp, double d_temp, double T_temp,
double P_temp, double x_temp )
      {  double
Re_temp,Prandtl_temp,temp,k_temp,D_temp,mu_temp,H_temp,s_temp,v_temp,cp_temp,x
m_temp,mw_mix_temp;

        tmix_l(T_temp,P_temp,x_temp,&k_temp,&D_temp,&mu_temp);
        mix_l(T_temp,P_temp,x_temp,&H_temp,&s_temp,&v_temp);
        mixcp_l(T_temp,P_temp,x_temp,&cp_temp);
        xm_temp = (x_temp/mw_nh3)/((1 - x_temp)/mw_h2o + x_temp/mw_nh3);
        mw_mix_temp = (1-xm_temp) * mw_h2o + xm_temp * mw_nh3;
        Re_temp=Re_co(m_temp,B_temp,mu_temp);
        Prandtl_temp=Prandtl(mu_temp,cp_temp,x_temp,k_temp);

      // Source: Sernes et al J Heat Transfer Trans ASME v101 n1 1979 p 176-178
```

```
//
  temp1=(k_temp)*0.01925*pow(Re_temp,0.24)*pow(Prandtl_temp,0.66)*pow(pow
((mu_temp*v_temp)/mw_mix_temp,2)/9.8,-0.334);
// Source: Parken and Fletcher 1990
//
  temp2=(k_temp)*0.042*pow(Re_temp,0.15)*pow(Prandtl_temp,0.53)*pow(pow((
mu_temp*v_temp)/mw_mix_temp,2)/9.8,-0.334);
// Source: Chun and Seban 1971 for wavy laminar flow
//temp3=(k_temp)*0.821*pow(Re_temp,-
0.22)*pow(pow((mu_temp*v_temp)/mw_mix_temp,2)/9.8,-0.334);
//temp=(k_temp)*3.8e-
3*pow(Re_temp,0.4)*pow(pow((mu_temp*v_temp)/mw_mix_temp,2)/9.8,-
0.334)*pow(Prandtl_temp,0.65);
// Source: Gimbutis 1975 from Kim paper
//
  temp4=(k_temp)*0.39*pow(Re_temp,0.21)*pow(Prandtl_temp,0.36)*pow(pow((m
u_temp*v_temp)/mw_mix_temp,2)/9.8,-
0.334)*pow(pow((mu_temp*v_temp)/mw_mix_temp,2)/(9.8*pow(d_temp,3)),0.12);
// Source: Dhorokhov 1975 from Garimella paper
//
  thickness=pow((3*m_temp*mu_temp*v_temp*v_temp)/(B_temp*9.81*mw_mix_t
emp*mw_mix_temp),0.3334);
```

```
//
  temp5=(k_temp/d_temp)*1.03*pow(Re_temp,0.4)*pow(Prandtl_temp,0.4)*pow((t
hickness/(2*3.14*d_temp)),0.4);
// Source: page 411, equation 7.57 of incropera
//
  temp=(k_temp/d_temp)*(0.3+(((0.62*pow(Re_temp,0.5)*pow(Prandtl_temp,0.333
4))/pow(1+pow(0.4/Prandtl_temp,0.6667),0.25)))*pow(1+pow(Re_temp/282000,0.625),0.
8));
//Wilke correlation for wavy laminar case
  delta=0.91*pow(Re_temp,0.33)*pow(pow((mu_temp*v_temp)/mw_mix_temp,2)/9
.8,0.334);
  temp=(k_temp/delta)*1.88;
//temp=(k_temp/delta)*0.029*pow(Re_temp,0.533)*pow(Prandtl_temp,0.344);
//delta=pow(pow((mu_temp*v_temp)/mw_mix_temp,2)/9.8,0.334);
//temp=(k_temp/delta)*1.76*pow(Re_temp,-0.333);

  temp22=temp;
  return temp;
}

double K_l(double m_temp, double d_temp, double T_temp, double P_temp, double
x_temp )
```

```
{  double
Re_temp,Sc_temp,temp,k_temp,D_temp,mu_temp,H_temp,s_temp,v_temp,xm_temp,mw_
mix_temp;

  tmix_l(T_temp,P_temp,x_temp,&k_temp,&D_temp,&mu_temp);
  mix_l(T_temp,P_temp,x_temp,&H_temp,&s_temp,&v_temp);
  xm_temp = (x_temp/mw_nh3)/((1 - x_temp)/mw_h2o + x_temp/mw_nh3);
  mw_mix_temp = (1-xm_temp) * mw_h2o + xm_temp * mw_nh3;

//Re_temp=Re_l(m_temp,d_temp,mu_temp);
  Re_temp=(1/0.6)*Re_co(m_temp,B,mu_temp);
  Sc_temp=Sc(mu_temp,v_temp,x_temp,D_temp);
// Source: Yih from "mass_transfer_in" check the unit of K_l
  temp=(1/v_temp)*(pow(10,-
9)*D_temp*0.01099*pow(Re_temp,0.3955)*pow(Sc_temp,0.5))/pow(pow((mu_temp*v_t
emp)/mw_mix_temp,2)/9.81,0.3334);
  temp33=temp;
  return temp;
}

double h_v1(double m_ltemp, double m_vtemp, double b_temp, double B_temp,
double d_temp, double T_ltemp,double T_vtemp, double P_temp, double x_temp, double
y_temp)
```

```
{double Re_temp,Prandtl_temp,u_temp,thickness,temp;
  double xm_temp,mw_mixl_temp,ym_temp,mw_mixv_temp;
  double H_ltemp,s_ltemp,v_ltemp;
  double H_vtemp,s_vtemp,v_vtemp,cp_vtemp;
  double k_vtemp,D_vtemp,mu_vtemp;
  double k_ltemp,D_ltemp,mu_ltemp;
//double Dh_temp;

  tmix_l(T_ltemp,P_temp,x_temp,&k_ltemp,&D_ltemp,&mu_ltemp);
  mix_l(T_ltemp,P_temp,x_temp,&H_ltemp,&s_ltemp,&v_ltemp);
  tmix_v((T_vtemp+T_ltemp)/2,P_temp,y_temp,&k_vtemp,&D_vtemp,&mu_vtemp
);
  mix_v((T_vtemp+T_ltemp)/2,P_temp,y_temp,&H_vtemp,&s_vtemp,&v_vtemp);
  mixcp_v((T_vtemp+T_ltemp)/2,P_temp,y_temp,&cp_vtemp);
  xm_temp=(x_temp/mw_nh3)/((1-x_temp)/mw_h2o+x_temp/mw_nh3);
  ym_temp=(y_temp/mw_nh3)/((1-y_temp)/mw_h2o+y_temp/mw_nh3);
  mw_mixl_temp=(1-xm_temp)*mw_h2o+xm_temp*mw_nh3;
  mw_mixv_temp=(1-ym_temp)*mw_h2o+ym_temp*mw_nh3;
  thickness=pow((3*m_ltemp*mu_ltemp*v_ltemp*v_ltemp)/(B_temp*9.81*mw_mi
xl_temp*mw_mixl_temp),0.3334);
  u_temp=(m_vtemp*v_vtemp)/(mw_mixv_temp*B_temp*(b_temp-2*thickness));
  //b_temp=b_temp-0.5*d_temp-2*thickness;
  //Dh_temp=(4*B_temp*b_temp)/(2*(B_temp+b_temp));
```

```
  Re_temp=Re_v(v_vtemp,y_temp,u_temp,d_temp,mu_vtemp);
  Prandtl_temp=Prandtl(mu_vtemp,cp_vtemp,y_temp,k_vtemp );
// Source: page 410, equation 7.55b of incropera. possible improvement can be
zhukauskas equation 7.56
  temp=(k_vtemp/d_temp)*0.683*pow(Re_temp,0.466)*pow(Prandtl_temp,0.3334);
  //temp=(k_vtemp/Dh_temp)*7.541;
  temp44=temp;
  return temp;
}

double h_v2(double m_ltemp, double m_vtemp, double b_temp, double B_temp,
double T_ltemp,double T_vtemp, double P_temp, double x_temp, double y_temp)
{double Re_temp,Prandtl_temp,u_temp,thickness,temp;
  double xm_temp,mw_mixl_temp,ym_temp,mw_mixv_temp;
  double H_ltemp,s_ltemp,v_ltemp;
  double H_vtemp,s_vtemp,v_vtemp,cp_vtemp;
  double k_vtemp,D_vtemp,mu_vtemp;
  double k_ltemp,D_ltemp,mu_ltemp;
  double Dh_temp;

  tmix_l(T_ltemp,P_temp,x_temp,&k_ltemp,&D_ltemp,&mu_ltemp);
  mix_l(T_ltemp,P_temp,x_temp,&H_ltemp,&s_ltemp,&v_ltemp);
```

```
        tmix_v((T_vtemp+T_ltemp)/2,P_temp,y_temp,&k_vtemp,&D_vtemp,&mu_vtemp
);
        mix_v((T_vtemp+T_ltemp)/2,P_temp,y_temp,&H_vtemp,&s_vtemp,&v_vtemp);
        mixcp_v((T_vtemp+T_ltemp)/2,P_temp,y_temp,&cp_vtemp);
        xm_temp=(x_temp/mw_nh3)/((1-x_temp)/mw_h2o+x_temp/mw_nh3);
        ym_temp=(y_temp/mw_nh3)/((1-y_temp)/mw_h2o+y_temp/mw_nh3);
        mw_mixl_temp=(1-xm_temp)*mw_h2o+xm_temp*mw_nh3;
        mw_mixv_temp=(1-ym_temp)*mw_h2o+ym_temp*mw_nh3;
        thickness=pow((3*m_ltemp*mu_ltemp*v_ltemp*v_ltemp)/(B_temp*9.81*mw_mi
xl_temp*mw_mixl_temp),0.3334);
        u_temp=(m_vtemp*v_vtemp)/(mw_mixv_temp*B_temp*(b_temp-2*thickness));
        b_temp=b_temp-2*thickness;
        Dh_temp=(4*B_temp*b_temp)/(2*(B_temp+b_temp));
        Re_temp=Re_v(v_vtemp,y_temp,u_temp,Dh_temp,mu_vtemp);
        Prandtl_temp=Prandtl(mu_vtemp,cp_vtemp,y_temp,k_vtemp );
      // Source: page 410, equation 7.55b of incropera. possible improvement can be
zhukauskas equation 7.56
      //temp=(k_vtemp/d_temp)*0.683*pow(Re_temp,0.466)*pow(Prandtl_temp,0.3334);
        temp=(k_vtemp/Dh_temp)*7.541;
        temp44=temp;
        return temp;
      }
```

```
double U(double d_o_temp,double d_i_temp, double B_temp, double k_t_temp,
double mc_temp, double Tc_temp, double Pc_temp, double m_temp, double T_temp,
double P_temp, double x_temp)
{double h_ci_temp,h_co_temp,temp;
  double
u_l_temp,H_temp,s_temp,v_temp,k_temp,D_temp,mu_temp,mw_mix_temp,xm_temp;

  h_ci_temp=h_ci(mc_temp,d_i_temp,Tc_temp,Pc_temp);
  mix_l(T_temp,P_temp,x_temp,&H_temp,&s_temp,&v_temp);
  tmix_l(T_temp,P_temp,x_temp,&k_temp,&D_temp,&mu_temp);
  xm_temp = (x_temp/mw_nh3)/((1 - x_temp)/mw_h2o + x_temp/mw_nh3);
  mw_mix_temp = (1-xm_temp) * mw_h2o + xm_temp * mw_nh3;
// Sources: page 40 of bird and stewart
  u_l_temp=((mw_mix_temp*9.81)/(3*mu_temp*v_temp))*pow((3*m_temp*mu_te
mp*v_temp*v_temp)/(9.81*mw_mix_temp*mw_mix_temp),0.6667);
  h_co_temp=h_co(m_temp,B_temp,d_o_temp,(T_temp+Tc_temp)/2,P_temp,x_tem
p);
// Sources: page 62 of incropera
  temp=1/((1/h_ci_temp)+(d_o-d_i)/(2*k_t_temp)+(1/h_co_temp));
  temp55=temp;
  return temp;
}
```

```
double h_l(double m_temp, double d_temp, double T_temp, double P_temp, double
x_temp )
{double Sc_temp, Prandtl_temp, K_temp,temp;
 double k_temp,D_temp,mu_temp,H_temp,s_temp,v_temp,cp_temp;

 tmix_l(T_temp,P_temp,x_temp,&k_temp,&D_temp,&mu_temp);
 mix_l(T_temp,P_temp,x_temp,&H_temp,&s_temp,&v_temp);
 mixcp_l(T_temp,P_temp,x_temp,&cp_temp);
 Prandtl_temp=Prandtl(mu_temp,cp_temp,x_temp,k_temp );
 Sc_temp=Sc(mu_temp,v_temp,x_temp,D_temp);
 K_temp=K_l(m_temp, d_temp, T_temp, P_temp, x_temp );
 temp=cp_temp*K_temp*1000*pow((Sc_temp/Prandtl_temp),0.6667);
 temp66=temp;
 return temp;

}

double K_v1(double m_ltemp, double m_vtemp, double b_temp, double B_temp,
double d_temp, double T_ltemp,double T_vtemp, double P_temp, double x_temp, double
y_temp)
{double Sc_temp,Prandtl_temp,h_temp,temp;
 double H_vtemp,s_vtemp,v_vtemp,cp_vtemp;
```

```
        double k_vtemp,D_vtemp,mu_vtemp;

        tmix_v(T_vtemp,P_temp,y_temp,&k_vtemp,&D_vtemp,&mu_vtemp);
        mix_v(T_vtemp,P_temp,y_temp,&H_vtemp,&s_vtemp,&v_vtemp);
        mixcp_v(T_vtemp,P_temp,y_temp,&cp_vtemp);
        Prandtl_temp=Prandtl(mu_vtemp,cp_vtemp,y_temp,k_vtemp );
        Sc_temp=Sc(mu_vtemp,v_vtemp,y_temp,D_vtemp);
        h_temp=h_v1(m_ltemp,m_vtemp,b_temp,B_temp,d_temp,T_ltemp,T_vtemp,P_te
mp,x_temp,y_temp);
        temp=h_temp/(cp_vtemp*1000*pow((Sc_temp/Prandtl_temp),0.6667));
        temp77=temp;
        return temp;
      }

      double K_v2(double m_ltemp, double m_vtemp, double b_temp, double B_temp,
double T_ltemp,double T_vtemp, double P_temp, double x_temp, double y_temp)
      {double Sc_temp,Prandtl_temp,h_temp,temp;
        double H_vtemp,s_vtemp,v_vtemp,cp_vtemp;
        double k_vtemp,D_vtemp,mu_vtemp;

        tmix_v(T_vtemp,P_temp,y_temp,&k_vtemp,&D_vtemp,&mu_vtemp);
        mix_v(T_vtemp,P_temp,y_temp,&H_vtemp,&s_vtemp,&v_vtemp);
        mixcp_v(T_vtemp,P_temp,y_temp,&cp_vtemp);
```

```
        Prandtl_temp=Prandtl(mu_vtemp,cp_vtemp,y_temp,k_vtemp );
        Sc_temp=Sc(mu_vtemp,v_vtemp,y_temp,D_vtemp);
        h_temp=h_v2(m_ltemp,m_vtemp,b_temp,B_temp,T_ltemp,T_vtemp,P_temp,x_te
mp,y_temp);
        temp=h_temp/(cp_vtemp*1000*pow((Sc_temp/Prandtl_temp),0.6667));
        temp77=temp;
        return temp;
      }

      double Pressure(double d_temp, double Np_temp, double m_temp, double B_temp,
double Tc_temp, double P_ctemp )
      {  double
G_temp,H_temp,s_temp,k_temp,D_temp,mu_temp,v_temp,Re_temp,f,temp,temp1,temp2,t
emp3;

        mix_l(Tc_temp,P_ctemp,0.0,&H_temp,&s_temp,&v_temp);
        tmix_l(Tc_temp,P_ctemp,0.0,&k_temp,&D_temp,&mu_temp);
        Re_temp=Re_ci(m_temp,d_temp,mu_temp);
        f=pow(0.79*log(Re_temp)-1.64,-2);

      // Source: kuppang handbook, page 288 chapter 5
      //  G is mass velocity (density*velocity)
        G_temp=(4*m_temp)/(3.1416*d_temp*d_temp);
```

```
  temp1=((0.5+0.5)*Np_temp*G_temp*G_temp*v_temp)/(2*mw_h2o);
  temp2=(f*Np_temp*B_temp*G_temp*G_temp*v_temp)/(2*mw_h2o*d_temp);
  temp3=(4*Np_temp*G_temp*G_temp*v_temp)/(2*mw_h2o);
  temp=temp1+temp2+temp3;
  return temp;
}
```

LIST OF REFERENCES

Akita, K., and Yoshida, F., 1974, "Bubble size, interfacial area and liquid phase mass transfer coefficient in bubble columns," Industrial and Engineering Chemistry Process Design and Development, 13, pp. 84-91.

Ameel, T. A., Kim, K. J., and Wood, B. D., 1997, "Non-absorbable gas effects on heat and mass transfer in wavy laminar falling film absorption," Solar Energy, 6, pp. 301-311.

Benzeguir, B., Setterwall, F., and Uddholm, H., 1991, "Use of a wave model to evaluate falling film absorber efficiency," International Journal of Refrigeration, 14, pp. 292-296.

Beutler, A., Greiter, I., Wagner, A., Hohhmann, L., Schreier, S., and Alefeld, G., 1996, "Surfactants and fluid properties," International Journal of Refrigeration, 19, pp. 342-346.

Bhavaraju, S. M., Russell, T. W. F., and Blanch, H. W., 1978, "The design of gas sparged devices for viscous liquid systems," AIChE Journal, 24, pp. 454-466.

Briggs, S.W., 1971, "Concurrent, crosscurrent, and countercurrent absorption in ammonia-water absorption refrigeration," ASHRAE Transactions, 77, pp. 171-175.

Chilton, T. H., and Colburn, A. P., 1934, "Mass transfer (Absorption) coefficients," Industrial and Engineering Chemistry, 26, pp. 1183-1187.

Churchill, S.W., and Ozoe, H., 1973, "Correlations for laminar forced convection with uniform heating in flow over a plate and in developing and fully developed flow in a tube," ASME Journal of Heat Transfer, 95, pp. 78-84.

Colburn, A. P., and Drew, T. B., 1937, "The condensation of mixed vapours," AIChE Transactions, 33, pp. 197-212.

Cosenza, F., and Vliet, G. C., 1990, "Absorption in falling water/LiBr films on horizontal tubes," ASHRAE Transactions, 96, pp. 693.

Daltrophe, N. C., Jelinek, M., and Borde, I., 1993, "Heat and mass transfer in a jet ejector for absorption systems," Proceedings of the International Absorption Heat Pump Conference, New Orleans, Louisiana, ASME AES-31, pp. 327-332.

Deng, S. M., and Ma, W. B., 1999, "Experimental studies on the characteristics of an absorber using LiBr/H_2O solution as working fluid," International Journal of Refrigeration, 22, pp. 293-301.

El-Sayed, Y. M., and Tribus, M., 1985, "Thermodynamic properties of ammonia-water mixtures: theoretical implementation for use in power cycle analysis," ASME Special Publication: Analysis of Energy Systems, ASME AES-1, pp. 89-95.

Fernández-Seara, J., Sieres, J., and Vázquez, M., 2002, "Simultaneous heat and mass transfer of a packed distillation column for ammonia-water absorption refrigeration systems," International Journal of Thermal Sciences, 41, pp. 927-935.

Frank, M., Kuipers, J. and Swaaij, W., 1996, "Diffusion coefficients and viscosities of CO2 + H2O, CO2 + CH3OH, NH3 + H2O, and NH3 + CH3OH liquid mixtures," Journal of Chemical and Engineering Data, 41, pp. 297-302.

Fuller, E. N., Schettler, P.D., and Giddings, J.C., 1965, "A comparison of methods for predicting gaseous diffusion coefficients," Journal of Gas Chromatography, 3, pp. 222-227.

Fuller, E. N., Ensley, K., and Giddings, J. C., 1969, "Diffusion of halogenated hydrocarbons in Helium. Effect of Structure on Collison Cross Sections," Journal of Physical Chemistry, 73, pp. 3679-3685.

Fujita, H., Takahama, H., Yabashi, H., and Takagi, K., 1980, "Effects of wall roughnesses on heat and mass transfer in countercurrent flow of air and water film," Heat Transfer – Japanese Research, 9, pp. 42-53.

Garimella, S., 2000, "Microchannel components for absorption space-conditioning systems," ASHRAE Transactions, pp. 453-462.

Gommed, K., Grossman, G., and Keonig, M. S., 1999, "Numerical model of ammonia-water absorption inside a vertical tube," Proceedings of the International Sorption Heat Pump Conference, Munich, Germany, pp. 275-281.

Gommed, K., Grossman, G., and Keonig, M. S., 2001, "Numerical study of absorption in a laminar falling film of ammonia-water," ASHRAE Transactions, pp. 453-462.

Goswami, D. Y., 1995, "Solar thermal power-status of technologies and opportunities for research," Proceedings of the 2nd ASME-ISHMT Heat and Mass Transfer Conference, Tata-McGraw Hill Publishers, New Delhi, India, pp. 57-60.

Goswami, D. Y., 1998, "Solar thermal technology: present status and ideas for the future," Energy Sources, 20, pp. 137-145.

Goswami, D. Y., and Xu, F., 1999, "Analysis of a New Thermodynamic Cycle for Combined Power and Cooling Using Low and Mid Temperature Solar Collectors," Journal of Solar Energy Engineering, 121, pp. 91-97.

Helbing, U., Wuerfel, R., and Fratzscher, W., 2000, "Comparative investigations of non-adiabatic absorption in film flow and bubble flow," Chemical Engineering and Technology, 23, pp. 1081-1085.

Herbine, G. S., Perez-Blanco, H., 1995, "Model of an ammonia-water bubble absorber," ASHRAE Transactions, 101, pp. 1324-1332.

Herold, K. E., Radermacher, R., and Klien, S. A., 1996, Absorption Chillers and Heat Pump, CRC Press Inc.

Hozawa, M., Inoue, M., Sato, J., and Tsukada, T., 1991, "Marangoni convection during steam absorption into aqueous LiBr solution with surfactant," Journal of Chemical Engineering of Japan, 24, pp. 209-214.

Hu, X., and Jacobi, A. M., 1996a, "The intertube falling film part 1 – Flow characteristics, mode transitions and hysteresis," ASME Journal of Heat Transfer, 118, pp. 616-625.

Hu, X., and Jacobi, A. M., 1996b, "The intertube falling film part 2 – Mode effects on sensible heat transfer to a falling liquid film," ASME Journal of Heat Transfer, 118, pp. 626-633.

Hu, X., and Jacobi, A. M., 1998, "Departure-site spacing for liquid droplets and jets falling between horizontal circular tubes," Experimental Thermal and Fluid Science, 16, pp. 322-331.

Huang, B. J., 1990, "A precise measurement of temperature difference using thermopiles," Experimental Thermal and Fluid Science, 3, pp. 265-271.

Ibrahim, O. M., and Klein, S. A., 1996, "Absorption power cycles," Energy, 21, pp. 21-27.

Incropera, F. P., and DeWitt, D. P., 2002, Fundamentals of Heat and Mass Transfer, 5th Edition, John Wiley & Sons Inc., New York.

Infante Ferreira, C. A., Keizer, C., and Machielsen, C. H. M., 1984, "Heat and mass transfer in vertical tubular bubble absorber for ammonia-water absorption refrigeration systems," International Journal of Refrigeration, 7, pp. 348-357.

Islam, R., Md., Wijeysundera, N. E., and Ho, J. C., 2003a, "Evaluation of heat and mass transfer coefficients for falling-films on tubular absorbers," International Journal of Refrigeration, 26, pp. 197-204.

Islam, R., Md., Wijeysundera, N. E., and Ho, J. C., 2003b, "Performance study of a falling-film absorber with a film-inverting configuration," International Journal of Refrigeration, 26, pp. 909-917.

Isshiki, N., Ogaka, K. and Sasaki, K., 1988, "Studies on mechanism and enhancement of absorption heat and mass transfer," Absorption Heat Pumps, Proceedings of Workshop by Commission of the European Communities, London, pp. 399-408.

Jamieson, D. T., Irving, J. B., and Tudhope, J. S., 1975, Liquid Thermal Conductivity: A Data Survey to 1973, H. M. Stationary Office, Edinburg.

Jeong, S., Lee, S. K., and Koo, K., 1998, "Heat transfer performance of a coiled tube absorber with working fluid of ammonia/water," ASHRAE Transactions, 104, pp. 1577-1583.

Kakaç, S., Shah, R. C., and Aung, W., 1987, Handbook of Single-Phase Convective Heat Transfer, John Wiley & Sons Inc., New York.

Kang, Y. T., and Christensen, R. N., 1993, "Development of a counter-current model for a vertical fluted tube GAX absorber," Proceedings of the International Absorption Heat Pump Conference, New Orleans, Louisiana, ASME AES-31, pp. 7-16.

Kang, Y. T., and Christensen, R. N., 1995, "Transient analysis and design model of a LiBr-H2O absorber with rotating drums," ASHRAE Transactions, 101, pp. 1163-1173.

Kang, Y. T., Chen, W., Christensen, R. N., 1996a, "Design of ammonia-water condenser with a fluted tube," ASHRAE Transactions, 102, pp. 587-595.

Kang, Y. T., Chen, W., Christensen, R. N., 1996b, "Development of design model for a rectifier in GAX absorption heat pump systems," ASHRAE Transactions, 102, pp. 963-972.

Kang, Y. T., Chen, W., Christensen, R. N., 1997, "A generalized component design model by combined heat and mass transfer analysis in NH3-H2O absorption heat pump systems," ASHRAE Transactions, 103, pp. 444-453.

Kang, Y. T., Christensen, R. N., and Kashiwagi, T., 1998, "Ammonia-water bubble absorber with a plate heat exchanger," ASHRAE Transactions, 104, pp. 1565-1575.

Kang, Y. T., Akisawa, A., and Kashiwagi, T., 1999, "Visualization and model development of Marangoni convection in NH3-H2O system," International Journal of Refrigeration, 22, pp. 640-649.

Kang, Y. T., Akisawa, A., and Kashiwagi, T., 2000a, "Analytical investigation of two different absorption modes: falling film and bubble types," International Journal of Refrigeration, 23, pp. 430-443.

Kang, Y. T., Nagano, T., and Kashiwagi, T., 2002b, "Visualization of bubble behavior and bubble diameter correlation for NH3-H2O bubble absorption," International Journal of Refrigeration, 25, pp. 127-135.

Kang, Y. T., Nagano, T., and Kashiwagi, T., 2002c, "Mass transfer correlation of NH3-H2O bubble absorption," International Journal of Refrigeration, 25, pp. 878-886.

Kashiwagi, T., 1988, "Basic mechanism of absorption heat and mass transfer enhancement by the Marangoni effect," Newsletter, IEA Heat Pump Center, 6, pp. 2-6.

Killion, J. D., and Garimella, S., 2001, "A critical review of models of coupled heat and mass transfer in falling-film absorption," International Journal of Refrigeration, 24, pp. 755-797.

Kim, B., 1998, "Heat and mass transfer in a falling film absorber of ammonia-water absorption systems," Heat Transfer Engineering, 19, pp. 53-63.

Kim, K. J., Berman, N. S., and Wood, B. D., 1993, "Experimental investigation of enhanced heat and mass transfer mechanisms using additives for vertical falling film absorber," Proceedings of the International Absorption Heat Pump Conference, New Orleans, Louisiana, ASME AES-31, pp. 41-47.

Kim, K. J., Berman, N. S., and Wood, B. D., 1996, "The interfacial turbulence in falling film absorption: effects of additives," International Journal of Refrigeration, 19, pp. 322-330.

Kulankara, S., Verma, S., and Herold, K. E., 1999, "Theory of heat/mass transfer additives in absorption chillers," Proceedings of the ASME Advanced Energy Systems Division, Nashville, Tennessee, 39, pp. 199–206.

Kumar, A., Degaleesan, T. E., Laddha, G. S., and Hoelscher, H. E., 1976, "Bubble swarm characteristics in bubble columns," Canadian Journal of Chemical Engineering, 54, pp. 503-508.

Kutateladze, S. S., 1972, "Elements of the hydrodynamics of gas-liquid systems," Fluid Mechanics-Soviet Research, 1, 29-50.

Lee, K. B., Chun, B. H., Lee, J. C., Hyun, J. C., and Kim, S. H., 2002, "Comparison of heat and mass transfer in falling film and bubble absorbers of ammonia-water," Experimental Heat Transfer, 15, pp. 191-205.

Martin, C., 2004, Study of cooling production with a combined power and cooling thermodynamic cycle, Ph.D. dissertation, University of Florida, Gainesville, FL.

Mason, E. A., and Saxena, S. C., 1958, "Approximate formula for the thermal conductivity of gas mixtures," Physics of Fluids, 1, pp. 361-369.

Meacham, J. M., and Garimella, S., 2002, "Experimental demonstration of a prototype microchannel absorber for space-conditioning systems," Proceedings of the International Sorption Heat Pump Conference, Shanghai, China, pp. 24-27.

Meacham, J. M., and Garimella, S., 2003, "Modeling of local measured heat and mass transfer variations in a microchannel ammonia-water absorber," ASHRAE Transactions, 109, pp. 412-422.

Meacham, J. M., and Garimella, S., 2004, "Ammonia-water absorption heat and mass transfer in microchannel absorbers with visual confirmation," ASHRAE Transactions, 110, pp. 525-532.

Medrano, M., Bourouis, M., Perez-Blanco, H., and Coronas, A., 2003, "A simple model for falling film absorption on vertical tubes in the presence of non-absorbables," International Journal of Refrigeration, 26, pp. 108-116.

Merrill T. L., Setoguchi T, and Perez-Blanco H., 1995, "Passive heat transfer enhancement techniques applied to compact bubble absorber design," Journal of Enhanced Heat Transfer, 2, pp. 199-208.

Merrill T. L., and Perez-Blanco H., 1997, "Combined heat and mass transfer during bubble absorption in binary solutions," International Journal of Heat and Mass Transfer, 40, pp. 589-603.

Miller, W. A., and Perez-Blanco, H., 1993, "Vertical-tube aqueous LiBr falling film absorption using advanced surfaces," ASME Transaction of International Absorption Heat Pump Conference, 31, pp. 185-202.

Min, J., and Webb, R.L., 2002, "Long-term wetting and corrosion characteristics of hot water treated aluminum and copper fin stocks," International Journal of Refrigeration, 25, pp. 1054-1061.

Mitrovic, J., 1986, "Influence of tube spacing and flow rate on heat transfer from a horizontal tube to a falling liquid film," Proceedings of the 8th International Heat Transfer Conference, San Francisco, California, 4, pp. 1949-1956.

Möller, R., and Knoche, K. F., 1996, "Surfactants with NH3-H2O," International Journal of Refrigeration, 19, pp. 317-321.

Pachhapur, A. S., and Rane, M. V., 1998, "Review of various absorber designs used in absorption systems," Presented at IIR Conference on Emerging Trends in Refrigeration and Air-Conditioning, New Delhi, India.

Palmer, S. C., and Christensen, R. N., 1996, "Experimental investigation and model verification for a GAX absorber," Proceedings of International Ab-Sorption Heat Pump Conference, Montréal, Canada, pp. 367-374.

Park, C. W., Kim, S. S., Cho, H. C., and Kang, Y. T., 2003, "Experimental correlation of falling film absorption heat transfer on micro-scale hatched tubes," International Journal of Refrigeration, 26, pp. 758-763.

Pathanjali, C., and Rahman, M. M., 1996, "Numerical simulation of gas absorption to a thin liquid film over a rotating disk in the presence of simulataneous chemical reaction," Proceeding of the Intersociety Energy Conversion Engineering Conference, Washington, DC, 2, pp. 1055-1066.

Perez-Blanco, H. A., 1988, "A model of an ammonia-water falling film absorber," ASHRAE Transactions, 94, pp. 467-483.

Petukhov, B. S., 1970, Heat transfer and friction in turbulent pipe flow with variable physical properties, Irvine, T. F., and Hartnett, J. P., eds., Advances in Heat Transfer, Academic Press, New York, 7, pp. 503-565.

Potnis, S. V., Gomezplata, A., Papar, R. A., Anand, G., and Erickson, D. C., 1997, "GAX component simulation and validation," ASHRAE Transactions, 103, pp. 454-459.

Price, B. C., and Bell, K. J., 1974, "Design of binary vapor condensers using the colburn-drew equations," AIChE Symposium Series-Heat Transfer-Research and Design, 70, pp. 163-171.

Reid, R. C., Prausnitz, J. M., and Poling, B. E., 1987, The Properties of Gases and Liquids, McGraw-Hill, New York.

Rignac, J. P., Huor, M. H., and Bugarel, R., 1988, "Heat and mass transfers in heat pump absorber: Study of film tubular absorbers with tangential feed and turbulence promoters," Absorption Heat Pumps: Proceedings of a Workshop by Commission of the European Communities, London, pp. 362-371.

Roques, J. F., Dupont, V., and Thome, J. R., 2002, "Falling film transitions on plain and enhanced tubes," Journal of Heat Transfer, 124, pp. 491-499.

Ruhemann, M., 1947, "A study of the transfer of heat and matter in an ammonia absorber," Transactions of the Institute of Chemical Engineers, pp. 158-162.

Schwarzer, B., Rahbar, M. S., and LeGoff, P., 1993, "A novel type of falling film heat and mass exchanger," Proceedings of the International Absorption Heat Pump Conference, New Orleans, Louisiana, ASME AES-31, pp. 179-183.

Schweitzer, P. A., 1998, Encyclopedia of Corrosion Technology, Marcel Dekker, Inc., New York.

Schweitzer, P. A., 2000, Mechanical and Corrosion-Resistant Properties of Plastics and Elastomers - Corrosion Technology, Marcel Dekker, Inc., New York.

Shah, R. K., and London, A. L., 1978, Laminar Flow Forced Convection in Ducts, Academic Press, New York.

Selim, A. M., and Elsayed, M. M., 1999a, "Performance of a packed bed absorber for aqua ammonia absorption refrigeration system," International Journal of Refrigeration, 22, pp. 283-292.

Selim, A. M., and Elsayed, M. M., 1999b, "Interfacial mass transfer and mass transfer coefficient in aqua ammonia packed bed absorber," International Journal of Refrigeration, 22, pp. 263-274.

Strenger, U., and Setterwall, F., 1993, "Investigations on lamellas in an absorption heat pump," Proceedings of the International Absorption Heat Pump Conference, New Orleans, Louisiana, ASME AES-31, pp. 149-153.

Sujatha, K. S., 1999, "Experiments on a bubble absorber," International Communications on Heat and Mass Transfer, 26, pp. 975-984.

Tamm, G., 2003, Experimental Investigation of an Ammonia-Based Combined Power and Cooling Cycle, Ph.D. dissertation, University of Florida, Gainesville, FL.

Tang, Z., and Lu, B. Y. C., 1991, "Droplet spacing of falling film flow on horizontal tube bundles," Proceedings of the 18th International Congress of Refrigeration, Montréal, Canada, 2, pp. 474-478.

Terasaka, K., Oka, J., and Tsuge, H., 2002, "Ammonia absorption from a bubble expanding at a submerged orifice into water," Chemical Engineering Science, 57, pp. 3757-3765.

Tongu, S., Makino, Y., Ohnishi, K., and Nakatsugawa, S., 1993, "Practical operating of small-sized air-cooled double-effect absorption chiller-heater by using lithium bromide and aqueous," Proceedings of the International Absorption Heat Pump Conference, New Orleans, Louisiana, ASME AES-31, pp.125-132.

Treybal, R. E., 1980, Mass Transfer Operations, McGraw-Hill, New York.

Wallis, G.B., 1969, One-dimensional Two-phase Flow, McGraw-Hill, New York.

Wallis, G. B., 1970a, "Annular two-phase flow: Part 1. A simple theory," ASME Journal of Basic Engineering, 92, pp. 59-72.

Wallis, G. B., 1970b, "Annular two-phase flow: Part 2. Additional effects," ASME Journal of Basic Engineering, 92, pp. 73-82.

Wei, Y-H, and Jacobi, A. M., 2002, "Vapor-shear, geometric, and bundle-depth effects on the intertube falling-film modes," Proceedings of 1st International Conference on Heat Transfer, Fluid Mechanics, and Thermodynamics, Kruger Park, South Africa, pp. 40-46.

Wilke, C. R., 1950, "A viscosity equation for gas mixtures," Journal of Chemical Physics, 18, pp. 517-519.

Xu, F., and Goswami, D. Y., 1999, "Thermodynamic properties of the ammonia-water mixtures for power-cycle applications," Energy, 24, pp. 525-536.

Yang, R., and Jou, D., 1995, "Heat and mass transfer of absorption process for the falling film flow inside a porous medium," International Journal of Heat and Mass Transfer, 38, pp. 1121-1126.

Yang, R., and Wood, B. D., 1993, "Experimental study for heat and mass transfer in wavy film absorption with the presence of non-absorbable gases," Chemical Engineering Communications, 125, pp. 77-90.

Yaws, C. L., 1995, Handbook of Thermal Conductivity, Gulf Publishing Company, Houston.

Yaws, C. L., 1995, Handbook of Viscosity, Gulf Publishing Company, Houston.

Yih, S. M., and Chen, K. Y., 1982, "Gas absorption into wavy and turbulent falling liquid films in a wetted-wall column," Chemical Engineering Communications, 17, pp. 123-136.

Yih, S. M., 1986, "Modeling heat and mass transport in falling liquid films," Handbook of Heat and Mass Transfer: Mass Transfer and Reactor Design, N. P. Cheremisinoff, eds., Gulf Publishing Company, Houston, pp. 111–120.

Ziegler, B., and Trepp, C., 1984, "Equations of state for ammonia-water mixtures," International Journal of Refrigeration, 7, pp. 101-106.

BIOGRAPHICAL SKETCH

Nitin Goel was born on 30th December 1978 in Dankaur, a historical village located about 30 miles southeast of New Delhi, India. He was brought up in an industrial town of Ghaziabad which also borders the capital of India. He received his bachelor's degree in mechanical engineering from the Indian Institute of Technology-Bombay, India, in 2001. In the same year, he enrolled into the direct-PhD program in the Department of Mechanical Engineering at the University of Florida. His initial research included a feasibility study of solar heating a manatee refuge located in southeast Florida, and various hydrogen production technologies. In fall 2002, he started working on the absorption-condensation processes in absorption based thermodynamic cycles as his dissertation topic.

Nitin received the 2004 Graduate Student Award from the American Society of Mechanical Engineers (ASME) – Solar Energy Division for his doctoral research in the field of solar energy. His research interests include absorption refrigeration, solar thermal energy and hydrogen production.